

University of Windsor

Scholarship at UWindsor

Electronic Theses and Dissertations

Theses, Dissertations, and Major Papers

1-1-2019

Impacts of climate change on the hydrological regime in the Olifants River, South Africa

Afanur Rahman Talukder
University of Windsor

Follow this and additional works at: <https://scholar.uwindsor.ca/etd>

Recommended Citation

Talukder, Afanur Rahman, "Impacts of climate change on the hydrological regime in the Olifants River, South Africa" (2019). *Electronic Theses and Dissertations*. 8180.
<https://scholar.uwindsor.ca/etd/8180>

This online database contains the full-text of PhD dissertations and Masters' theses of University of Windsor students from 1954 forward. These documents are made available for personal study and research purposes only, in accordance with the Canadian Copyright Act and the Creative Commons license—CC BY-NC-ND (Attribution, Non-Commercial, No Derivative Works). Under this license, works must always be attributed to the copyright holder (original author), cannot be used for any commercial purposes, and may not be altered. Any other use would require the permission of the copyright holder. Students may inquire about withdrawing their dissertation and/or thesis from this database. For additional inquiries, please contact the repository administrator via email (scholarship@uwindsor.ca) or by telephone at 519-253-3000ext. 3208.

**Impacts of climate change on the hydrological regime in the Olifants River, South
Africa**

By

Afanur Rahman Talukder

A Thesis

Submitted to the Faculty of Graduate Studies
through the Department of Civil and Environmental Engineering
in Partial Fulfillment of the Requirements for
the Degree of Master of Applied Science
at the University of Windsor

Windsor, Ontario, Canada

2019

© 2019 Afanur Rahman Talukder

Impacts of climate change on the hydrological regime in the Olifants River, South Africa.

by

Afanur Rahman Talukder

APPROVED BY:

C. Houser

Faculty of Science

R. Balachandar

Department of Civil and Environmental Engineering

E. Riddell

Krugar National Park, SANPARKS, South Africa

T. Bolisetti, Advisor

Department of Civil and Environmental Engineering

12 December 2019

DECLARATION OF ORIGINALITY

I hereby certify that I am the sole author of this thesis and that no part of this thesis has been published or submitted for publication.

I certify that, to the best of my knowledge, my thesis does not infringe upon anyone's copyright nor violate any proprietary rights and that any ideas, techniques, quotations, or any other material from the work of other people included in my thesis, published or otherwise, are fully acknowledged in accordance with the standard referencing practices. Furthermore, to the extent that I have included copyrighted material that surpasses the bounds of fair dealing within the meaning of the Canada Copyright Act, I certify that I have obtained a written permission from the copyright owner(s) to include such material(s) in my thesis and have included copies of such copyright clearances to my appendix.

I declare that this is a true copy of my thesis, including any final revisions, as approved by my thesis committee and the Graduate Studies office, and that this thesis has not been submitted for a higher degree to any other University or Institution.

ABSTRACT

Olifants River watershed one of the largest river basins in South Africa, which is home for one of the most important natural parks in the world, Kruger National Park (KNP). The activities in this watershed generate 6% of the Gross Domestic Product. It requires a minimum amount of water termed as ecological reserve for sustaining the ecohydrology which is often jeopardized due to the water scarcity. The objective of this study is to assess the impact of climate change on the hydrologic regime in the Olifants River watershed.

A hydrological model is developed using Soil and Water Assessment Tool (SWAT). The model was calibrated using multisite data (2003-2008) and validated (2009-2012) by comparing the simulated results with the observed streamflow data. The Nash Sutcliffe Efficiency (NSE), Kling Gupta Efficiency (KGE) and Percent Bias (PBIAS) for the Mamba (B7H015) flow station are found to be 0.60, 0.80, -2.21% and 0.56, 0.63, -0.47% for the calibration and validation period, respectively. The same are 0.52, 0.65 19.26% and 0.74, 0.81, 8.82% for the calibration and validation periods for Blyde (B6H005) station.

The calibrated model is forced with the bias corrected future climate data extracted from Coordinated Regional Climate Downscaling Experiment (CORDEX) for nine climate ensembles under moderate (rcp4.5) and high (rcp8.5) emission scenarios for mid-century (2041-2070) and end-century (2071-2100) periods. The results indicate that the annual average temperature is projected to increase by 1.7°C to 4.6°C by the end century compared to the base period (1985-2005). The mean annual precipitation is projected to decrease in the future by 12-29%. The minimum flow (0.5 m³/s) availability at B7H015 for the ecological reserve of KNP would decrease 2-12% in the future.

DEDICATION

To my beloved parents

ACKNOWLEDGEMENTS

First of all, I would like to thank the almighty for giving me the strength, patience and blessings to accomplish this endeavour.

I would like to thank my wife, Farzana, son Abrar and daughter Ayat for their endless support and commitments towards my MASc study.

I sincerely appreciate my supervisor, Dr. Tirupati Bolisetti, for his continuous support and guidance during the MASc study at University of Windsor. I thank him for providing the technical and financial support during this journey.

I sincerely acknowledge the program reader, Dr. Ram Balachandar and outside program reader, Dr. Chris Houser for their valuable time and suggestions to improve the quality of the research.

I am taking this opportunity to thank special committee member Dr. Eddie Riddell for sharing his knowledge and experience about the study area. I also thank him for attending the meetings and sharing the data.

I express my gratitude to Mr. Hugo Retief for sharing his insights about the study area and sparing his valuable time attending the meetings and presentations.

I acknowledge South African Weather Service, Department of Environmental Affairs South Africa, Department of Water and Sanitation South Africa, Climate Hazards Group InfraRed Precipitation with Station data, Moderate Resolution Imaging Spectroradiometer, International Centre for Tropical Agriculture, and Food and Agriculture Organization for sharing the data.

My gratitude goes to the university of Windsor for providing the entrance scholarship.

I like to thank my research groupmate Dr. Vinod Chilkoti for assisting me at various stages of the research. His in-depth knowledge in hydrology and modelling tools helped me a lot to solve the challenges encountered during the research.

Finally, I like to thank all my fellow graduate students Israt, Monika, Saranya and others with whom I shared the office.

CONTENTS

DECLARATION OF ORIGINALITY	iii
ABSTRACT.....	iv
DEDICATION.....	v
ACKNOWLEDGEMENTS.....	vi
LIST OF TABLES.....	xiv
LIST OF ABBREVIATIONS.....	xv
CHAPTER I.....	1
INTRODUCTION	1
1.1 Background	1
1.2 Problem Definition.....	2
1.3 Objectives.....	3
1.4 Structure of the Thesis.....	4
CHAPTER II.....	5
LITERATURE REVIEW	5
2.1 Overview	5
2.2 Hydrologic Cycle	5
2.3 Water Budget.....	6
2.4 Hydrologic Models.....	6
2.5 Model Classification	7
2.6 Model Selection.....	9
2.7 SWAT Application.....	10
2.8 SWAT Applications in Climate Change Impact Studies	10
2.9 General Circulation Model (GCM).....	11
2.10 Downscaling of GCM	12
2.11 Bias Correction.....	12
2.11.1 Linear Scaling.....	13
2.11.2 Quantile Mapping.....	14
2.12 Climate change impact on water resources in South Africa and the Olifants basin	14

2.13 Research gap and potential: climate change and water resources in Olifants basin	16
CHAPTER III	18
METHODOLOGY	18
3.1 Overview	18
3.2 Watershed Description	19
3.3 Soil and Water Assessment Tool (SWAT)	21
3.4 SWAT User Interface.....	23
3.5 Data Description.....	23
3.5.1 Digital Elevation Model (DEM).....	24
3.5.2 Soil Data	25
3.5.3 Landuse Data	26
3.5.4 Climate Data	28
3.5.5 River Flow Data.....	33
3.5.6 Dams	35
3.6 Model Setup	36
3.7 Water Use.....	37
3.8 Climate Change Impact Assessment.....	39
3.9 Trend Analysis	41
3.9.1 Mann Kendall (M-K) Test.....	41
3.9.2 Sen’s Slope	41
CHAPTER IV	42
RESULTS AND DISCUSSION.....	42
4.1 Overview	42
4.2 Impacts of Water Use on Streamflow	42
4.3 Sensitivity Analysis.....	45
4.4 Calibration and Validation	47
4.4.1 Nash-Sutcliffe Efficiency (NSE).....	48
4.4.2 Kling Gupta Efficiency (KGE).....	48
4.4.3 Percent Bias (PBIAS).....	48
4.4.4 Calibration and Validation Performance	49
4.5 Uncertainty Analysis.....	50
4.6 Water Budget Analysis.....	51

4.7 Climate Change Impacts	53
4.7.1 Precipitation Projection	53
4.7.2 Temperature Projection	58
4.7.3 Flow Projection.....	65
4.7.4 Hydrograph Comparison	68
4.7.5 Flow Duration Curve (FDC) Comparison	69
4.8 Spatial Distribution of Precipitation Change	70
4.9 Spatial Distribution of Potential Evapotranspiration Change	71
4.10 Spatial Distribution of Water Yield Change	73
CHAPTER V	75
CONCLUSIONS AND RECOMMENDATIONS	75
5.1 Conclusions	75
5.2 Recommendations	76
REFERENCES	78
ANNEXURES	92
Annexure 1: List of available precipitation station	92
Annexure 2: List of climate model ensembles	92
Annexure 3: Projected precipitation maps for the future periods	93
Annexure 4: Projected temperature maps for the future periods	105
Annexure 5: Projected PET maps for the future periods	113
Annexure 6: Projected water yield maps for the future periods.....	117
Annexure 7: Projected Flow Duration Curves at Mamba for future periods	121
Annexure 8: Trend analysis plots for projected temperatures.....	125
Annexure 9: Change in annual hydrological components from base period	127
Annexure 10: Extracting climatic data from CHIRPS or CORDEX in R	133
Annexure 11: Publisher’s permission	134
VITA AUCTORIS	137

LIST OF FIGURES

Fig. 2-1 Hydrologic Cycle (Adapted after Brutsaert, 2005).....	5
Fig. 3-1 Methodology flowchart.....	18
Fig. 3-2 Olifants River watershed location map.....	19
Fig. 3-3 Olifants River basin topography.	24
Fig. 3-4 Soil classification within the study area.....	25
Fig. 3-5 Landuse classes within the study area.....	27
Fig. 3-6 Precipitation stations within the study area (a) observed (b) gridded.....	30
Fig. 3-7 Temperature stations within the study area (a) observed (b) gridded.....	30
Fig. 3-8 Annual average precipitation comparison between CHIRPS and Observed at (a) B1E001, (b) B1E003, (c) B4E003, and (d) B7E007 stations	31
Fig. 3-9 Monthly precipitation comparison between CHIRPS and Observed at.....	31
(a) B1E001, (b) B1E003, (c) B4E003, and (d) B7E007 stations.....	31
Fig. 3-10 Monthly maximum temperature comparison between MODIS and Observed at (a) Hoedspruit, (b) Lydenburg, (c) Oudestad, and (d) Witbank stations	32
Fig. 3-11 Monthly minimum temperature comparison between MODIS and Observed at (a) Hoedspruit, (b) Lydenburg, (c) Oudestad, and (d) Witbank stations	32
Fig. 3-12 Difference in minimum temperature between Observed and MODIS at (a) Hoedspruit, (b) Lydenburg, (c) Oudestad, and (d) Witbank stations.....	33
Fig. 3-13 Monthly precipitation and streamflow comparison over time at Balule.....	34
Fig. 3-14 Monthly precipitation and streamflow comparison over time at Mamba.....	34
Fig. 3-15 Monthly precipitation and streamflow comparison over time at Blythe	34
Fig. 3-16 Major dams in the Oilfants River basin	36
Fig. 3-17 Delineation of sub watersheds.	37
Fig. 3-18 Upper, Middle and Lower Olifants River.	38
Fig. 3-19 Crop calendar of South Africa	39
Fig. 3-20 (a) Comparison of monthly median precipitation and mean PET across the study area, and (b) Monthly consumptive water use	39
Fig. 4-1 Comparison of observed and simulated streamflows at Mamba (B7H015) gauging station (without considering consumptive water use).....	43

Fig. 4-2 Comparison of observed and simulated streamflows at Mamba (B7H015) gauging station (considering consumptive water use).....	43
Fig. 4-3 Comparison of monthly observed (1 st bar from left) and simulated streamflows at Mamba (B7H015) gauging station (without considering consumptive water use)	44
Fig. 4-4 Comparison of monthly observed (1 st bar from left) and simulated streamflow at Mamba (B7H015) gauging station (considering consumptive water use).....	44
Fig. 4-5 Model parameters sensitivity statistics in the Olifants River basin	46
Fig. 4-6 Monthly streamflow calibration results: (a) Mamba and (b) Blythe	49
Fig. 4-7 Monthly streamflow validation results: (a) Mamba and (b) Blythe.....	49
Fig. 4-8 Illustration of the best streamflow estimation and 95 percent uncertainty band at the beginning of the uncertainty analysis at Mamba (B7H015)	51
Fig. 4-9 Illustration of the best streamflow estimation and 95 percent uncertainty band at the end of the uncertainty analysis at Mamba B7H015	51
Fig. 4-10 Simulated annual water budget for the period 2003-2012 in the Olifants basin	52
Fig. 4-11 Spatial distribution of hydrological components for the period 2003-2012; (a) average annual precipitation, (b) potential evapotranspiration and (c) water yield.....	53
Fig. 4-12 Monthly mean precipitation comparison in the study area between base future periods for (a) rcp 4.5 mid-century, (b) rcp 4.5 end-century, (c) rcp 8.5 mid-century, and (d) rcp 8.5 end-century.....	56
Fig. 4-13 Monthly mean precipitation comparison in the study area between base and mid-century for rcp 4.5 scenario	56
Fig. 4-14 Monthly mean precipitation comparison in the study area between base and end-century for rcp 4.5 scenario	57
Fig. 4-15 Monthly mean precipitation comparison in the study area between base and mid-century rcp 8.5 scenario	57
Fig. 4-16 Monthly mean precipitation comparison in the study area between base and end-century for rcp 8.5 scenario	58
Fig. 4-17 Daily maximum temperature comparison at monthly time step between base and future period for (a) rcp 4.5 mid-century, (b) rcp 4.5 end-century, (c) rcp 8.5 mid-century and iv) rcp 8.5 end-century	60

Fig. 4-18 Daily minimum temperature comparison at monthly time step between base and future periods for (a) rcp 4.5 mid-century, (b) rcp 4.5 end-century, (c) rcp 8.5 mid-century and iv) rcp 8.5 end-century	60
Fig.4-19 Monthly timeseries, linear regression analysis and annual Mann-Kendall statistics of daily maximum temperature for rcp 8.5 mid-century for the study area.....	61
Fig. 4-20 Monthly timeseries, linear regression analysis and annual Mann-Kendall statistics of daily maximum temperature for rcp 8.5 end-century for the study area.	61
Fig. 4-21 Monthly timeseries, linear regression analysis and annual Mann-Kendall statistics of daily maximum temperature for rcp 8.5 mid-century for the study area.	62
Fig. 4-22 Monthly timeseries, linear regression analysis and annual Mann-Kendall statistics of daily maximum temperature for rcp 8.5 end-century for the study area.	62
Fig. 4-23 Monthly mean flow comparison between base and future periods at Mamba (B7H015); (a) rcp 4.5 mid-century, (b) rcp 4.5 end-century, (c) rcp 8.5 mid-century, and (d) rcp 8.5 end-century.....	65
Fig. 4-24 Boxplot of monthly mean flow comparison at Mamba for rcp4.5 mid-century	66
Fig. 4-25 Boxplot of monthly mean flow comparison at Mamba for rcp4.5 end-century	66
Fig. 4-26 Boxplot of monthly mean flow comparison at Mamba for rcp8.5 mid-century	67
Fig. 4-27 Boxplot of monthly mean flow comparison at Mamba for rcp8.5 end-century	67
Fig. 4-28 Historical and future flow hydrographs with ranges for, (i) rcp 4.5 mid-century, (ii) rcp 4.5 end-century, (iii) rcp 8.5 mid-century, and (iv) rcp 8.5 end-century at Mamba	68
Fig. 4-29 Historical and future Flow Duration Curves (FDC's) for (i) rcp 4.5 mid-century, (ii) rcp 4.5 end-century, (iii) rcp 8.5 mid-century, and (iv) rcp 8.5 end-century at Mamba	69
Fig. 4-30 Change in precipitation across the Olifants River basin from base to (i) rcp 4.5 mid-century, (ii) rcp 4.5 end-century, (iii) rcp 8.5 mid-century, and (iv) rcp 8.5 end-century	71
Fig. 4-31 Change in PET across the Olifants River Basin from base to (i) rcp 4.5 mid-century, (ii) rcp 4.5 end-century, (iii) rcp 8.5 mid-century, and (iv) rcp 8.5 end-century	72

Fig. 4-32 Change in water yield across the Olifants River Basin from base to (i) rcp 4.5 mid-century, (ii) rcp 4.5 end-century, (iii) rcp 8.5 mid-century, and (iv) rcp 8.5 end-century
..... 73

LIST OF TABLES

Table 3-1: Soil classification used in Olifants watershed modelling	26
Table 3-2: Landuse Classification adopted in Olifants watershed modelling.....	27
Table 3-3: List of major dams inside the Olifants River basin	35
Table 3-4: List of CORDEX climate model ensembles used in this study	40
Table 4-1: Sensitivity ranking of model parameters considered in the sensitivity analysis	46
Table 4-2: Range of calibrated parameters and final fitted values used in the modelling	47
Table 4-3: Performance statistics for calibration and validation at monthly time step....	50
Table 4-4: Percent change in the seasonal and annual mean precipitation in mid and end century periods for rcp 4.5 and 8.5, from the base period in the Olifants River basin	55
Table 4-5: Changes in maximum temperature during future period when compared to those of base period in °C	59
Table 4-6: Change in minimum temperature during future period when compared to those of base period in °C	59
Table 4-7: Statistics of Mann-Kendall analysis (τ and P) and Sen's slope (β_1) of daily minimum temperature at annual time step during the future periods for the rcp 4.5 scenario	63
Table 4-8: Statistics of Mann-Kendall analysis (τ and P) and Sen's slope (β_1) of daily maximum temperature at annual time step during the future periods for the rcp 4.5 scenario	63
Table 4-9: Statistics of Mann-Kendall analysis (τ and P) and Sen's slope (β_1) of daily minimum temperature at annual time step during the future periods for the rcp 8.5 scenario	64
Table 4-10: Statistics of Mann-Kendall analysis (τ and P) and Sen's slope (β_1) of daily maximum temperature at annual time step during the future periods for the rcp 8.5 scenario	64
Table 4-11: Flow exceedance for minimum flow ($0.5 \text{ m}^3/\text{s}$) at Mamba	70

LIST OF ABBREVIATIONS

AR5	Fifth Assessment Report
CHIRPS	Climate Hazards Group InfraRed Precipitation with Station data
CN	Curve Number
CORDEX	Coordinated Regional Climate Downscaling Experiment
DEM	Digital Elevation Model
FAO	Food and Agriculture Organization
GCM	General Circulation Model
GDP	Gross Domestic Product
GHG	Greenhouse Gases
GIS	Geographic Information System
HRU	Hydrologic Response Unit
IPCC	Intergovernmental Panel on Climate Change
KNP	Kruger National Park
MAP	Mean Annual Precipitation
MODIS	Moderate Resolution Imaging Spectroradiometer
NOAA	National Oceanic and Atmospheric Administration
NSE	Nash Sutcliffe Efficiency
PBIAS	Percent Bias
PDM	Probability Distribution Model
PET	Potential Evapotranspiration
RCM	Regional Climate Model
SA	Sensitivity Analysis
SWAT	Soil and Water Assessment Tool
t_{\max}	Daily Maximum Temperature
t_{\min}	Daily Minimum Temperature
USDA	United States Department of Agriculture
UTM	Universal Transverse Mercator
WHAT	Web-based Hydrograph Analysis Tool
WMO	World Meteorological Organization

CHAPTER I

INTRODUCTION

1.1 Background

Climate is typically defined as the average weather over a long period, generally 30 years according to the World Meteorological Organization (WMO). The climate of a region is generated by a complex and interactive atmospheric system by involving large number of physical, chemical and biological processes among the atmosphere, the hydrosphere, the cryosphere, the land surface and the biosphere (IPCC, 2007). The climate is dynamic, and it varies both temporally and spatially (Kwon et al., 2008). Over the last 4.5 billion years, the earth's climate gradually changed with the evolution of the earth (Kasting et al., 1988; Kasting, 1993). However, the earth's climate is changing rapidly since the 19th century, which is apparent from the analysis of the observations of various parameters such as the global mean temperature rise, the global mean sea level rise, the increase in frequency of extreme weather events, declining of snow and ice cover, etc. (Levitus et al., 2012; Immerzeel et al., 2010; Barnett et al., 2005). The causes of this climate change are attributed to both natural and anthropogenic factors, but human induced perturbation of atmospheric composition is mainly responsible for the recent global warming (Crutzen, 2006; Lott et al., 2013; Stott et al., 2004; Tett et al., 1999).

Some of the gases in the atmosphere provide a radiation blanket to keep the earth's surface warm, the phenomenon is commonly known as the greenhouse effect, and these gases are known as the greenhouse gases (GHGs) (Meinshausen et al., 2009; Satterthwaite, 2008; Lashof and Ahuja, 1990). GHGs occupy a small portion of the atmosphere but have profound effects on climate. The primary GHGs gases include water vapor, carbon dioxide (CO₂), nitrous oxide (N₂O), methane (CH₄), chlorofluorocarbons (CFCs) and ozone (O₃). All of them are strongly associated with anthropogenic activities except the water vapour. However, CO₂ is at the center of interest because of its abundance and longevity (Rodhe, 1990). The atmospheric concentration of CO₂ has been increasing at an alarming rate since the beginning of the industrialization epoch primarily due to burning of fossil fuel and deforestation (Canadell et al., 2007). CO₂ is a heat trapping gas and has a strong correlation with temperature. Present concentration of CO₂ is 411 ppm which is unprecedented over the last 420,000 years (NOAA,

2019). The continuous emission of greenhouse gas is the root cause of increasing temperature which is one of the dominant driving forces behind excessive snow melting and precipitation, extreme flooding, droughts, etc. (IPCC, 2007).

The Intergovernmental Panel on Climate Change (IPCC) is a United Nations (UN) body that was established in 1988 to assess the climate change and its impact on human and nature. In its Fifth Assessment Report (AR5), IPCC predicts that the average global temperature could rise in between 1.1°C to 6.4°C by the end of the 21st century. In addition to temperature rise, the enhanced GHGs will also stimulate the interactive and complex climate system. For instance, the precipitation is directly influenced by warming, as heating increases the evapotranspiration, causing frequent and intense droughts (Dai, 2013). On the other hand, atmospheric water holding capacity increases 7% with 1°C increase of temperature which will cause heavy downpour events like storms and flooding (Trenberth, 2011). In addition to the water quantity, the quality will also be hampered by the changes in the mobility, dilution and chemical reaction kinetics of contaminants (Whitehead et al., 2009). The climate change has the potential to exacerbate the already stressed water resources and jeopardize the water resources planning and management strategies developed based on the historical hydrologic data as assumption of stationarity is obsolete under climate change scenario. Therefore, analysis of hydrologic regime under different climate change scenarios is imperative to develop long term water resources management strategies.

1.2 Problem Definition

Olifants River basin is one of the primary drainage regions of South Africa. Significant mining, agricultural, industrial activities and intensive irrigation schemes are concentrated in this watershed. The activities within the catchment produces six percent of the GDP of South Africa. Moreover, it is one of the major rivers flowing through Kruger National Park (KNP) which is one of the largest conservation areas in South Africa (Van et al., 2008). KNP attracts more than one million tourists per year and it's also an attractive destination for the international tourists (Mathivha, et al., 2017). The present water resources of Olifants watershed are highly stressed, and the demands are increasing rapidly (Arranz, et al., 2007). The estimated shortfall is 243 Mm³ by 2025 according to Department of Water

Affairs and Forestry (DWAF) (McCartney, 2004). Droughts have been reported in every decade which impact the activities of the KNP at great extent. KNP requires certain amount of minimum water termed as ecological reserve to maintain the activities which largely depend on the water availability in the Olifants river (Pringle, 2001). However, the availability of this minimum water under changing climate is unclear and the investigation become more complex due to the highly temporal and spatial variability of rainfall in the Olifants River basin. This rainfall variability affects almost every aspect of human life ranging from flood control, water supply, agricultural productivity and to wildlife. Moreover, all these aspects are also likely to be affected by climate change (Gallego et al., 2011). The projections indicate that climate change could result in loss of 66% animal species in the KNP (Fischlin et al., 2007). Furthermore, South African region is one of the most vulnerable regions in Africa due to low adaptive capacity and widespread poverty (Callaway, 2004). Because of the high spatial and temporal variability of rainfall in South Africa, water resources are at the epicenter of projected climate change matrix. However, to date there are only few studies that assessed the hydrological responses of climate change for South African and Olifants region. These studies are necessary for developing future water resources planning and management strategies (Nkhonjera, 2017). Most of the studies have been carried out at regional and country level scale using General Circulation Model (GCM). These coarse scale studies have drawbacks in terms of concealing the complex hydrological interaction at the local watershed scale (Schulze, 2000; Kusangaya et al., 2014). Studies also reveal that the impacts of climate change vary over different places, depending on the geographic location and weather of that region (Zhang et al., 2007). As a result, hydrological modelling based study at the watershed scale using Regional Climate Model (RCM) would be very helpful in assessing the climate change impacts and developing adaptation measures.

1.3 Objectives

The overall objective of this study is to assess the impact of climate change for the Olifants River basin and investigate the availability of ecological flow for KNP. The specific objectives are to:

- 1) Develop hydrological simulation model for the Olifants River watershed and perform the water budget analysis.
- 2) Analyse parameter sensitivity of the model.
- 3) Assess the climate change impacts on the hydrological regime with emphasis on streamflows and analyse the minimum water availability to maintain ecological flow for KNP.

1.4 Structure of the Thesis

The thesis is divided into five chapters. This introductory chapter provides background information on the climate change and the Olifants River basin. The next chapter presents literature review on watershed hydrology, hydrologic modelling, climate models and bias correction. Chapter 3 renders the description of Olifants River basin. It further provides the detailed methodology adopted for hydrological modelling using Soil and Water Assessment Tool (SWAT). Chapter 4 presents the results and discussion on sensitivity analysis, calibration and validation of the model and climate change impact assessment. Chapter 5 concludes the thesis including summary of the results.

CHAPTER II LITERATURE REVIEW

2.1 Overview

This chapter presents a review of the literature on watershed hydrology, hydrologic models and climate models. It also includes the review of studies on the climate change impacts on water resources within the South Africa focusing the Olifants River basin to comprehend the present state of the knowledge.

2.2 Hydrologic Cycle

The hydrologic cycle describes the movement and interaction of water through its all phases i.e. atmosphere, land surface, open water, subsurface, etc. (Bedient et al., 2008). This cycle is continuous, has no beginning or ending. Precipitation, evapotranspiration, infiltration, overland flow and baseflow are the primary components of the hydrologic cycle. Understanding of the hydrologic cycle is essential to assess the changes in various hydrological processes under climate change conditions (Donnelly et al., 2017).

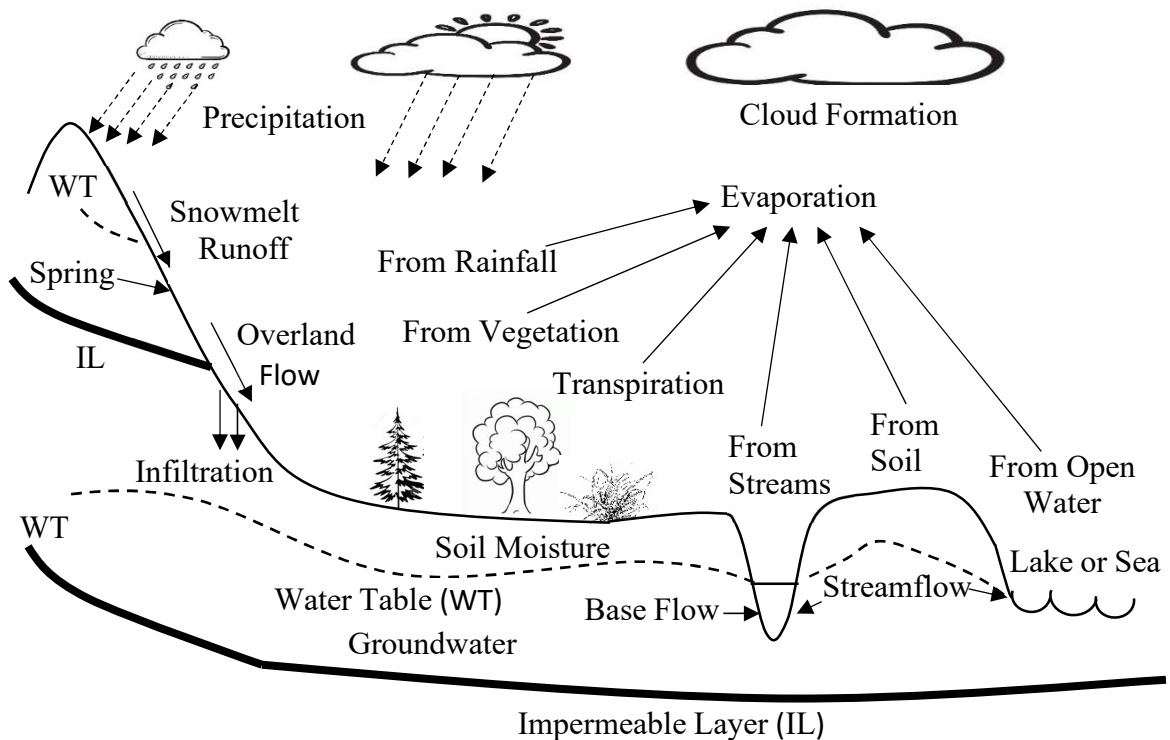


Fig. 2-1 Hydrologic Cycle (Adapted after Brutsaert, 2005)

2.3 Water Budget

Water budget quantifies various components of hydrologic cycle within a control volume per unit time based on the conservation of mass (Healy et al., 2007). It also states that the difference between water flowing into and out of a given area is balanced by a change in water storage (Sahoo et al., 2011). Water budget, in general, for an area can be written as:

$$\text{Water inputs} - \text{Water outputs} = \text{Change in storage} \quad \text{Eq. 2-1}$$

The water inputs include precipitation, surface and ground water inflow, anthropogenic inputs like wastewater or artificial recharge. Whereas the water outputs are evapotranspiration, surface and ground water outflow and water abstractions (Owen, 1995).

Simple yet universal water budget equation is applicable for all space and time scales, ranging from studies of rapid sand infiltration in a soil column to analysis of continental scale floods over periods of decades or millennia (Healy et al., 2007). However, the processes involved in the water budgets are difficult to quantify because of their complex natural and anthropogenic interactions. Water budget analysis is the prerequisite to model continuous streamflow data. Moreover, water budget also helps to gain insights into the surface and ground water interactions (Liang, 2003). Water budget analysis is the most useful tool to identify the changes as it can quantify the water availability under changing scenarios. Water budget analysis can be used for protecting sources of drinking water, residential and industrial developments, municipal water supplies, dam construction, irrigation, stormwater management and water conservation. (Conservation Ontario, 2001). In general, water budget is a valuable tool for developing long term planning of water supply, conserving water quality and quantity and protecting the environment.

2.4 Hydrologic Models

The term “model” illustrates the set of equations or algorithms that are used to simulate the characteristics of a physical system and refers to the available software tools that automate the solution of the equations representing the system (Shoemaker et al., 2005). Hydrologic models are the simplification of the real world system yet useful tool for the researchers and the decision makers to examine and predict the effect of watershed processes and

management practices on soil and water resources (Whipple, 1996; Moriasi et al., 2007; Sorooshian, 2008). Though, initially hydrologic modelling was developed to solve simple engineering problems like flood estimation or design of stormwater system, reservoir spillway, now with the advancement of computational resources it can be used to analyse much more complex phenomena like large scale flooding, effects of changes in landuse or climate (Arnold et al., 1998a). Moreover, much more knowledge can be gained about the watershed during data collection, model parameterization. In addition, output can be analyzed spatially and temporally at different scales. In a nutshell, the ability to quantify the impacts of watershed management strategies have made the hydrologic models a useful tool for water resources planning, development and management (Singh et al., 2002).

2.5 Model Classification

Hydrologic model can be classified in many ways depending on the characteristics, such as time step, spatial scale, events and processes to be modelled (Merritt et al., 2003). In general, depending on the physical processes the watershed model can be categorized in two different ways: empirical (black box) or physically based (mechanistic) (Al-Amin et al., 2013). Empirical models (black box) are developed from the input-output relationship or experiment without describing the features and physical processes of the hydrological system (Devia et al., 2015). They are generally the simplest model and have the least time and cost involvement. These models assume stationarity and valid only within the boundaries which restricts the model capability to simulate changing scenarios (Shoemaker et al., 2005; Devia et al., 2015).

Physically based models constitute with the important governing laws associated with the hydrologic cycle and have a logical structure similar to the real world system being modelled (Rahman, 2008). They integrate various processes, inputs and generate outputs based on the laws of physics and chemistry (Al-Amin et al., 2013). Physically based models are more complex and accurate compared to empirical model as they produce quantitative outputs based on the understanding of the underlying functional mechanism of the processes. These models range from simple conceptual model to fully distributed physically based models. The former one depicts only major hydrological processes whereas the latter one models individual hydrological, biological, geological and chemical

process using well established theoretical equations. However, the lack of comprehensive input data or holistic information about the system preclude the feasibility of having a truly fully distributed physically based model. The mechanistic models can be bifurcated into lump and distributed models depending on the spatial distribution of the watershed process and parameters (Merritt et al., 2003). Lumped models disregard the spatial heterogeneity and consider the whole watershed as a single unit (Sorooshian, 2008). They use average values to represent various processes over the whole watershed to generate output at the outlet. Such models assume uniform conditions throughout the system and do not consider spatial distribution of the following: 1) the input variables, such as rainfall and temperature 2) the parameter characterizing physical processes such as topography, and 3) the output processes such as streamflow (Mekonnen, 2016).

In contrast, distributed models account the spatial variability of the processes and outputs in the watershed analysis (Merritt et al., 2003). Distributed models can be further divided into semi distributed or fully distributed based on the methodology of incorporating the spatial heterogeneity. Semi distributed hydrological models divide the watershed into sub-watershed then perform lumped calculation at the sub-watershed level. Example of semi distributed models include TOPMODELS (Beven et al., 1979), Soil and Water Assessment Tool (SWAT)(Arnold et al., 1998b) and WATFLOOD (Kouwen, 1988). Conceptual definition of topographic units, identification of similar hydrological response unit (HRU) and grouping of similar HRUs calling Group Response Unit (GRU) are the basis of TOPMODELS, SWAT and WATFLOOD model, respectively. On the other hand, fully distributed models discretized the study area into grids or finite elements to depict spatial heterogeneity where governing equations are solved numerically. The SHE (Abbott et al., 1986) is a fully distributed model where parameterization in the horizontal and vertical direction are achieved by orthogonal grid network and horizontal column square box at each grid cell accordingly. It uses 1-D model for river flow, 2-D model for overland flow and 3-D model for groundwater flow. Fully distributed models generally require more information and parametrization compared to lumped model, which incur concomitant increase of expense and effort, that often limit the realization of these models for large basin. However, semi-distributed models are capable of providing useful results

economically and efficiently for water management problems (Arnold et al., 1998b; Pomeroy et al., 2007).

2.6 Model Selection

Nowadays the growing number of available models are making the selection process harder than ever before. Every model has its own advantages and disadvantages. However, the following factors should be considered for selecting a model : a) goals, objectives or hypothesis of the project, b) potential use of the model results, c) characteristics of the watershed, d) other factors which include temporal and spatial scale, data requirements, calibration requirements, acceptance and uses of the model within different communities, ease of use, modeller expertise, available support and time (Engel et al., 2007). For the present study, the following factors are considered to select the model; the model should be:

- able to assess the climate change impact and simulate watershed
- able to incorporate water management operation as the study area is highly regulated
- able to perform the continuous simulation
- based on readily available data considering data scarcity of the region
- able to accept elevation changes
- computationally efficient for large area and long duration
- freely available along with source code, well documented and user friendly

Shoemaker et al. (2005) reviewed sixty five hydrological models which were used as the starting point for the model selection. Based on the anticipated modelling results, SWAT model is selected in the present research for modelling of Olifants River basin as it's a user-friendly software with an outstanding graphical user interface for pre and post processing. Moreover, it is capable to include reservoir and agricultural management practices like irrigation. In addition, SWAT is one of the most widely used hydrological software in the world because of its numerous advantages that include computational efficiency, modularity, ability to predict long term impact, multiple geographic information system (GIS) interface, ability to use readily available global dataset, online resources of supporting document, availability of reliable user and developer support, other supporting

software, inclusion of several processes like sediment, nutrient, pesticide and bacteria, open access of source code (Gassman et al., 2010).

2.7 SWAT Application

Numerous studies have been carried out using SWAT since its creation and it has emerged as one of the most widely used watershed simulation models to solve a wide range of problems. SWAT has gained international acceptance and globally over 600 peer-reviewed journal paper related to SWAT model evidence the fact (Gassman et al., 2010). The model has been used in many government projects across the United States (U.S.) and Europe to study direct assessment of climate change and anthropogenic influences on water resources. In U.S., SWAT is used for the Hydrologic Unit Model of the U.S. (HUMUS) with the goal to simulate hydrologic and pollutant loss impact of agricultural and municipal water use to buttress U.S. Department of Agriculture (USDA) in the analysis of U.S. Resources Conservation Act Assessment of 1997. The model also being used to support myriad of projects in U.S., couple of them are worth mentioning which include assessment and evaluation of watershed conservation practices under USDA Conservation Effects Assessment Project (Mausbach et al., 2004), Total Maximum Daily Load (TMDL) analysis for impaired water to determine pollutant source and potential solution under 1972 U.S. Clean Water Act. In Europe, use of SWAT model has been reported in many projects which include quantify the impact of climate change on five different watersheds under Climate Hydrochemistry and Economics of Surface-water System (CHESS) funded by European Commission Environment and Climate Research Programme (Arnold et al., 2005), assess the ability of SWAT to estimate non-point source pollution sponsored by European Commission Energy, Environment and Sustainable Development. In South Africa, only a limited number of studies has been conducted using SWAT model primarily due to lack of data. Govender (2005) studied the applicability of SWAT model in South Africa found strong simulation result for a small (0.68 km²) watershed.

2.8 SWAT Applications in Climate Change Impact Studies

SWAT model has been successfully applied by various researchers in assessing the climate impacts on hydrologic regime. Muttiah and Wurbs (2002) studied the impact of climate change in the 73,000 km² San Jacinto River Basin of Texas using SWAT model. They

compared the historical streamflow with the future (2040 -2059) streamflow, generated by SWAT model based on the extracted GCM climatic data. They found higher mean flow in the future due to significant increases in the floods and high flows, but reduction in the normal and low flows.

Gosain et al. (2006) simulated the impact of climate change on the streamflow for 2041-2060 period in 12 major river basins in India ranging in size from 16,680 km² to 871,800 km². Overall decrease in surface runoff but more frequent flood and drought is predicted under the climate change scenario compared to control period of 1981-2000.

Rosenberg et al. (2003) simulated the effect of downscaled Hadley Centre General Circulation Model (HadCM2 GCM) climate projections on water yield in the 18 major water resources regions of U.S. for the period 2035 to 2095. The results indicate significant change in the water yield and a shift in the seasonality i.e. early snowmelt in the western basin. The study also provided insights into future water management as the extreme precipitation event and water yield are projected to increase in most of the region. However, Water yield is projected to decrease in the western Great Plains of Kansas, Colorado and Nebraska which could severely affect the agriculture and nearby population. Stone et al. (2001) also found significant seasonal change in water yield in Missouri river basin by inputting downscaled climate projections into SWAT which were generated by nesting Regional Climate Model (RCM) into GCM. These studies depicted that SWAT can be used to project the impact of climate change on hydrological regime and evaluation watershed management decisions in a river basin (Rahman et al., 2012).

2.9 General Circulation Model (GCM)

General Circulation Models (GCMs) are climate models that numerically solve multiple governing equations related to atmospheric processes and generate climatic parameters under different greenhouse gas emission scenarios. GCMs are the major source of information about the future climate. GCMs started developing since 1960, however, most models were not able to incorporate the major components, such as atmosphere, land surface, ocean, biosphere, etc., until 1990 due to lack of advance computer technology (IPCC, 2001). These models solve the fundamental conservation laws of mass, momentum and energy which are discretized by finite element or finite difference method. Climate

models require equation of state and moisture for atmosphere and ocean. The state equation for the atmosphere relates pressure, density, temperature while for the ocean it relates pressure, temperature, density and salinity (Warren et al., 2005). Over the past few decades climate models adequately reproduced the observed features of recent climate and emerged as a promising tool for estimating future climate change (IPCC, 2007). Despite growing confidence in climate models, uncertainties and coarse resolution (approximately 200 km X 200 km grid) restrict the direct use of GCMs output for local application (Grotch and MacCracken, 1991). Therefore, GCM outputs need to be downscaled for climate change impact assessment at watershed scale.

2.10 Downscaling of GCM

Downscaling can be defined as a technique to improve the GCMs resolution to generate local scale weather. There are two fundamental methods of downscaling a) statistical downscaling, and b) dynamic downscaling (Fowler et al., 2007). Statistical downscaling is based on the relation between local meteorological variable and climate variables generated by the GCM. It depends on the long term weather record rather than the physical features of a region such as topography (Wilby et al., 1997). On the other hand in dynamic downscaling Limited Area Model or Regional Climate Model (RCM) is used to extract local-scale weather data from large-scale GCM data by setting coarse scale GCM data as the boundary conditions (Wilby et al., 1997). This process improves parameterization of physical processes and increase the temporal and spatial resolution. Moreover, regional characteristics like extreme events, orographic precipitation, etc., can be adequately simulated by this technique (Fowler et al., 2007). However, the studies found that bias correction of the RCM downscaled data are required before using it as an input for hydrological and climate change impact study (Wood et al., 2004).

2.11 Bias Correction

Bias is the systematic errors which can be defined as the differences between the observed and simulated weather variables from the climate models (GCMs/RCMs). Coarse spatial resolution, simplified physics and thermodynamic processes, lack of comprehensive knowledge of climate system processes are the driving factors behind bias (Navarro-Racines et al., 2015). Bias correction is very important before using climate model data to

generate realistic results (Piani et al., 2010). A transfer function is applied to perform the bias correction of the climate model data and generally assumption of the stationarity is the basis of bias correction which means that whatever is the bias in the past will remain in the future (Teutschbein et al., 2012). There are different methods for bias correction which ranges from simple method such as linear scaling to complex method like quantile mapping.

2.11.1 Linear Scaling

Linear scaling method applies the correction based on the mean values and matches mean of the corrected value with that of the observed value and retains the variations pattern (Fang et al., 2015). For precipitation the bias is calculated by the ratio of the average monthly observed over average monthly simulated historical data. However, in case of the temperature bias is calculated by deduction of average monthly simulated historical data from average monthly observed data. Finally, the monthly bias is applied to the future data. In case of precipitation the future data is multiplied with the bias whereas for temperature the bias is added to the future data to get bias corrected data (Lenderink et al., 2007). The linear scaling can be formulated as:

$$P_{bias} = \frac{P_{(avg)obs}}{P_{(avg)hi}} \quad \text{Eq. 2-2}$$

$$P_{bias(corrected)} = P_{bias} * P_{mod} \quad \text{Eq. 2-3}$$

Where P_{bias} is the precipitation bias for a month, $P_{(avg)obs}$ is the monthly average value of the month in consideration of the observed data period, $P_{(avg)his}$ is the monthly average value of the month in consideration of the historical data period, $P_{bias(corrected)}$ is the precipitation bias and P_{mod} is the future precipitation data from climate model.

$$T_{bias} = T_{(avg)obs} - T_{(avg)his} \quad \text{Eq. 2-4}$$

$$T_{bias(corrected)} = T_{bias} + T_{mod} \quad \text{Eq. 2-5}$$

Where T_{bias} is the temperature bias for a month, $T_{(avg)obs}$ is the monthly average value of temperature of the month in consideration of the observed data period, $T_{(avg)his}$ is the monthly average value of temperature of the month in consideration of the historical data

period, $T_{bias(corrected)}$ is the temperature bias and T_{mod} is the future temperature data from climate model.

2.11.2 Quantile Mapping

The quantile mapping corrects mean, quantiles, standard deviation as well as wet day frequency. This method is applicable for all potential distribution of precipitation and widely used for the correction of RCMs precipitation data (Wilcke et al., 2013). The adjustment for precipitation using quantile mapping can be formulated using empirical Cumulative Distribution Function (eCDF) (Fang et al., 2015).

$$P_{bias(corrected),m,d}^i = eCDF_{obs,m}^{-1}(eCDF_{raw,m}^i(P_{raw,m,d}^i)) \quad \text{Eq. 2-6}$$

Where $P_{bias(corrected),m,d}^i$ is the bias corrected precipitation on d^{th} day of i^{th} month, $P_{raw,m,d}^i$ is raw climate model precipitation on d^{th} day of i^{th} month and $eCDF_{obs,m}^{-1}$, $eCDF_{raw,m}^i$ are computed from respective data for the observation (obs) and raw model (raw) periods.

2.12 Climate change impact on water resources in South Africa and the Olifants basin

Climate change is a major challenge in South Africa and the concern is growing as the temperature is rising at a higher rate than the global average for the last five decades along with the increased frequent extreme rainfall events (Ziervogel et al., 2014). Fifth Assessment Report (AR5) of IPCC buttress the apprehension by projecting 3-6 °C temperature increase in South Africa for rcp 8.5 by the 2081-2100 period from 1986-2005 period. Overall, South Africa has unreliable episodic rainfalls which result in frequent extreme events like droughts and floods (Singh et al., 2014). Climate change has the potential to further exacerbate the problems by changing the water balance i.e. reduction of water availability and increased number of extreme events (Schulze et al., 2001). Moreover, agriculture, biodiversity, hydropower supply and water borne diseases are intrinsically related to the hydrology (Bates et al., 2008). The impacts of climate change could be devastating because of the low adaptive capacity of this region (Callaway, 2004; Kusangaya et al., 2014). Given the circumstances, climate change poses significant threat to the water resources and necessitates further investigation of the hydrologic cycle and hydrological regime (Ziervogel et al., 2014).

Temperature has profound effect on the hydrologic cycle. An increase in temperature can increase evaporation and change the precipitation pattern which leads to overall intensification of the process. Kusangaya et al. (2014) found a warming trend of temperature in both observed and remote sensing derived record in South Africa which concurred with other studies (Hughes et al., 1996; Kruger et al., 2004). According to Dennis et al. (2012) who predicted that the climatic changes in South African temperature include a general warming throughout the country. In the Olifants River basin, Singh et al., (2014) found an increasing and coherent pattern in temperature. In this study, the mean annual temperature increase was found 2.4°C and 4.6 °C, respectively for the 2046-2065 and 2081-2100 period for the high emission scenario (A2 scenario) and for the moderate emission scenario (B1 scenario) the respective increases were 1.9 °C and 2.5 °C from the 1961-2005 period. The temperature increase projected by Singh et al., (2014) agrees with the trend reported in the Fourth Assessment Report (AR4) of IPCC (IPCC, 2007). Cullis et al. (2011) used synthetically generated climate data in this basin and predicted an increase in temperature of around 1.0°C and 2.2 °C by 2025 and 2050. In summary, all the studies concur that the temperature has increased and will keep increasing in the future (Nkhonjera, 2017).

Precipitation is the key driver of the hydrological cycle and any change in the intensity, duration and frequency will impact the water resources directly (Yilmaz et al., 2011). Paucity and discrepancy in the observational data preclude the determination of the annual precipitation trend in many parts of the African continent (Nikulin et al., 2012; Niang et al., 2014). Precipitation projection possesses higher uncertainty, spatial and seasonal dependency than the temperature projection (Orlowsky et al., 2012; Rowell, 2012). The limited number of studies done on the impacts of climate change on water resources in South Africa did not concur on the precipitation trend and magnitude (Nkhonjera, 2017). For instance, IPCC (2007) predicted precipitation decrease in the South African region while Tadross et al. (2011) projected an increase. In the Olifants River basin, Singh et al., (2014) found significant uncertainties in the projected precipitation as the GCM models project both increase and decrease in the future precipitation. Cullis et al. (2011) predict a progressive increase in the precipitation of around 5% and 10% by 2025 and 2050 respectively for the Olifants basin.

Runoff is the portion of precipitation that flows over the land (Nkhonjera, 2017). The climate change impact on runoff in a catchment depends on the sensitivity of the catchment to the climatic variables like precipitation, temperature, evaporation, etc. (IPCC, 2014). Catchment sensitivity is mainly a function of the runoff coefficient. In general, runoff holds an intrinsic relation with precipitation and climate change would equally affect the runoff just like the precipitation. IPCC (2007) projected 10-30% reduction of river runoff and water availability in the tropical Africa because of climate change. Limpopo basin is an expansion of Olifants catchment where 35-45% runoff decrease is projected in the future due to climate change (Arnell, 1999; Zhu et al., 2010).

A climate change study in the Olifants river basin has been carried out by Cullis et al. (2011) using synthetically generated climate data. Due to the high variability of the downscaled rainfall projections, Cullis et al. (2011) created synthetic time series of temperature and precipitation for dry, intermediate and wet condition for future period using historical climatic data. The synthetic data then forced with the Pitman rainfall-runoff model to determine the surface runoff impact. The results indicate high sensitivity of surface runoff with the potential climate change with wetter winter and drier summer.

Another, climate change study in the Olifants river basin has been carried out by Singh et al. (2014) using statistically downscaled climate data from GCM. The future runoff was computed by driving the downscaled GCM data into the lumped Probability Distribution Model (PDM) developed by Moore (2007). Overall decrease in the Mean Annual Runoff (MAR) is found for both 2046-2065 and 2081-2100 period compared to 1961-2000. Moreover, higher MAR reduction is projected during the 2081-2100 period.

2.13 Research gap and potential: climate change and water resources in Olifants basin

Until now, a limited number of studies on the impacts of climate change on hydrological regime have been carried out in the Olifants river basin. Moreover, these studies used synthetic and statistically downscaled GCM climate data which suffers from stationarity, coarse scale resolution, respectively. In addition, the future climatic data is forced with the empirical/lumped models which have limitation in adopting the physical features. These limitations necessitate further research on the climate change impacts (a) using dynamically downscaled RCM projections; which is better than the synthetic and statistical

downscaling of GCM data as it incorporates the physical attributes at finer scale, (b) forcing the RCM data with physically based semi distributed SWAT model to simulate the runoff.

CHAPTER III

METHODOLOGY

3.1 Overview

The overall methodology broadly falls into data collection, model development and output analysis (Fig. 3-1). Both static and dynamic data are required for this study. The static data include the topographic, landuse and soil whereas the dynamic data include precipitation, temperature and streamflow. The hydrological model SWAT is adopted for this study that requires GIS layers of the static data and numeric values of the dynamic climatic data at daily time step to simulate the streamflow. The simulated streamflow is checked against the observed streamflow to evaluate the model performance. To achieve a satisfactory model performance exhaustive sensitivity analysis, calibration and validation have been carried out in SWAT-CUP. After that, the calibrated model is forced with the dynamically downscaled climatic data to assess the climate change impacts. To this end, the hydrological components i.e. precipitation, temperature, evapotranspiration, flow, etc., are compared between the historical period (1985-2005) and two future time horizons namely mid-century (2041-2070) and end century (2071-2100).

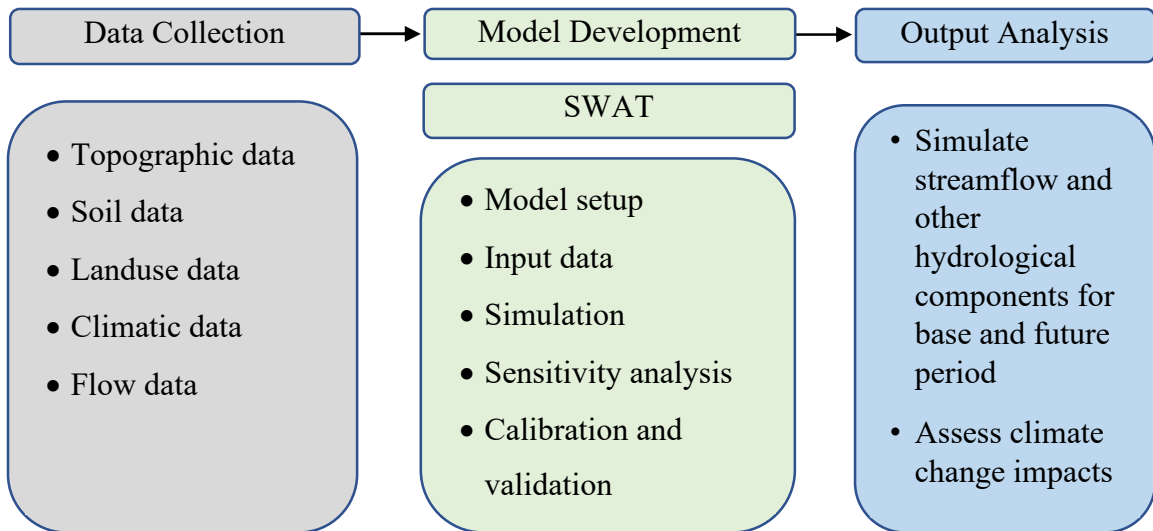


Fig. 3-1 Methodology flowchart

3.2 Watershed Description

The Olifants River basin (Fig.3-2) covers approximately 73,700 km² of northeastern region of the South Africa including portion of the Gauteng, Mpumalanga and Limpopo province. The Olifants River originates from Trichardt city in the province of Gauteng then flows through the province of Mpumalanga and Limpopo and finally flows through the Kruger National Park (KNP) before draining into Indian Ocean. The major tributaries of Olifants River are Klein Olifant, Blyde and Steelpoort rivers on the right bank and Wilge, Elands, Moses and Ga-Selati rivers on the left bank. The basin stretches between latitudes 22.60⁰ S-26.50⁰ S and longitudes 28.30⁰ E-31.90⁰ E and the river reach is 770 km long (McCartney, 2004).

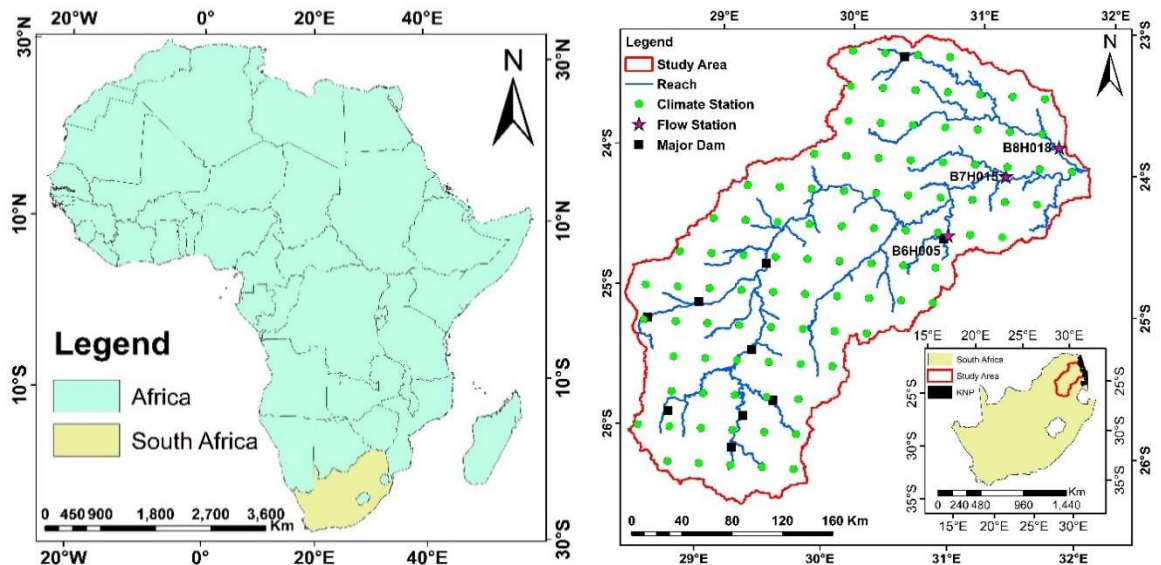


Fig. 3-2 Olifants River watershed location map.

This watershed is the home of 3.2 million people and contributes approximately six percent to the Gross Domestic Product (GDP) and diversified economic activities ranging from mining, which include coal, copper, platinum, iron, industrial and agricultural activities including power plant, intensive irrigation scheme are concentrated here. Besides the river flows through the KNP which attracts more than a million tourists each year. Most of the mining and industrial facilities are located in the upper reaches near the towns of Witbank and Middleburg in Mpumalanga.

The climatic conditions differ significantly within the catchment, primarily driven by the variation of the elevation of the catchment. The area is divided into highveld (upper side on the west) and lowveld (lower side on the east) separated by the escarpment which oriented approximately north- south. The altitude of the highveld ranges from 1,200 m to 2,400 m while that of the lowveld is less than 800 m. The temperature varies between 18⁰-34⁰ C in summer (October to April) and 5⁰-26⁰ C in winter (May to September). Maximum temperatures are experienced in January whereas the minimum occurs in July. The mean annual temperature is 16⁰ C for the whole watershed, however that is 14⁰ C for the highveld and 22⁰ C for the lowveld. The distribution of mean annual temperature and mean annual precipitation (MAP) hold a strong relation with the elevation, with precipitation being higher at higher elevation and temperature decreasing (Schulze et al., 2007).

The movement of air masses within the inter tropical coverage zone (ITCZ) exerts great influence on the climate of the basin. During the summer, high land temperature creates low pressure which brings an inflow of moisture with maritime air masses from the Indian Ocean. In contrast, in the winter, low land temperature produces continental high pressure, which results in regional dry season. As a result, the rainfall is seasonal and largely occurs during the summer period. The mean annual precipitation for the entire catchment is recorded as 630 mm with peak rainfall occurring in January and February (Arranz et al., 2007). However, the rainfall pattern is irregular, the coefficient of variation is greater than 0.25 across most of the catchment (McCartney, 2004). The highest MAP occurs along the escarpment because of the orographic effect, ranges from 800 mm to 1,500 mm. In the highveld area, MAP ranges between 500 mm to 800 mm while in the lowveld it lies between 500 mm to 600 mm. Evaporation varies across the catchment; the highest is reported in the north and west. The mean annual evapotranspiration (MAE) has been reported to lie between 1,450 mm to 1,700 mm for the entire watershed (McCartney, 2004; Lange et al., 2005). Runoff reflects the spatial and temporal distribution of the rainfall. The mean annual runoff is 37.5 mm which is approximately six percent of the mean annual precipitation. The flow has significant inter-annual variation and severe drought observed in most decades (McCartney, 2004).

The catchment geology mainly consists of igneous and metamorphosed rocks. Granite is the most abundant rock though frequent dolomite intrusions in the form of dykes and sills are found. For instance, a large dolomitic intrusion known as the escarpment divides the watershed into highveld and lowveld (Roy, 2005). The watershed is characterized by five major types of soils, i.e. cambic arenosols, chromic luvisols, chromic vertisols, orthic acrisols and rhodic ferralsols (Gyamfi et al., 2016).

The primary landuse practices in the Olifants catchment include grazing, agricultural, mining, industry, forestry, rural and urban settlements. The land in the upper Olifants is highly urbanized whereas the middle and lower parts are relatively undeveloped. The upper Olifants is rich in minerals and extensive mining occurs in this area. The stretches between the upper and middle Olifants are highly fertile which starkly contrasts with the low percentage arable land of South Africa (Annandale et al., 2001). As a result, this transitional area is primarily used for agriculture and extensive irrigation, particularly around the Loskop dam. In contrast, the lower Olifants is typically rural and ecotourism is the main industry.

The grass land and range brush cover two-thirds of the study area. The grass land is found at the higher altitude with the characteristics of high summer rainfall and low temperature. The agricultural area covers approximately 11,000 km² (15%) of the study area which includes commercial and rainfed/subsistence farming. The commercial farming primarily consists of large farm and uses substantial portion of the water through intense irrigation. Commercial forestry occurs in the high rainfall area especially near the escarpment (Arranz et al., 2007).

3.3 Soil and Water Assessment Tool (SWAT)

SWAT is a continuous watershed simulation model which operates at a daily or sub daily time step to simulate the hydrological balance and watershed management practices (Gassman et al., 2007). It is a physically based model developed by Agricultural Research Service (ARS) of United States Department of Agriculture (USDA). The model has undergone continuous improvement and modification since creation. The model is capable of predicting the long term impact of land management practices on water, sediment and agricultural chemical yields with changing soil, land use and management conditions

(Arnold et al., 1998a). SWAT is a computationally efficient model that simulate overland flow, lateral flow, base flow, irrigation, water management practices, climate change and other features (Neitsch et al., 2011).

SWAT models several different physical processes inside the watershed. Instead of dividing the watershed into orthogonal grid, SWAT divides the watershed into sub-basins based on the Digital Elevation Model (DEM) in a fashion that overland flow of all ground area inside a sub-basin contribute to the stream segment located inside the sub-basin. The sub-basins are further divided into Hydrologic Response Unit (HRU) which are unique overlay combinations of similar landuse, soil and slope. After discretization and HRU definition, SWAT simulates the hydrologic cycle into two major phases: a) land phase, and b) water or routing phase. The model performs all the computations at the HRU level then aggregated at the sub-basin and basin outlet. The land phase controls the amount of water, nutrient, pesticide and sediment loadings to the main channel inside a subbasin. The water or routing phase controls the movement of water, nutrients, etc., through the stream network to the outlet. The following water balance equation is applied at the HRU level of the land phase to simulate the flow and water quality variables:

$$SW_t = SW_0 + \sum_{i=1}^n (R_{day} - Q_{surf} - E_a - w_{seep} - Q_{gw}) \quad \text{Eq. 3-1}$$

Where SW_t and SW_0 are the final and initial water content (mm), respectively, R_{day} is amount of precipitation on day i (mm), Q_{surf} is amount of surface runoff on day i (mm), E_a is amount of evapotranspiration on day i (mm), w_{seep} is amount of water entering in the unsaturated zone from soil profile on day i (mm), Q_{gw} is amount of groundwater flow return to the stream (baseflow) on day i (mm). The surface runoff is computed using either the Green Ampt method (Green and Ampt, 1911) or modified curve number (CN) method (USDA Soil Conservation Service, 1972). Potential evapotranspiration is estimated using one of the three methods: a) Penman-Monteith (Penman and Monteith, 1965); b) Priestley-Taylor (Priestley and Taylor, 1972); and c) Hargreaves (Hargreaves et al., 1985). In this study, the surface runoff and potential evapotranspiration is estimated based on modified CN and Penman-Monteith method, respectively. Actual evaporation is calculated using an approach similar to Ritchie (1972). The rate of percolation depends on the hydraulic conductivity and available water holding capacity of soil. The lateral flow in the soil is

governed by the conductivity, slope, soil water content and estimated by a kinematic storage model based on water mass balance and continuity equation developed by Sloan et al. (1983). The shallow aquifer, connected to the stream, is either recharged through percolation or delivered water to the stream as baseflow depending on the storage.

SWAT has the capability to simulate climate change and water management scenarios. The climatic input i.e., precipitation, temperature can be manipulated by changing the adjustment factors to simulate the climate change. However, dynamically downscaled bias corrected climatic data are used in this study for determining the impact of climate change.

3.4 SWAT User Interface

ArcGIS-SWAT is the graphical user interface of SWAT which is developed by integrating ArcView GIS and SWAT with a view to provide a user-friendly modelling environment to facilitate the preprocessing, interfacing and post processing of the SWAT model. The interface helps the user to keep the processes in sequential order, starting from delineation of the streams and ending with analysis or calibration of the model. The ArcGIS-SWAT interface comprises of dynamic and static geodatabase. The dynamic geodatabase contains information related to the study area while the static geodatabase keeps the look up tables and files for default parameter values. The interface is organized into multiple components: 1) delineation of watershed, 2) HRU definition, 3) weather generation, 4) input parameterization and editing, 5) model run, 6) read and map results, and 7) calibration tool (Olivera et al., 2006). ArcSWAT 2016 with guided user interface ArcMap 10.3.1 is used for this study.

3.5 Data Description

SWAT model requires data on various climate parameters, such as daily precipitation and temperature, topographic data like DEM, soil characteristics, landuse and so on for hydrological simulation. The necessary precipitation and temperature data for developing the model are obtained from the Climate Hazards Group InfraRed Precipitation with Station data (CHIRPS) and MODIS (Moderate Resolution Imaging Spectroradiometer). The required geographical information system (GIS) layers like digital elevation map (DEM), land use and soil data are obtained from International Centre for Tropical

Agriculture (CIAT) (<http://srtm.csi.cgiar.org>), Department of Environmental Affairs, South Africa (https://egis.environment.gov.za/data_egis/data_download/current), Food and Agriculture Organization (FAO) (<http://www.fao.org/land-water/land/land-governance/land-resources-planning-toolbox/category/details/en/c/1026564>) respectively. The observed streamflow data for calibration and validation are obtained from Department of Water and Sanitation, South Africa.

3.5.1 Digital Elevation Model (DEM)

Digital Elevation Model (DEM) is the digital representation of land surface elevation with respect to a specific datum which is generally mean sea level. A GIS layer of DEM, an array of square cells associated with elevation value, is used in SWAT to delineate the watershed and stream based on the elevation. For Olifants River watershed modelling, 90 m resolution Shuttle Radar Topography Mission (SRTM) DEM (Fig. 3-3) is obtained from CIAT. The DEM has the projection Cape UTM under zone 34S. It is evident from the DEM that the elevation of the watershed ranges from 0-2400 m and the overall slope of the watershed is towards the northeast direction. In general, the watershed is divided into highveld and lowveld landscapes separated by escarpment, which is apparent in the DEM.

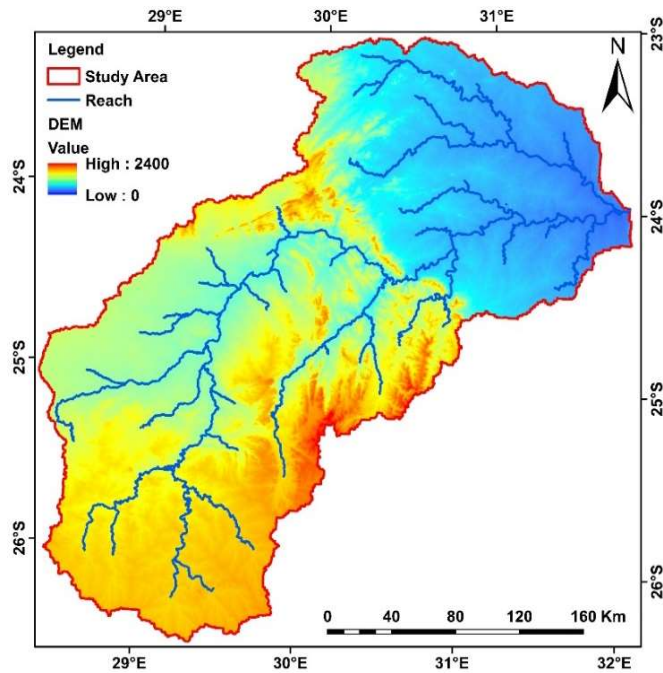


Fig. 3-3 Olifants River basin topography.

3.5.2 Soil Data

Generally, the soils data use by SWAT can be categorized in two groups like physical properties and chemical properties. Physical properties of soil play a vital role in the hydrological process of a watershed as it controls the movement of air and water through the soil profile, whereas, chemical properties describe the nutrients in the soil. The input data for chemical properties of soil is optional while the physical properties are required. The global FAO soil data at 1:5,000,000 scale was adopted for the watershed (<http://www.fao.org/land-water/land/land-governance/land-resources-planning-toolbox/category/details/en/c/1026564/>). The soil map (Fig. 3-4) and classification (Table 3-1) show that the substantial portion of the soil is sandy loam which occupies 64.9% of the area whereas the sandy clay loam and clay occupies 17.2 % and 17.9% of the watershed, respectively. It's apparent from the soil map that the major portion of the lowveld area consists sandy loam, while clay and sandy clay loam covers the major portion in the high veld.

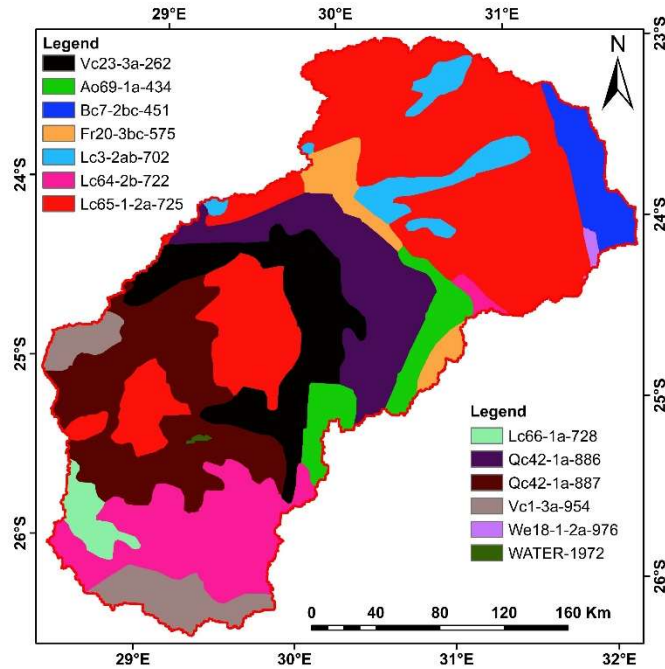


Fig. 3-4 Soil classification within the study area.

Table 3-1: Soil classification used in Olifants watershed modelling

Name	Type	Area(km²)	Percent
Lc65-1-2a-725	Sandy Loam	23697	34.35
Qc42-1a-887	Sandy Loam	9812	14.22
Lc64-2b-722	Sandy Clay Loam	7429	10.77
Vc23-3a-262	Clay	6836	9.91
Qc42-1a-886	Sandy Loam	6524	9.46
Vc1-3a-954	Clay	3405	4.94
Ao69-1a-434	Sandy Loam	2855	4.14
Lc3-2ab-702	Sandy Clay Loam	2653	3.85
Bc7-2bc-451	Sandy Clay Loam	2407	3.49
Fr20-3bc-575	Clay	1965	2.85
Lc66-1a-728	Sandy loam	1184	1.72
We18-1-2a-976	Sandy Loam	164	0.24
WATER-1972	Water	48	0.07

3.5.3 Landuse Data

Landuse plays a vital role in hydrologic modelling as the distribution of water largely depends on it. Moreover, it has an intrinsic relation with the evapotranspiration, infiltration, surface and subsurface flow. The 2013-14 South African national land cover data set derived from the Landsat 8 imagery having 30 m x 30 m resolution was adopted for the simulation. The landuse data was obtained from Department of Water and Sanitation, South Africa (https://egis.environment.gov.za/data_egis/data_download/current). It is apparent from the landuse classification (Fig. 3-5) that the range land and agricultural land are the dominant types of landuse in this study area. The range land and agricultural land cover 72.5 and 15.6 percent of the study area, respectively (Table 3-2). Agricultural activities occupy only 15.6 percent of the total area, however, it consumes substantial amount of water because of the intensive irrigation and commercial farming.

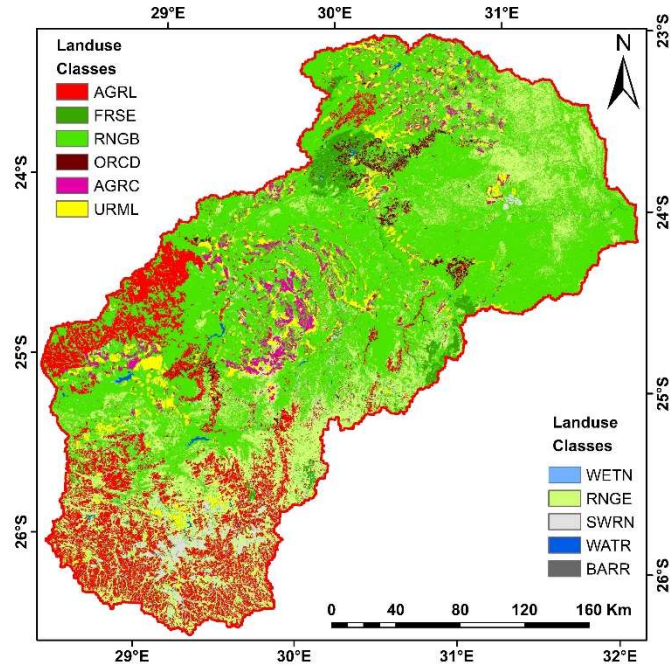


Fig. 3-5 Landuse classes within the study area.

Table 3-2: Landuse Classification adopted in Olifants watershed modelling

Landuse	Code	Area (ha)	Percentage (%)
Range-Brush	RNGB	3502494	50.8
Range-Grasses	RNGE	1498677	21.7
Agricultural Land-Generic	AGRL	863258	12.5
Residential-Med/Low Density	URML	316917	4.6
Agricultural Land-Close-grown	AGRC	211531	3.1
Forest-Evergreen	FRSE	145837	2.1
Southwestern US (Arid) Range	SWRN	130272	1.9
Wetlands-Non-Forested	WETN	88659	1.3
Orchard	ORCD	72720	1.1
Barren	BARR	43405	0.6
Water	WATR	24095	0.4

3.5.4 Climate Data

Climate data like daily precipitation, maximum and minimum temperature, wind speed, relative humidity and solar radiation are required for the simulation. Moreover, the geographical location and elevation of the climate stations are needed. There are only 13 observed precipitation stations [Fig. 3-6 (a)] and only eight stations having observed temperature data [Fig. 3-7 (a)] available within the study area. These limited number of climate stations are not adequate for hydrological modelling for an area of 73,700 km² characterized with high spatial and temporal rainfall and temperature variability. Precipitation is the major driver of the hydrological processes and good quality precipitation data is required for better simulation in SWAT model (Masih et al., 2011).

Satellite based observation of climatic variables, such as precipitation and temperature are available which can be used in conjunction with observed data for hydrological modelling (Hughes, 2006). Data from Climate Hazards Group InfraRed Precipitation with Station data (CHIRPS) has been used in different parts of the world i.e., Asia, Europe, North America, North Africa and the results suggested that it can be used in the Olifants River basin for hydrological modelling (Funk et al., 2015; Tuo et al., 2016; Paredes-Trejo et al., 2017; Caparoci et al., 2018). Moderate Resolution Imaging Spectroradiometer (MODIS) has gridded daily temperature data which has been used in different studies across the world (Vancutsem et al., 2010). MODIS temperature data blended with observed data has been used in this study. Due to the scarcity of observed data, satellite based precipitation and temperature data were obtained from CHIRPS and MODIS for developing the model. To this end, approximately 30 km x 30 km grid is adopted that resulted in 96 climatic stations [Fig. 3-6 (b) and Fig. 3-7 (b)] to extract the precipitation and temperature data at daily time step from the CHIRPS and MODIS, respectively. CHIRPS dataset (ftp://ftp.chg.ucsb.edu/pub/org/chg/products/CHIRPS-2.0/global_daily/netcdf/p05/) hosting the global precipitation has a resolution of 0.05 degree approximately equivalent to 5.5 km x 5.5 km grid whereas the MODIS land surface temperature dataset has a resolution of 1 km (Wan et al., 2015). MODIS dataset has been obtained using the Application for Extracting and Exploring Analysis Ready Samples (appEEARS) program.

For extracting and compiling the daily precipitation data from the CHIRPS global dataset a script was developed in R.

The annual and monthly mean of the satellite precipitation (CHIRPS) are compared with the observed precipitation obtained from Department of Water and Sanitation, South Africa. For this, CHIRPS precipitation is extracted at the same locations of the observed precipitation stations. The annual precipitation comparison is carried out from 1990 to 2017 period and the monthly comparison is performed based on the average of respective monthly data for the same period for all the thirteen observed station. A portion of the annual and monthly comparison is presented in the Fig. 3-8 and Fig 3-9, respectively. The observed and CHIRPS precipitation shows similar distribution pattern at annual and monthly time step but varies in quantity. In general CHIRPS underestimated the precipitation by ten percent in the Olifants River basin compared to the observed.

The similar comparison has been carried out between the satellite temperature (MODIS) and the observed temperature data acquired from South African Weather Service. Both minimum and maximum daily MODIS temperature follows the similar monthly distribution pattern of respective observed with varied quantity (Fig. 3-10 and Fig. 3-11). Moreover, daily maximum temperature exhibits more variation compared to daily minimum temperature. The MODIS temperatures are higher than the observed temperature in most of the cases. On an average the MODIS minimum and maximum daily temperature is respectively, 1.7°C and 4.0°C higher than the observed temperature.

The variation between the observed and MODIS daily minimum temperature is presented at Fig. 3-12 at monthly time step for the period 2001 to 2013. The difference is computed by deducting MODIS temperature from the observed thus the positive value indicates higher observed value and vice versa. In most of the time splits the temperature variation lies between $\pm 2^{\circ}\text{C}$. MODIS underestimated the winter temperature and overestimated the summer temperature at the Hoedspruit and Witbank locations. However, MODIS depicts higher temperature for the Oudestad station and no definite trend for the Lydenburg station.

Based on the comparison, the satellite based precipitation (CHIRPS) and temperature (MODIS) are corrected using linear bias correction method. Due to the unavailability of

wind speed, relative humidity and solar radiation data, they were simulated by the weather generator module in SWAT.

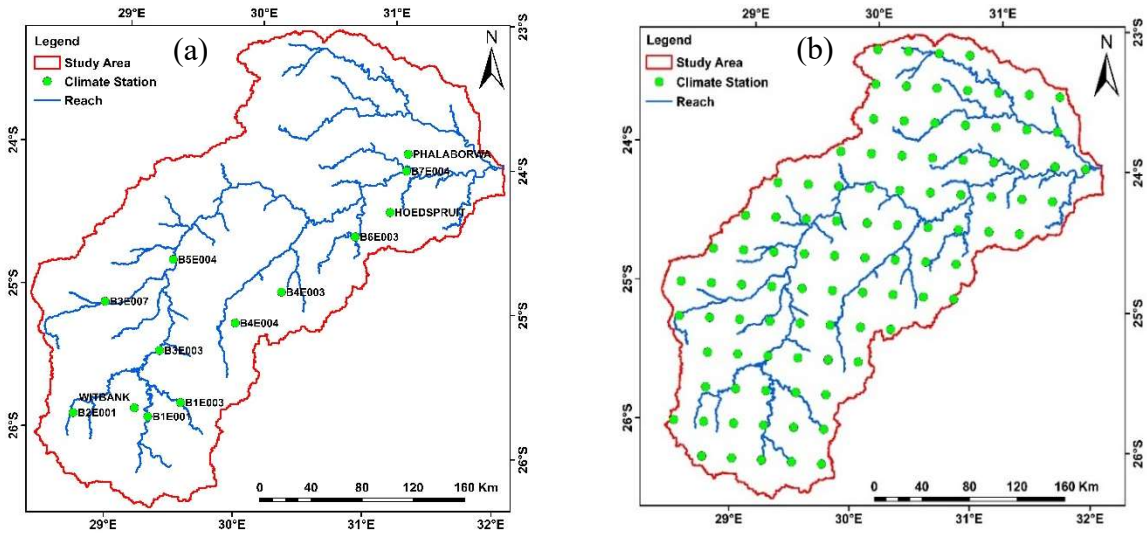


Fig. 3-6 Precipitation stations within the study area (a) observed (b) gridded

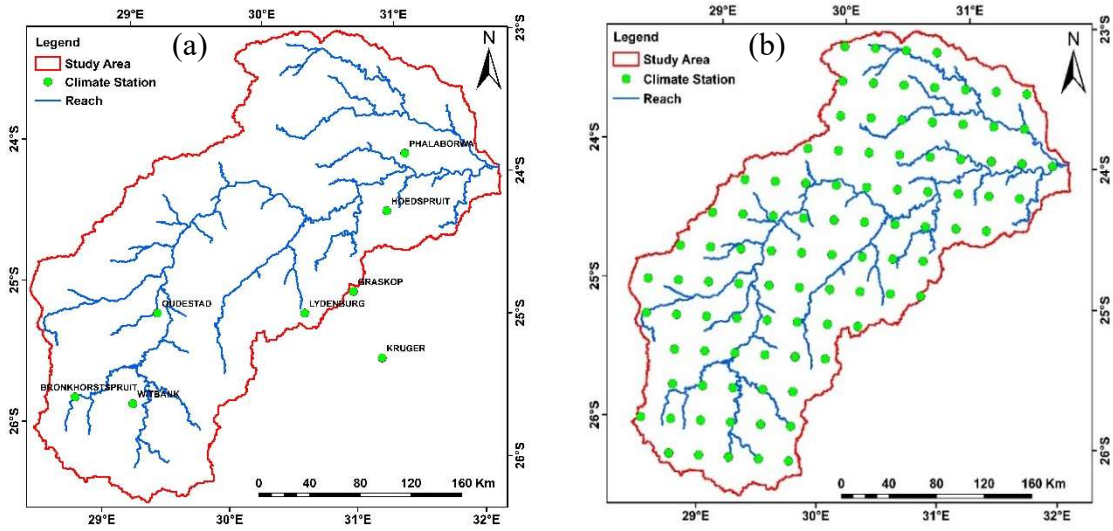


Fig. 3-7 Temperature stations within the study area (a) observed (b) gridded

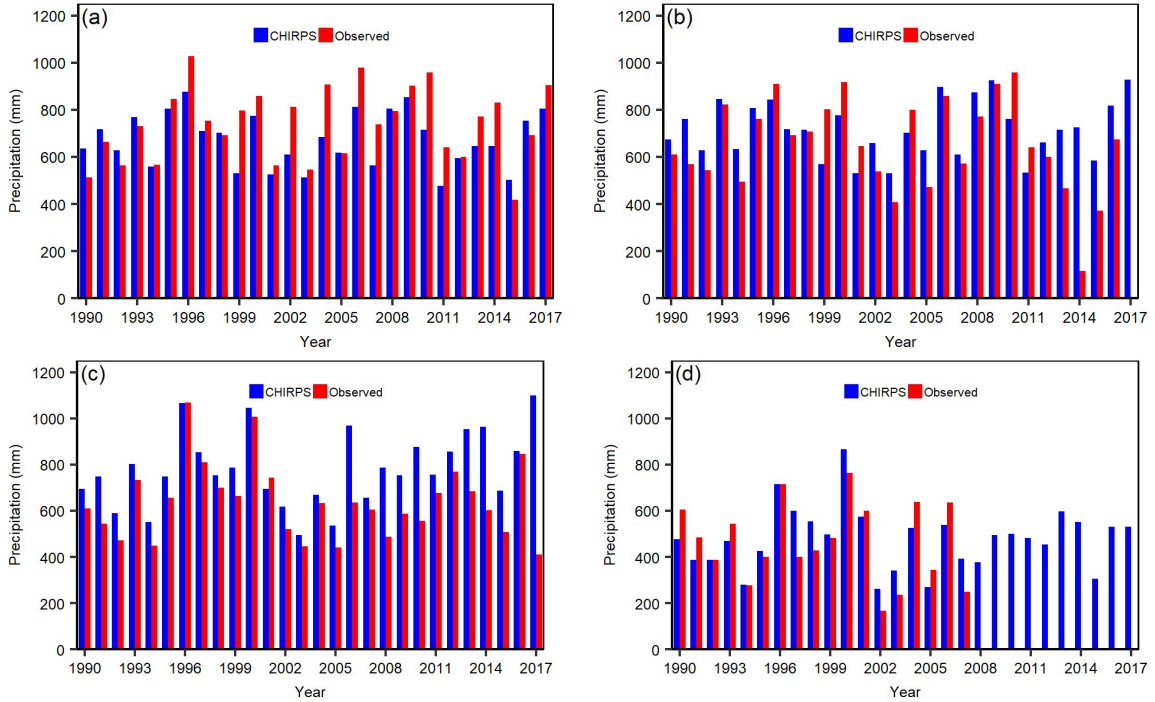


Fig. 3-8 Annual average precipitation comparison between CHIRPS and Observed at (a) B1E001, (b) B1E003, (c) B4E003, and (d) B7E007 stations

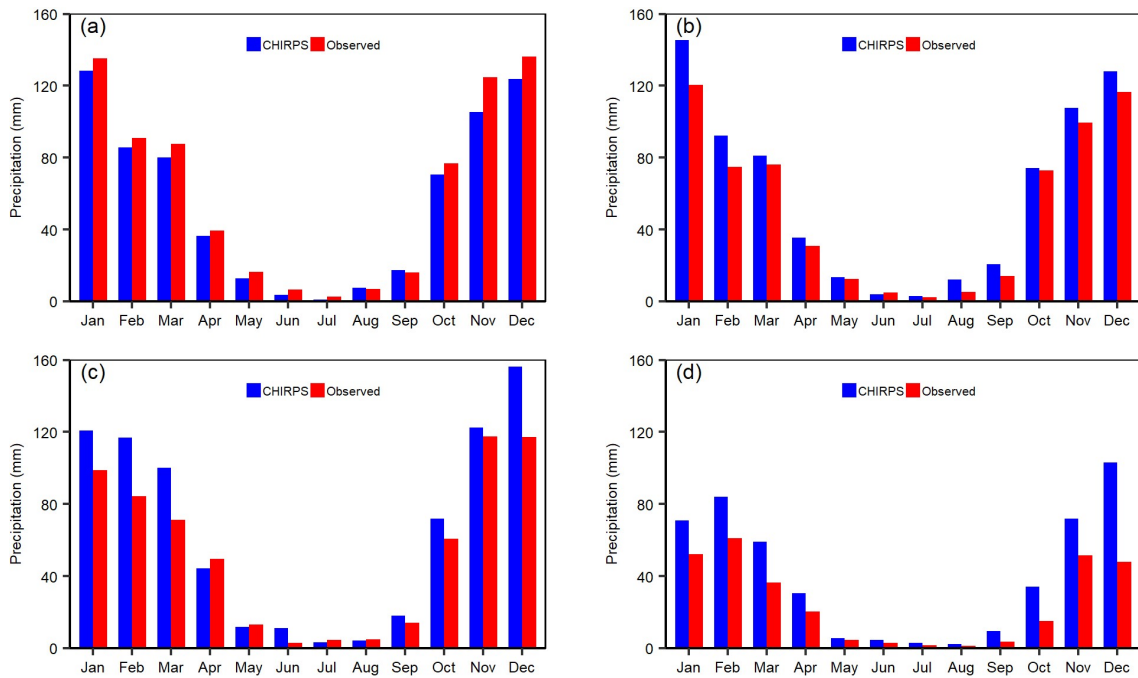


Fig. 3-9 Monthly precipitation comparison between CHIRPS and Observed at (a) B1E001, (b) B1E003, (c) B4E003, and (d) B7E007 stations

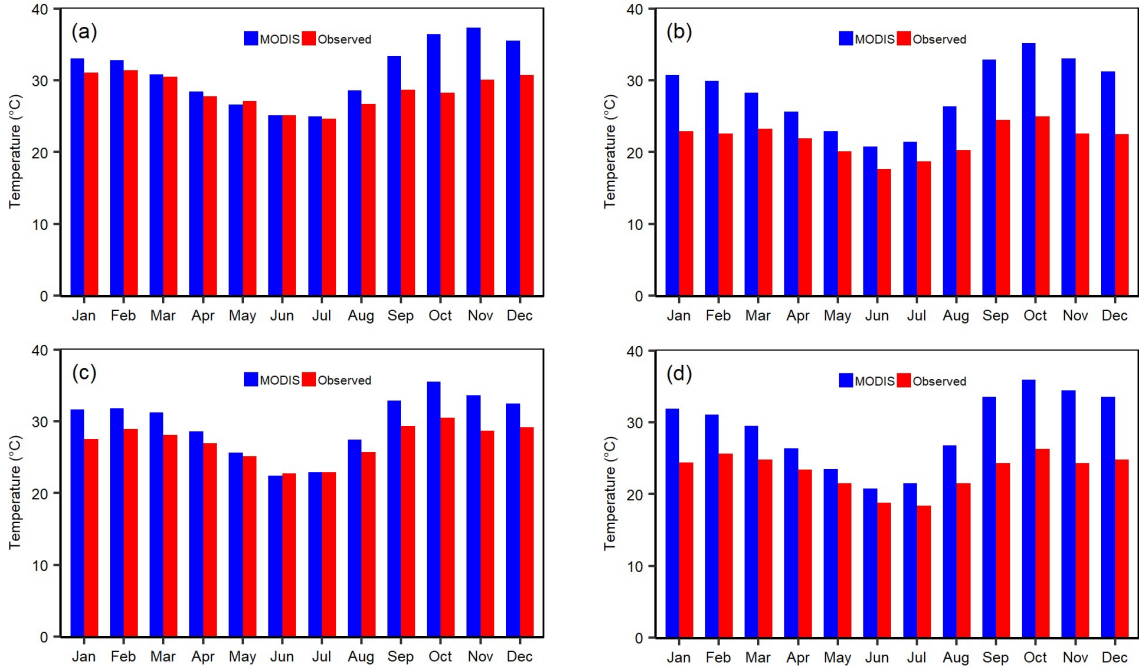


Fig. 3-10 Monthly maximum temperature comparison between MODIS and Observed at (a) Hoedspruit, (b) Lydenburg, (c) Oudestad, and (d) Witbank stations

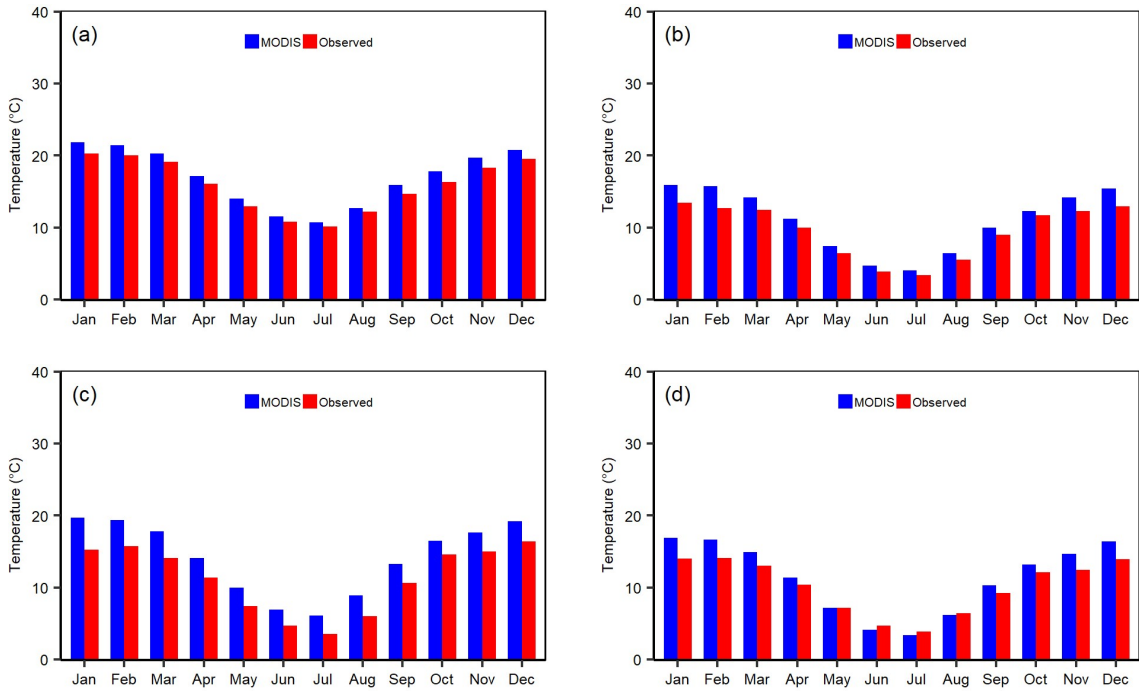


Fig. 3-11 Monthly minimum temperature comparison between MODIS and Observed at (a) Hoedspruit, (b) Lydenburg, (c) Oudestad, and (d) Witbank stations

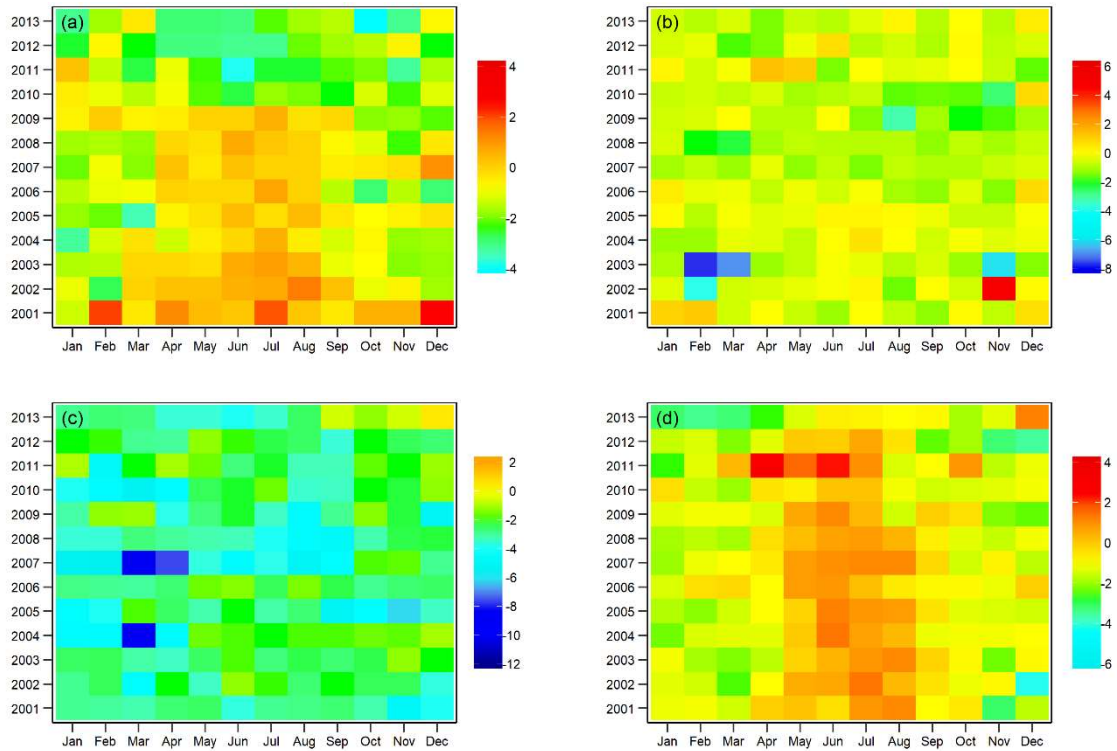


Fig. 3-12 Difference in minimum temperature between Observed and MODIS at (a) Hoedspruit, (b) Lydenburg, (c) Oudestad, and (d) Witbank stations

3.5.5 River Flow Data

Observed time series of streamflow, are required for calibration and validation of the model are collected from Department of Water and Sanitation, South Africa. There are several gauging stations within in the study area, however most of them do not have continuous data and only a few have continuous data. According to Arnold et al. (2012) the observed flow data should contain the dry, moderate and wet spell for the both calibration and validation time splits. In terms of model testing, the variation in the observed flow data is more important than the length of the data (Gan et al., 1997). The precipitation and observed stream for different streamflow monitoring stations were compared to identify the best/suitable stations for calibration and validation (Fig. 3-13, Fig. 3-14 and Fig. 3-15). The flow station Balule (B7H026) lacks data for the 1996 to 2009 and 2012-2014 time splits, thus it would not be a good choice for the model calibration and validation. In contrast, Blythe (B6H005) and Mamba (B7H015) possess continuous data and include the dry, intermediate and wet spells which can be grouped into different time horizons for the

model calibration and validation. Besides B7H015 and B6H005 reflect the monthly and seasonal flow pattern which include low flows during the dry seasons and high flows during the monsoon. In addition, B7H015 has 50,490 km² drainage area that covers more than two third of the study area thus represents the substantial hydrological processes within the study area. Moreover, streamflow at B7H015 has profound consequences on the water availability of the KNP. B6H005 has 2,200 km² catchment area, however, this catchment is least affected by the anthropogenic activities (McCartney, 2004). Finally, B6H005 and B7H015 stations data are selected for the calibration and validation of the model.

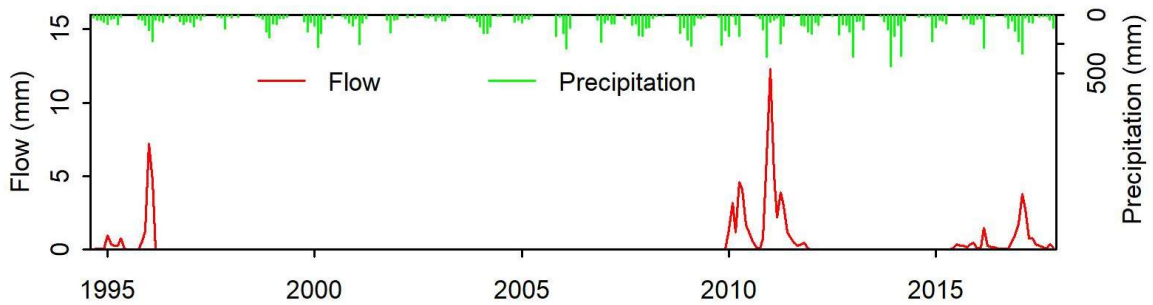


Fig. 3-13 Monthly precipitation and streamflow comparison over time at Balule.

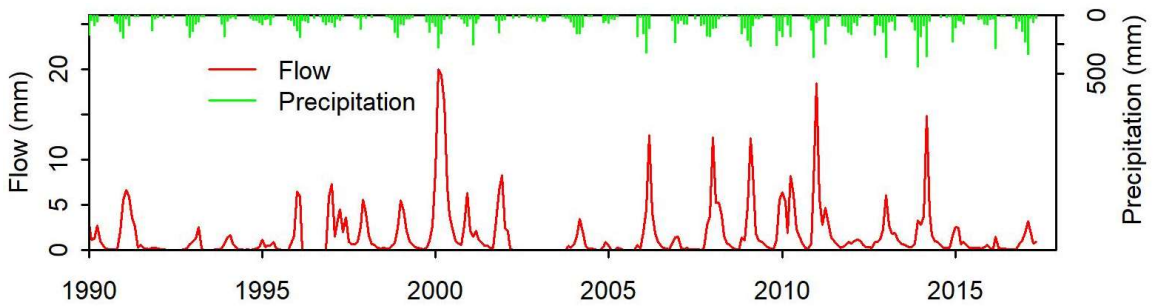


Fig. 3-14 Monthly precipitation and streamflow comparison over time at Mamba.

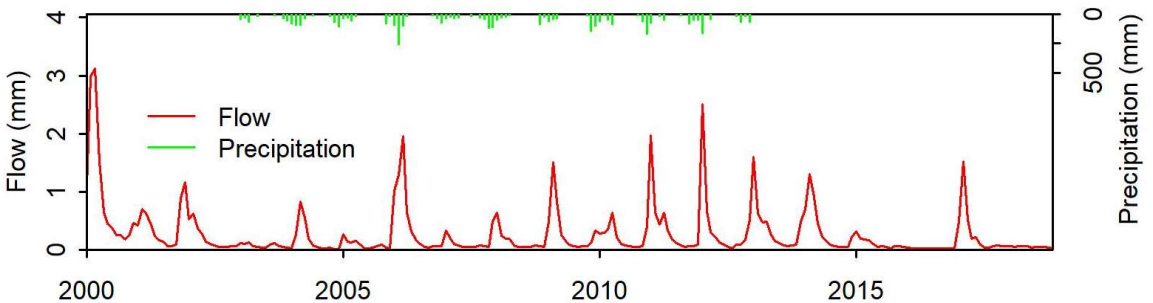


Fig. 3-15 Monthly precipitation and streamflow comparison over time at Blythe

3.5.6 Dams

There are more than 4,000 dams of different categories in Olifants River basin that store 1,472 Mm³ water (McCartney, 2004). However, 10 major dams (Fig. 3-16) included in the model store 1,167 Mm³ which represents approximately 80 percent of the total storage of the basin. The presence of dams modify the water movement by controlling the flow. In SWAT model, the dams are located on the stream and receive flow from the upstream subbasins. The water balance for a dam is described below:

$$V = V_{stored} + V_{flowin} - V_{flowout} + V_{pcp} - V_{evp} - V_{seep} \quad \text{Eq. 3-1}$$

Where V is the volume of water in the dam at the end of the day (m³), V_{stored} is the volume of the water stored at the beginning of the day (m³), V_{flowin} is the volume of water entering into the dam during the day (m³), $V_{flowout}$ is the volume of water flowing out from the dam during the day (m³), V_{pcp} is the volume of precipitation falling on the dam during the day (m³), V_{evp} is the volume of water removed from the dam through evaporation during the day (m³), V_{seep} is the volume of water lost through seepage (m³). The data on dams are collected from Department of Water Affairs, South Africa (Table 3-3). Unfortunately, the required data for water flowing out from the dams are not available. To overcome the paucity of the water flowing out data the simulated target storage method is set at a fashion where water will spill out from the dam if the level of storage in the dam crosses the principal storage volume.

Table 3-3: List of major dams inside the Olifants River basin

SL Name	Latitude	Longitude	Capacity (Mm ³)	Height (m)	Surface Area (km ²)	Starting Year
1 Loskop	-25.42	29.36	374	53	24.3	1939
2 Rhenosterkop	-25.10	28.92	206	35	37.2	1984
3 Middle Letaba	-23.28	30.40	172	34	18.8	1984
4 Flag Boshielo	-24.80	29.43	105	36	12.9	1987
5 Witbank	-25.89	29.32	104	42	12.1	1971
6 Bronkhorst Spruit	-25.89	28.73	58	32	8.6	1950
7 Blyderivierspoort	-24.54	30.80	54	71	2.4	1975
8 Middelburg	-25.77	29.55	48	36	4.7	1978
9 Rust De Winter	-25.23	28.53	27	31	4.7	1934
10 Kromfontein	-26.12	29.25	18	14	0.4	1990
Middle Coffey						

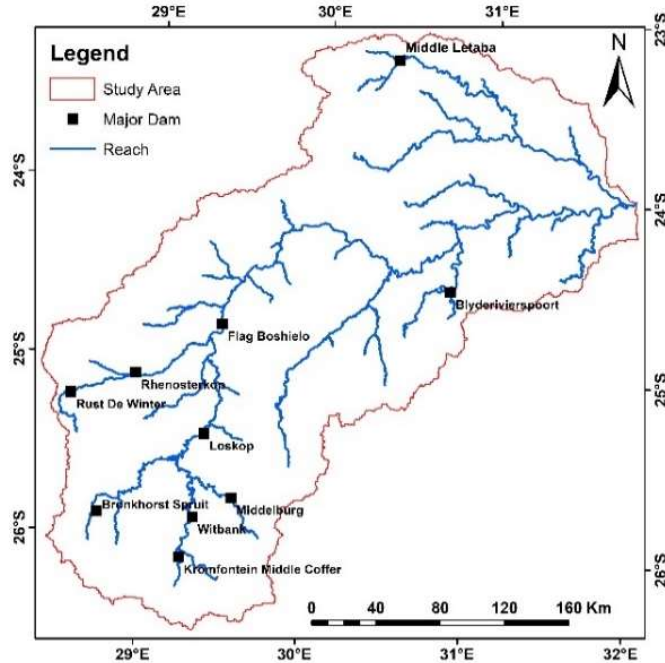


Fig. 3-16 Major dams in the Oilfants River basin

3.6 Model Setup

The ArcGIS-SWAT interface of version 2016 has been used to setup the model. Olifants River stream was delineated from the raster file of DEM. The DEM was masked by the known Olifants area shapefile to reduce the processing time. The outlet location of the basin was added to the model to calculate the flow paths based on DEM and outfall. The model testing streamflow stations were inserted manually to ensure that the creation of the subbasins around the stations. The locations of the major dams were provided using add reservoir option. Though the Olifants River basin covers 73,700 km², based on DEM and other information the watershed having an area of 68,978 km² was delineated and divided into 81 subbasins (Fig 3-17). The GIS layer of landuse and soil data are provided along with the user defined lookup tables to accomplish SWAT landuse and soil classification. After that, the percentage of the slope classes were defined. The Olifants River basin has a wide range of elevation and it's categorized into three types (Gyamfi et al., 2016a). These slope categories (a) level to mildly undulating (<8%), (b) rolling to hilly (8-30%) and (c) steeply dissected to mountains (>30%) were included in the model and the proportion in terms of the percentage of the study area were 79.5% ,16.5% and 4 %, respectively, for

(a), (b) and (c). The threshold values for landuse, soil and slope were set at 5%, 20% and 20%, respectively. The elevation bands were used to simulate the orographic rainfall in the vicinity of the escarpment. After model parameterization, the subbasins were further divided into 454 hydrologic response units (HRUs) depending on the homogeneity of landuse, soil type and slope. The accuracy of the model is dependant on the number of subbasins. Considering the number of climate stations, 81 subbasins are reasonable for the watershed. The model was set up for the period of March 1, 2000 to December 31, 2012 with three years as a warm-up period. Ninety six climatic stations precipitation and temperature data were used as input, however, the SWAT model used only sixty five stations data depending on the location of the station and centroid of the subbasin; each subbasin use only one climatic station that is the nearest to the centroid.

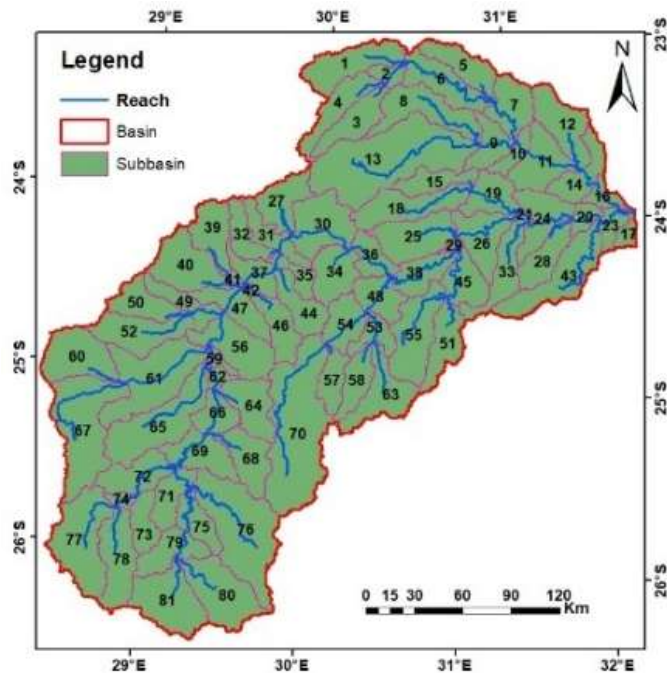


Fig. 3-17 Delineation of sub watersheds.

3.7 Water Use

The Olifants River basin can be divided into upper, middle and lower Olifants based on water use (Fig. 3-18). Upper catchment of the river uses water mainly for commerce and industry. Irrigation is the most dominant water user in the middle catchment and based on the irrigation practice the farming can be categorized into a) commercial farming and b)

subsistence farming. The first one heavily relies on intense irrigation and the latter one on rainfall. Commercial farming and mines are the major water user in the lower reaches of Olifants as well. Conservations and ecotourism are not the major water users but play vital role in earning foreign currency and creating jobs.

Total water demand for the watershed is estimated to be 1,016 Mm³ (McCartney, 2004). Agriculture is not the dominant land use but it consumes more than 50 percent of the water demand which equates approximately 540 Mm³ (Arranz et al., 2007). Maize, wheat, sorghum, etc. are the major crops grown in this area and maize is the most dominant (Akpalu et al., 2011). Maize is a summer crop and planted in between October to December in this region (Benhin, 2006). The comparison between monthly mean precipitation and potential evapotranspiration (PET) shows that PET is always higher than precipitation, indicating the need for irrigation [Fig. 3-20 (a)]. Moreover, as per the crop calendar of South Africa (Fig. 3-19) October to April is the cropping period for the summer crop. The crop estimation committee of South Africa reported that 97 percent of the total cropping occurs during the summer period in the Olifants River basin (DAFF, 2019; DAFF, 2018). It can be concluded that most of the irrigation and water consumption occurs during the summer and based on this conclusion a consumptive water use pattern is constructed for this study area [Fig. 3-20 (b)].

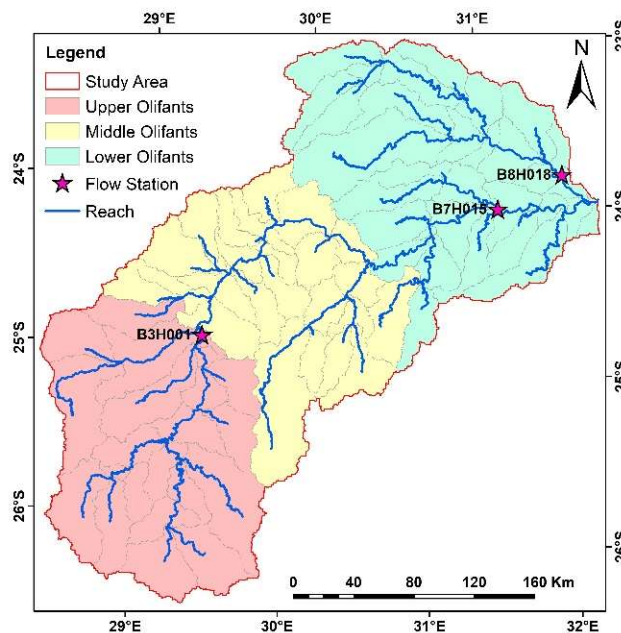


Fig. 3-18 Upper, Middle and Lower Olifants River.

Crop/Month	Oct	Nov	Dec	Jan	Feb	Mar	Apr	May	Jun	Jul	Aug	Sep
Maize												
Sorghum												
Wheat												

	Sowing		Growing		Harvesting
--	--------	--	---------	--	------------

Fig. 3-19 Crop calendar of South Africa

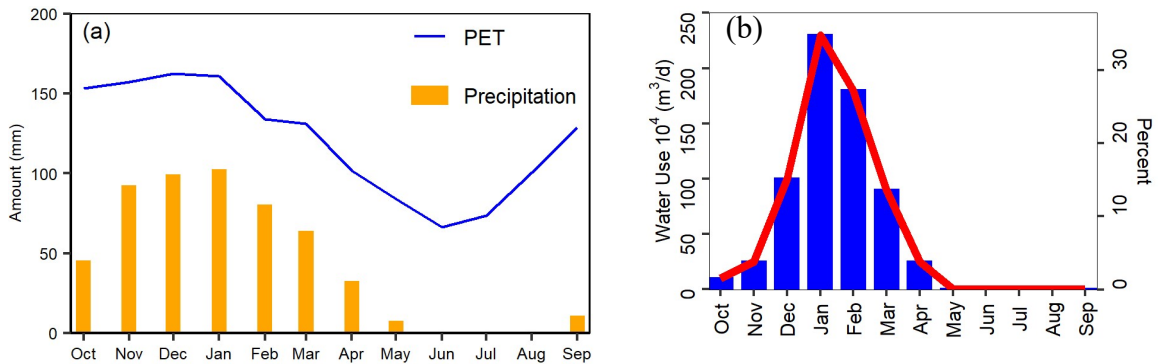


Fig. 3-20 (a) Comparison of monthly median precipitation and mean PET across the study area, and (b) Monthly consumptive water use

3.8 Climate Change Impact Assessment

Climate change impact assessment on hydrologic regime is performed by comparing the various processes of the hydrologic cycle between historical and future time horizons. To this end, the pre-calibrated model is forced with bias corrected historical and future climate data. The climate data for historical (1985-2005) and two scenario periods, mid-century (2041-2070) and end-century (2071-2100), have been used from an ensemble of nine regional climate models (Table 3-4). The RCMs are part of the Coordinated Regional Climate Downscaling Experiment (CORDEX). Two different emission scenarios are considered namely, rcp4.5 (moderate emission scenario) and rcp8.5 (high emission scenario). The available data under CORDEX project are grouped into 14 domains which encompassed most of the land surfaces throughout the globe (Chilkoti et al., 2017). The present study area lies within the domain-4 known as Africa (AFR) and the data related to the corresponding domain has been gathered from the climate models having the resolution of 0.44° x 0.44° (50 km x 50 km approximately). The climate projection contains numerous climatic variables. However, according the input requirement of the hydrological model, only precipitation, maximum and minimum near surface air temperature have been

extracted from the climate projection at the daily time step for the sixty five climatic stations SWAT used during the model development. A script is developed in R to extract and compile the climatic data.

Table 3-4: List of CORDEX climate model ensembles used in this study

SL	General Circulation Model (GCM)		Regional Climate Model (RCM)	
	GCM	Modelling Agency	RCM	Modelling Agency
M1	CanESM2	CCCma	RCA4	SMHI
M2	ECEARTH	ICHEC	CCLM4-8-17	IAES
M3	ECEARTH	ICHEC	HIRHAM5	DMI
M4	ECEARTH	ICHEC	RACMO22T	KNMI
M5	ECEARTH	ICHEC	RCA4	SMHI
M6	ECEARTH	ICHEC	REMO2009	GERICS
M7	HadGEM2	MOHC	CCLM4-8-17	IAES
M8	HadGEM2	MOHC	CRCM5	UQAM
M9	HadGEM2	MOHC	RCA4	SMHI

CCCma- Canadian Center for Climate Modelling and Analysis

SMHI- Swedish Meteorological and Hydrological Institute

ICHEC- Irish Center for High End Computing

IAES- Institute for Atmospheric and Environmental Sciences

DMI- Danish Meteorological Institute

KNMI- The Royal Netherlands Meteorological Institute

GERICS- The Climate Service Center Germany

MOHC- Met Office Hadley Centre

UQAM- Université du Québec à Montréal

3.9 Trend Analysis

3.9.1 Mann Kendall (M-K) Test

M-K test is a non-parametric rank-based test that has the capability to analyze the hydrometeorological dataset (Yue et al., 2002). It determines the trend and strength of the trend based on the indices τ and p value. if τ is positive then it indicates positive trend and vise versa, however zero indicates no trend. The p value describes the significance level or confidence level of the trend. For instance, p value of 0.05 indicates 95 percent of confidence level hence only 5 percent data falls outside the trend (Helsel et al., 1992). The test measures the difference between the later measure value and earlier measured values $(x_j - x_i)$, where $j > i$, and assign integer -1,0 and 1 for negative, zero and positive values. The test statistics can be written as

$$S = \sum_{i=1}^{n-1} \sum_{j=i+1}^n \text{sign}(x_j - x_i) \quad \text{Eq. 3-2}$$

$$\text{where } \text{sign}(x_j - x_i) = \begin{cases} -1, & \text{if } (x_i - x_j) < 0 \\ 0, & \text{if } (x_i - x_j) = 0 \\ 1, & \text{if } (x_i - x_j) > 0 \end{cases}$$

$$\tau = \frac{2S}{n(n-1)} \quad \text{Eq. 3-3}$$

3.9.2 Sen's Slope

Sen's slope is also a nonparametric test and is often performed together with M-K test to describe the slope of the trend (Helsel et al., 1992). It calculates the slope from the median of the paired slopes hence it is less sensitive towards the outliers. The Sen's slope can be expressed as

$$\beta_1 = \text{median} \left(\frac{x_j - x_i}{t_j - t_i} \right) \quad \text{Eq. 3-4}$$

where β_1 is the Sen's slope, x_j and x_i are the values of the timeseries data at t_j and t_i , respectively.

CHAPTER IV

RESULTS AND DISCUSSION

4.1 Overview

The results and discussion chapter mainly consist of the model performance, hydrological budget and climate change impacts assessment. The model performance includes the effect of water use, sensitivity analysis, calibration and validation and model uncertainty analysis. The consumptive water use estimated for this basin adopted in the model to better represent the reality and achieve better simulation. SWAT-CUP has been used to perform the sensitivity analysis, calibration and validation and model uncertainty analysis. In the hydrological budget analysis, the water budget has been analyzed and matched with the reported values.

The projected changes in precipitation, temperature and flow are analyzed and discussed in the climate change section. To this end, the hydrological components are compared between the historical and future periods. Results indicate significant increase in the projected temperature, general decrease in flow and precipitation with fluctuations. Moreover, spatial analysis has been performed and the results show that the high spatial variation will remain in the projected precipitation and flow.

4.2 Impacts of Water Use on Streamflow

The default monthly simulated streamflows are compared to the observed streamflow at Mamba flow station (B7H015) having a catchment area of 50,490 km² with and without considering the consumptive water use. There is a significant variation between the simulated and observed streamflow in the absence of consumptive water use (Fig. 4-1). It was learnt that the large amount water withdrawals are one of the reasons behind the poor simulation. Power generation, industrial, urban, rural, mining and irrigation are the main water consumption sectors in this catchment (McCartney , 2004). For proper estimation of the flows, the consumptive water uses need to be incorporated in the model. The consumptive use as estimated earlier and presented in Fig. 3-20 (b) was incorporated. The streamflow comparison subsequent to the consumptive use indicates a significant improvement in the model performance (Fig. 4-2). The mean monthly flows for each year

are plotted separately for two different cases which include (a) without water use (Fig. 4-3), and (b) with water use (Fig. 4-4). The simulation without water use captures the flow pattern but overestimates the high flow magnitudes. On the other hand, the presence of water use simulates the flow reasonably, however, there is room for improvements which is achieved during the calibration.

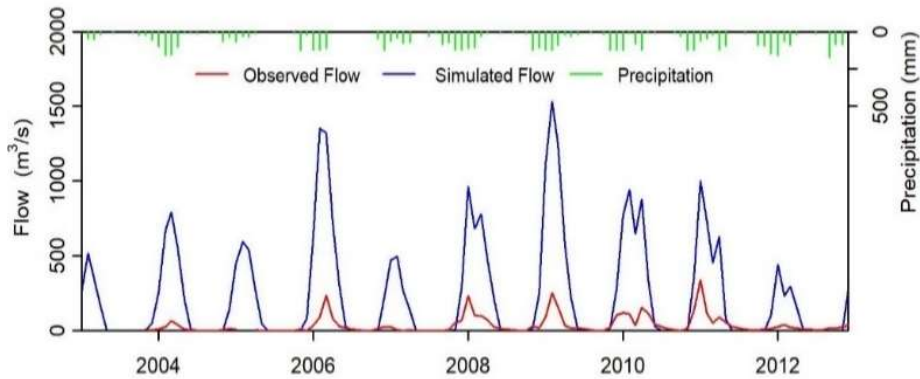


Fig. 4-1 Comparison of observed and simulated streamflows at Mamba (B7H015) gauging station (without considering consumptive water use)

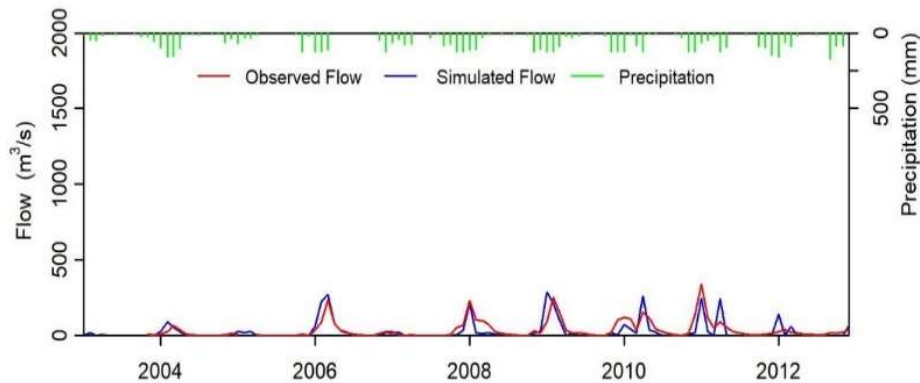


Fig. 4-2 Comparison of observed and simulated streamflows at Mamba (B7H015) gauging station (considering consumptive water use)

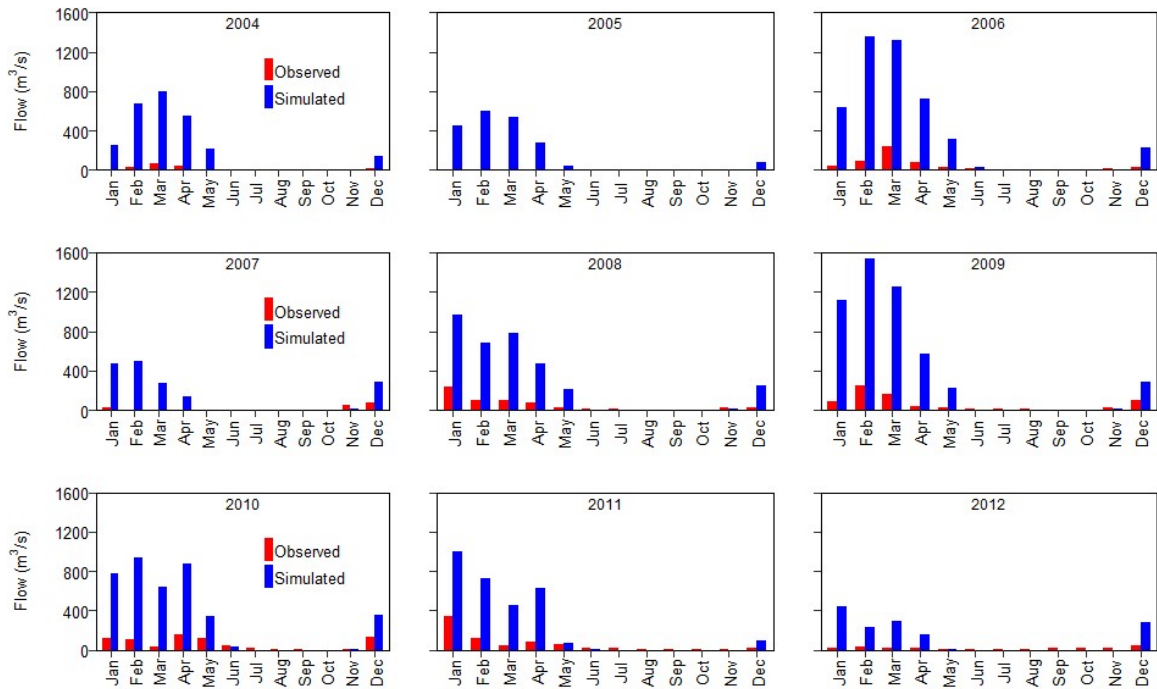


Fig. 4-3 Comparison of monthly observed (1st bar from left) and simulated streamflows at Mamba (B7H015) gauging station (without considering consumptive water use)

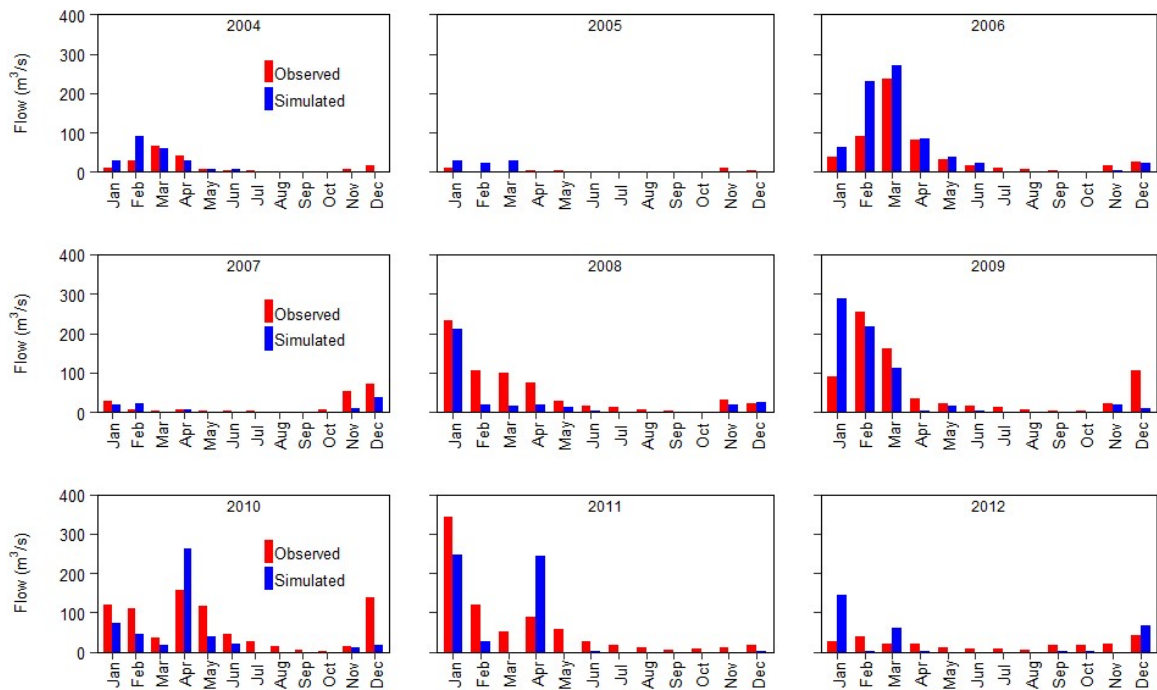


Fig. 4-4 Comparison of monthly observed (1st bar from left) and simulated streamflow at Mamba (B7H015) gauging station (considering consumptive water use)

4.3 Sensitivity Analysis

Hydrologic model needs to pass through calibration and validation process before utilizing it as a decision-making tool (Muleta et al., 2005). A semi-distributed watershed model has several parameters that represent the hydrologic processes in the watershed. Sensitivity analysis (SA) quantifies the changes in the model output corresponding to model inputs (Mai et al., 2019). SA helps to lower the number of parameters required tuning for the calibration. The objective of the SA is to determine the most sensitive parameters to ease the calibration process. There are two different types of SA namely, local or global. Local SA represents the change in model output in context to a specific input space whereas the global SA represents the model output response in the context of entire feasible model input space. Global SA is widely used as compared to the local SA, as it provides more information about the model sensitivity by considering the model input correlation (Göhler et al., 2013). SA analysis is also useful for model uncertainty analysis, model structural analysis and determining the relative importance of the model parameters (Mai et al., 2019).

SWAT Calibration and Uncertainty Program (SWAT-CUP) is a widely used tool to carry out the model sensitivity analysis. SWAT-CUP performs multiple regression analysis to quantify the parameter sensitivity statistics in terms of t-stat and p-value. The t-stat represents the sensitivity coefficient over its standard error, the large value indicates that the sensitivity coefficient is different from zero thus the parameter might be sensitive. On the other hand, the p-value represents the null hypothesis that the coefficient is zero i.e. has no effect. For instance, the p-value of 0.05 means that the probability of occurrence of no effect is 5% hence for the rest 95% cases the parameter would be sensitive. Therefore, the low p-value indicates that the parameter is sensitive.

SA of the Olifants basin hydrologic model was performed through SWAT-CUP. The results of the analysis are depicted in the Fig. 4-5. Fourteen model parameters were tested for sensitivity which include eight groundwater and six surface water parameters. Among them one groundwater and five surface water parameters are found to be sensitive and the Curve Number (CN2) is found to be the most sensitive parameter. Relative ranking of the sensitive parameters was presented in the Table 4-1.

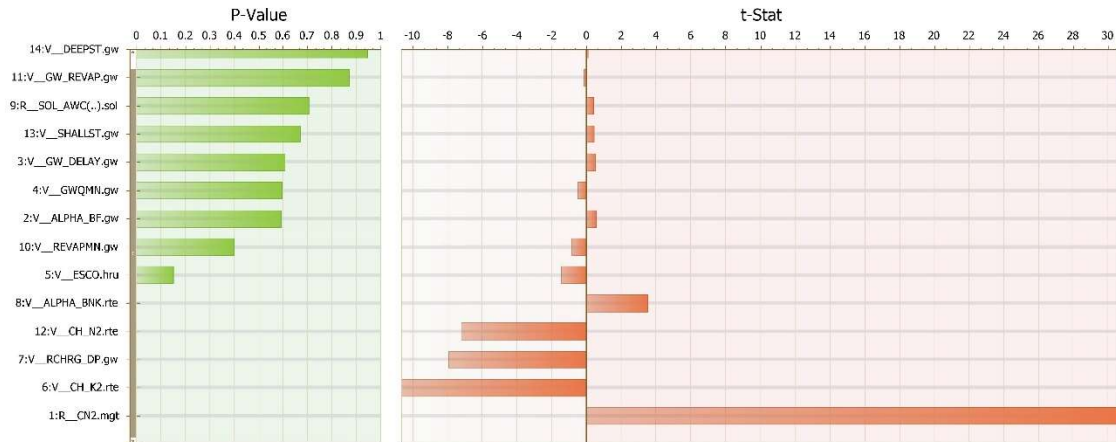


Fig. 4-5 Model parameters sensitivity statistics in the Olifants River basin

Table 4-1: Sensitivity ranking of model parameters considered in the sensitivity analysis

Parameter	Category	Description	Rank
CN2	Management	SCS runoff curve number	1
CH_K2	Main channel	Effective hydraulic conductivity in the main channel (mm/h)	2
RCHRG_DP	Groundwater	Deep aquifer percolation fraction	3
CH_N2	Main channel	Manning's n value for main channel	4
ALPHA_BNK	Main channel	Baseflow alpha factor for bank storage (days)	5
ESCO	HRU	Soil evaporation compensation factor	6
REVAPMN	Groundwater	Threshold depth of water in the shallow aquifer for "revap" to occur (mm)	7
ALPHA_BF	Groundwater	Baseflow alpha factor (days)	8
GWQMN	Groundwater	Threshold depth of water in the shallow aquifer required for return flow to occur (mm H ₂ O)	9
GW_DELAY	Groundwater	Groundwater delay (days)	10
SHALLST	Groundwater	Initial depth of water in the shallow aquifer (mm)	11
SOL_AWC	Soil	Soil available water storage capacity (mm H ₂ O/mm soil)	12
GW_REVAP	Groundwater	Groundwater "revap" coefficient	13
DEEPST	Groundwater	Initial depth of water in the deep aquifer (mm)	14

4.4 Calibration and Validation

Calibration is the process of finding optimal model parameters for achieving acceptable or higher level of performance of the model, whereas validation is the consistency checking of the calibration. Calibration is performed by changing the model parameters, while in validation the model parameters obtained during the calibration period are tested in an independent evaluation period. Generally, calibration and validation are performed with observed or experimental data of different periods. For instance, if 20 years of observed data are available, then 3-4 years data is used for warm up, one set of 7-8 years data are used for calibration and another set of 7-8 years data are used for validation. In this study, based on the available data, the model is set up for the period 2000 to 2012, out of which 2000-2002, 2003-2008, and 2009-2012 time periods are the warm-up, calibration and validation periods, respectively. SWAT-CUP software is used for calibration of the model and the calibrated parameter ranges as well as fitted values are presented in Table 4-2.

Table 4-2: Range of calibrated parameters and final fitted values used in the modelling

Parameter	Description	Range	Fitted Value
CN2	SCS runoff curve number	-0.2-0.2	0.19
CH_K2	Effective hydraulic conductivity in the main channel (mm/h)	0-50	31.5
RCHRG_DP	Deep aquifer percolation fraction	0-0.7	0.25
CH_N2	Manning's n value for main channel	0-0.2	0.15
ALPHA_BNK	Baseflow alpha factor for bank storage (days)	0-0.2	0.09
ESCO	Soil evaporation compensation factor	0-0.6	0.23
REVAPMN	Threshold depth of water in the shallow aquifer for "revap" to occur (mm)	100-300	218
ALPHA_BF	Baseflow alpha factor (days)	0-0.2	0.1
GWQMN	Threshold depth of water in the shallow aquifer required for return flow to occur (mm H ₂ O)	500-4500	675
GW_DELAY	Groundwater delay (days)	30-400	185
SHALLST	Initial depth of water in the shallow aquifer (mm)	500-1500	790
SOL_AWC	Soil available water storage capacity (mm H ₂ O/mm soil)	-0.1-0.1	-0.06
GW_REVAP	Groundwater "revap" coefficient	0.15-0.2	0.18
DEEPST	Initial depth of water in the deep aquifer (mm)	1500-2500	1970

4.4.1 Nash-Sutcliffe Efficiency (NSE)

NSE is a normalized statistic which is determined as unit minus square sum of difference between observed and simulated value over variance of observed value under the investigation period. NSE is calculated as

$$NSE = 1 - \frac{\sum_{i=1}^n (O_i - S_i)^2}{\sum_{i=1}^n (O_i - \bar{O})^2} \quad \text{Eq. 4-1}$$

where O_i and S_i are the observed value and simulated value respectively at time step ' i ', \bar{O} is the average observed value and n is the number of observations. NSE ranges between $-\infty$ to 1, where 1 represents the perfect value. NSE value greater than 0.5 is considered acceptable for monthly flow simulation in SWAT model.

4.4.2 Kling Gupta Efficiency (KGE)

The KGE (Gupta et al., 2009) measures the Euclidian distance of three components which include correlation, bias and variability from the ideal point. The values of KGE ranges from $-\infty$ to 1, where 1 represents the perfect match. KGE is less sensitive towards the extremes relative to the NSE. KGE enhances the bias and the variability measure considerably but slightly decrease the correlation compared to the NSE (Gupta et al., 2009). KGE can be expressed as follows

$$KGE = 1 - \sqrt{(r - 1)^2 + (\alpha - 1)^2 + (\beta - 1)^2} \quad \text{Eq. 4-2}$$

where, r is the linear regression coefficient between observed and simulated data

$$\alpha = \frac{\text{Coefficient of variation of simulated data}}{\text{Coefficient of variation of observed data}}, \text{ and } \beta = \frac{\text{Mean of simulated data}}{\text{Mean of observed data}}$$

4.4.3 Percent Bias (PBIAS)

PBIAS measures the average tendency of simulated data compared to its observed counterpart. It measures the overestimation or underestimation of simulated data in percentage. PBIAS is formulated as

$$PBIAS = \frac{\sum_{i=1}^n (O_i - S_i) * 100}{\sum_{i=1}^n O_i} \quad \text{Eq. 4-3}$$

where O_i and S_i are the observed value and simulated value respectively at time step ' i ' and n is the number of observations. The optimum value for PBIAS is 0 and low value

indicates accuracy of the model. PBIAS value range between -20% and 20% is considered acceptable for monthly flow simulation of SWAT model. The positive value indicates that the model is underestimating while the negative value represents overestimation of the model.

4.4.4 Calibration and Validation Performance

The model is calibrated (Fig. 4-6) and validated (Fig. 4-7) at two different stations (a) Mamba (B7H015) and (b) Blythe (B6H005) having catchment area of 54,500 km² and 2,200 km², respectively. The model performance classification of Moriasi et al. (2007) has been adopted as the reference for evaluating the results. Both quantitative and graphical technique are used to evaluate the performance of the hydrological model. The model evaluation statistics for calibration and validation (Table 4-3) show that there is a satisfactory agreement between the simulated and measured streamflows. The well-established model statistical performance indicator NSE and KGE are found to be greater than 0.5 and 0.6, respectively for both station during the model evaluation period. In addition, another well established model statistical performance indicator, PBIAS lies within the range of $\pm 20\%$. Moreover, the visual indicators like timeseries comparison during the low, average and high discharge period for the model calibration and validation period depicts fair agreement between the modelled and measured flows. The acceptable range of NSE, KGE and PBIAS along with the visual comparison confirmed the model satisfactory performance.

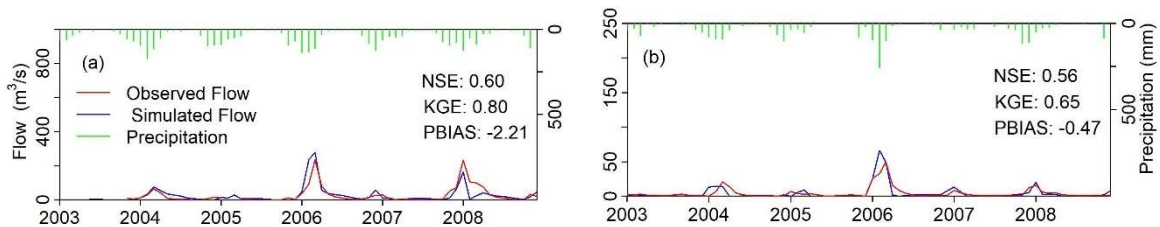


Fig. 4-6 Monthly streamflow calibration results: (a) Mamba and (b) Blythe

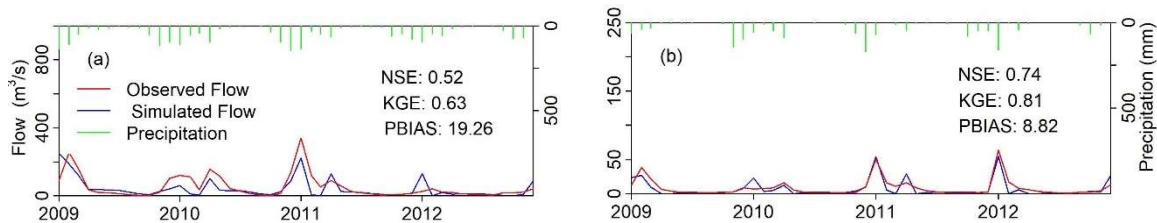


Fig. 4-7 Monthly streamflow validation results: (a) Mamba and (b) Blythe

Table 4-3: Performance statistics for calibration and validation at monthly time step

Station	Satisfactory value			Calibration			Validation		
	NSE ¹	PBIAS ²	KGE ¹	NSE	PBIAS	KGE	NSE	PBIAS	KGE
B7H015	0.50	± 20%	0.60	0.60	-2.21	0.80	0.56	-0.47	0.63
B6H005				0.52	19.26	0.65	0.74	8.82	0.81

¹Indicating minimum acceptable value, ²Indicating acceptable range

4.5 Uncertainty Analysis

Uncertainty analysis is very important to determine reliability of the model. Model uncertainty analysis is carried out using SWAT-CUP Sequential Uncertainty Fitting (SUFI-2), which considers all potential sources of uncertainty including input data, model conceptualization, parameterization and output. The uncertainty analysis result is expressed as 95 percent uncertainty (95 PPU), which is calculated at the 2.5% and 97.5% levels of the cumulative distribution of the output variable using Latin Hypercube Sampling method (Mckay et al., 2000). Two factors termed as P-factor and R-factor are used to express the result of the uncertainty analysis. P-factors represents the percentage of the behavioural data falls within the 95 PPU, while R-factor represents the thickness of the 95 PPU band (Abbaspour et al., 2015). The P-factor and R-factor, respectively, ranges between 0 to 1 and 0 to ∞. The numeric value of 1 and 0 represent the perfect match with observed for the P-factor and R-factor, respectively. The P-factor greater than 0.7 and R-factor less than 1 is considered satisfactory (Dabrowski, 2014). The P-factor and R-factor can be expressed as follows:

$$R - \text{factor} = \frac{\sum_{i=1}^n (Y_{i,97.5\%} - Y_{i,2.5\%})}{ns} \quad \text{Eq. 4-4}$$

$$P - \text{factor} = \frac{\sum_{i=1}^n I[Y_i]}{n} \quad \text{Eq. 4-5}$$

$$\text{with } I[Y_i] = \begin{cases} 1, & \text{if } Y_{i,2.5\%} < Y_i < Y_{i,97.5\%} \\ 0, & \text{else} \end{cases}$$

where, $Y_{i,97.5\%}$ and $Y_{i,2.5\%}$ are the upper and lower limit of 95 PPU, and s is the standard deviation of the observed flow.

The NSE is set as an objective function in this uncertainty analysis and the simulation having NSE equal to or greater than 0.5 is considered as behavioral. 500 simulations have been carried out to perform the uncertainty analysis which improved the model reliability by narrowing down the 95 PPU band (Fig.4-8 and Fig. 4-9). The results indicate that 35% of the observed streamflow data bracketed within the 95 PPU band with an R value of 0.26.

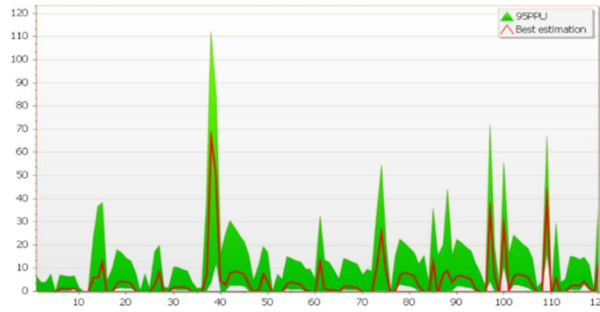


Fig. 4-8 Illustration of the best streamflow estimation and 95 percent uncertainty band at the beginning of the uncertainty analysis at Mamba (B7H015)

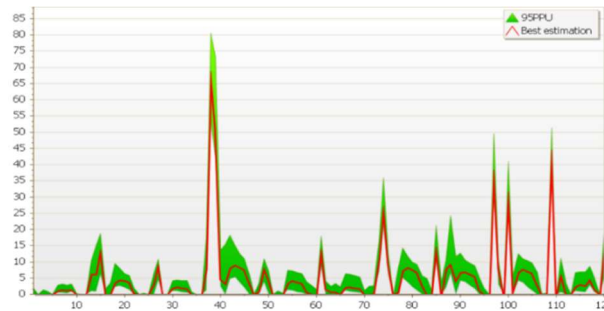


Fig. 4-9 Illustration of the best streamflow estimation and 95 percent uncertainty band at the end of the uncertainty analysis at Mamba (B7H015)

4.6 Water Budget Analysis

Water budget analysis of the hydrological model is performed at annual time step for the period 2003 to 2012. The model Mean Annual Precipitation (MAP) for that period is found 634 mm which showed good agreement with the observed MAP of 630mm. The values of the hydrological components are expressed as a percentage of MAP in the water budget analysis (Fig. 4-10). The hydrological budget depicts that 75.8 percent of the precipitation returns to the atmosphere as evapotranspiration, rest 24.2 percent contributes to the surface runoff, baseflow and seepage. The surface runoff, baseflow and seepage are found to be 6.3, 1.9 and 16.0 percent of the precipitation, respectively. The percentage of the

evaporation is consistent with the previous study of Gyamfi et al. (2016), who found the evaporation lies in between 70 to 78 percent of precipitation for this study area. Moreover, the surface runoff conforms with the study of McCartney (2004), who reported mean annual runoff is 6 percent of MAP for this region. Furthermore, Web-based Hydrograph Analysis Tool (WHAT) is used to separate the baseflow and surface runoff portion from the observed flow. WHAT results showed, the streamflow consists of 22% baseflow and 78% surface runoff, which is consistent with the respective simulation result having 23% baseflow and 77% surface runoff.

Spatial analysis of the average annual precipitation, potential evapotranspiration and water yield distribution across the Olifants River basin is performed at subbasin scale for the 2003 to 2012 time horizon (Fig. 4-11). The precipitation varied greatly over the study area ranging from 200 mm to 1000 mm with an average of 634 mm. The potential evapotranspiration varied significantly over the study area ranging from 1300 mm to 1900 mm with an average of 1600 mm. Higher potential evapotranspiration observed in the northeast area of the basin compared to the southwest area. The southeast portion characterize with higher elevation and lower temperature compared to the northeast portion of the basin which played a vital role behind such spatial distribution of the potential evapotranspiration. The water yield represents the net amount of water exiting the subbasin towards the outfall. The water yield follows the spatial distribution of the precipitation and ranges between 0 mm to 250 mm for the study area. In general, southwest portion yields more water compared to the northeast portion of the basin and the middle section yields the most water near the highveld region.

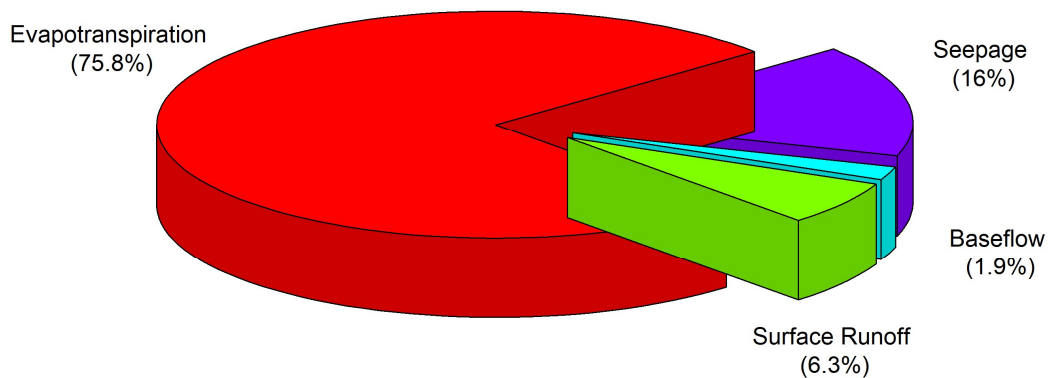


Fig. 4-10 Simulated annual water budget for the period 2003-2012 in the Olifants basin

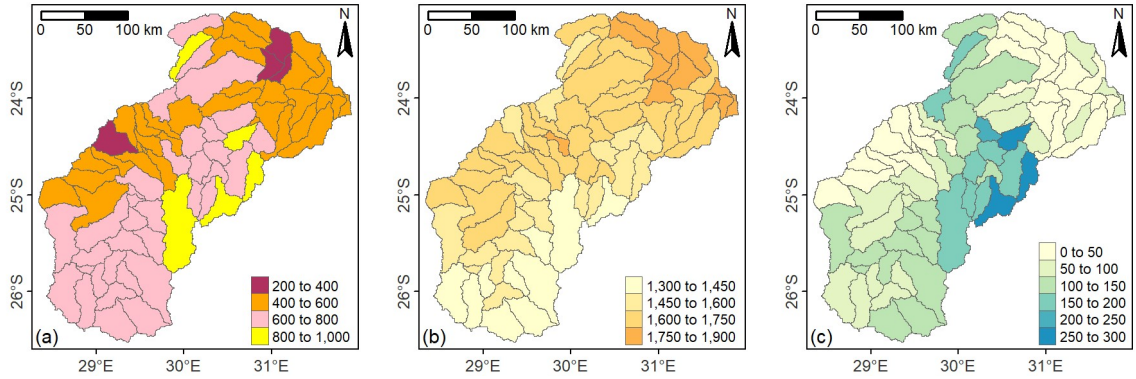


Fig. 4-11 Spatial distribution of hydrological components for the period 2003-2012; (a) average annual precipitation, (b) potential evapotranspiration and (c) water yield

4.7 Climate Change Impacts

Hydrological components such as precipitation, temperature, flow and so on are compared between the base and future periods in the subsequent sections to assess the climate change impacts. In South Africa the hydrological year starts from October and ends at September and this hydrological year has been adapted in the monthly comparison plots. Moreover, the time splits 1985-2005, 2041-2070 and 2071-2100 are named as base period, mid-century and end-century, respectively. Furthermore, base model results are compared with nine different climate ensembles which is denoted by B for base, and M1 to M9 for climate ensembles. The details of the abbreviated climate models are described in Table 3-4.

4.7.1 Precipitation Projection

Precipitation is compared between the base period and two future periods, namely (a) mid-century, and (b) end-century for the rcp4.5, and rcp8.5 at monthly time step (Fig. 4-12 to Fig. 4-16). Relative to the base period, the mean annual precipitation is projected to decrease, though the magnitude of the reduction varies across the nine climate ensembles. The mid-century and end-century seasonal precipitation pattern are projected similar to the base period. However, projection uncertainty in the summer precipitation is found to be higher compared to that of the winter during the future periods. Moreover, there will be more frequent extreme precipitation events in the future compare to the base period. The mean summer precipitation is projected to decrease by 8.72 to 17.68 percent while the winter will decrease by 16.67 to 46.72 percent.

The monthly precipitation comparisons between base and future periods are plotted separately for each month in the Fig. 4-13 to Fig. 4-16. The comparison for the rcp4.5 during mid century (Fig. 4-13) depicts that in the winter season the mean precipitation will decrease across the nine climate ensembles and the least amount of precipitation would occur during the month of July. However, fluctuation in the projected precipitation is found during the summer particularly in the month of December, January, March and April. In December and January, ECEARTH RACMO22T (M4) climate model ensemble exhibits an increase in the mean precipitation with respect to observed precipitation while rest eight climate models showed decrease. Four climate ensembles ECEARTH CCLM (M2), ECEARTH RCA4 (M5), ECEARTH REMO2009 (M6) and HADGEM RCA4 (M9) showed an increase in the mean monthly precipitation while others showed a decrease in March and the similar phenomena with higher magnitude is found in April. Comparing the interquartile ranges, it can be inferred that the more skewedness in precipitation is expected during the winter compared to the summer. Moreover, RCMs nested in the GCM named ECEARTH have estimated higher precipitation.

The comparison for the rcp4.5 during end-century (Fig. 4-14) depicts that in the winter season the mean precipitation will decrease across the climate models with one exception in ECEARTH RACMO22T (M4) during May, June, and August. Similar to the mid-century the least amount of precipitation would occur during the month of July. Moreover, fluctuation in the projected precipitation is found during the summer particularly in the month of January, February and March. Climate ensembles CanESM RCA4 (M1) and ECEARTH RACMO22T (M4) in January, ECEARTH RACMO22T (M4) and ECEARTH REMO2009 (M6) in February, and CanESM RCA4 (M1) and ECEARTH REMO2009 (M6) in March exhibits an increase in the mean precipitation with respect to the base period temperature while rest eight climate models showed decrease. Like the mid-century more skewedness in precipitation is expected during the winter compared to the summer. Moreover, the climate ensemble ECEARTH RACMO22T (M4) has estimated higher precipitation.

The comparison for the rcp8.5 during mid-century (Fig. 4-15) depicts that during the winter season the mean precipitation will decrease across the nine climate models with exception

in May and the least amount of precipitation would occur during the month of July. However, fluctuation in the projected precipitation is found during the summer especially in the month of January, February, March and April. Climate ensembles ECEARTH HIRHAM (M3) and ECEARTH RACMO22T (M4) in January, CanESM RCA4 (M1) and ECEARTH REMO2009 (M6) in February, ECEARTH REMO2009 (M6) in March and ECEARTH HIRHAM (M3), ECEARTH RACMO22T (M4) and ECEARTH REMO2009 (M6) in April exhibits an increased in the mean precipitation relative to observed while other climate ensembles showed decrease. Skewedness in precipitation is expected in both winter and summer precipitation. Moreover, RCMs nested in the GCM named ECEARTH have estimated higher precipitation.

The comparison for the rcp8.5 during mid-century (Fig. 4-16) depicts that the mean monthly precipitation is projected to decrease with a few exceptions in January, May, July and August. The least amount of precipitation would occur during the month of July. Climate model ensembles ECEARTH HIRHAM (M3) and ECEARTH RACMO22T (M4) in January, and ECEARTH RACMO22T (M4) projected increase in the mean precipitation during May, July and August relative to observed while other climate ensembles showed decrease. Moreover, RCMs nested in the GCM named ECEARTH have estimated higher precipitation.

Table 4-4: Percent change in the seasonal and annual mean precipitation in mid and end century periods for rcp 4.5 and 8.5, from the base period in the Olifants River basin

Scenario	Mid-century			End-century		
	Summer	Winter	Annual	Summer	Winter	Annual
rcp4.5	-16.26	-46.72	-26.41	-17.68	-18.57	-17.98
rcp8.5	-8.72	-16.67	-11.37	-15.06	-38.25	-22.79

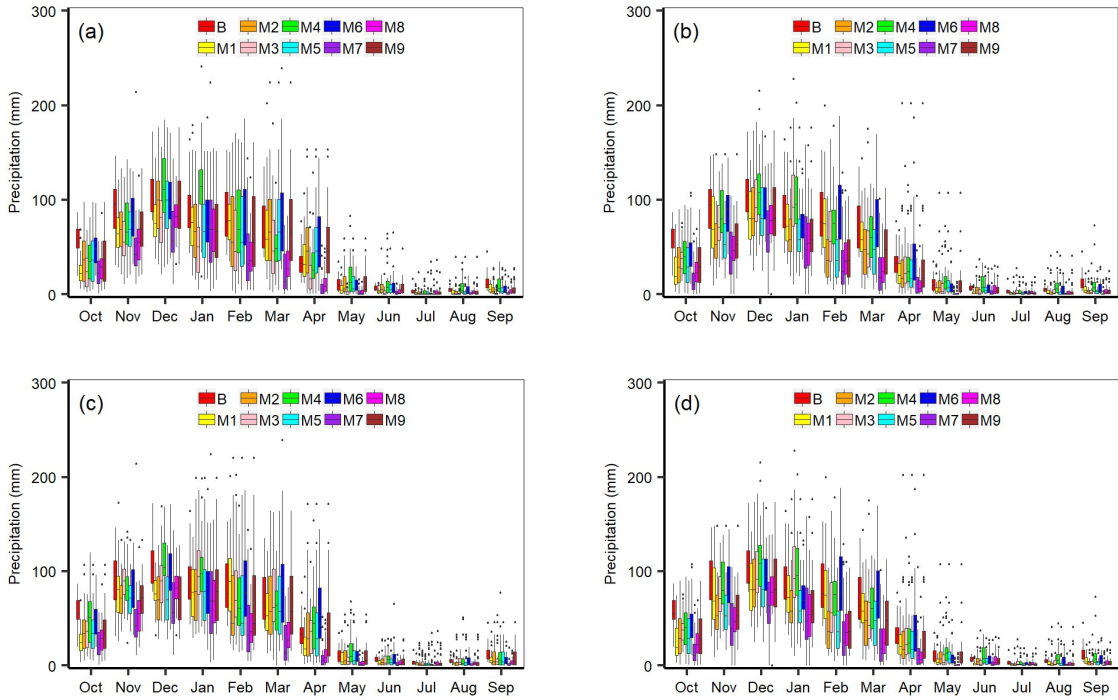


Fig. 4-12 Monthly mean precipitation comparison in the study area between base and future periods for (a) rcp 4.5 mid-century, (b) rcp 4.5 end-century, (c) rcp 8.5 mid-century, and (d) rcp 8.5 end-century

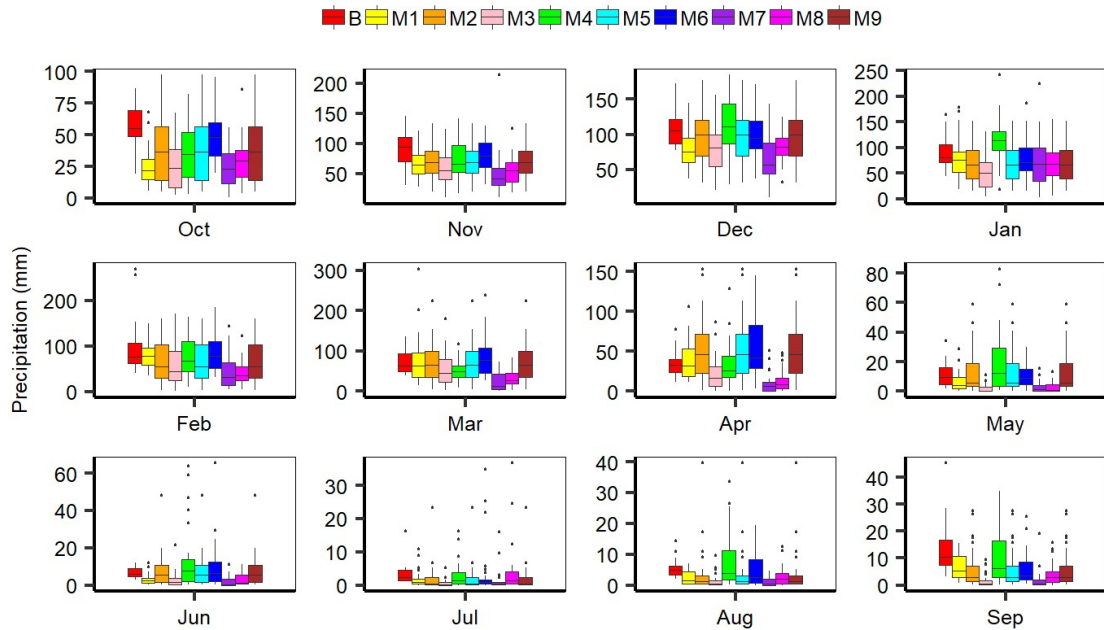


Fig. 4-13 Monthly mean precipitation comparison in the study area between base and mid-century for rcp 4.5 scenario

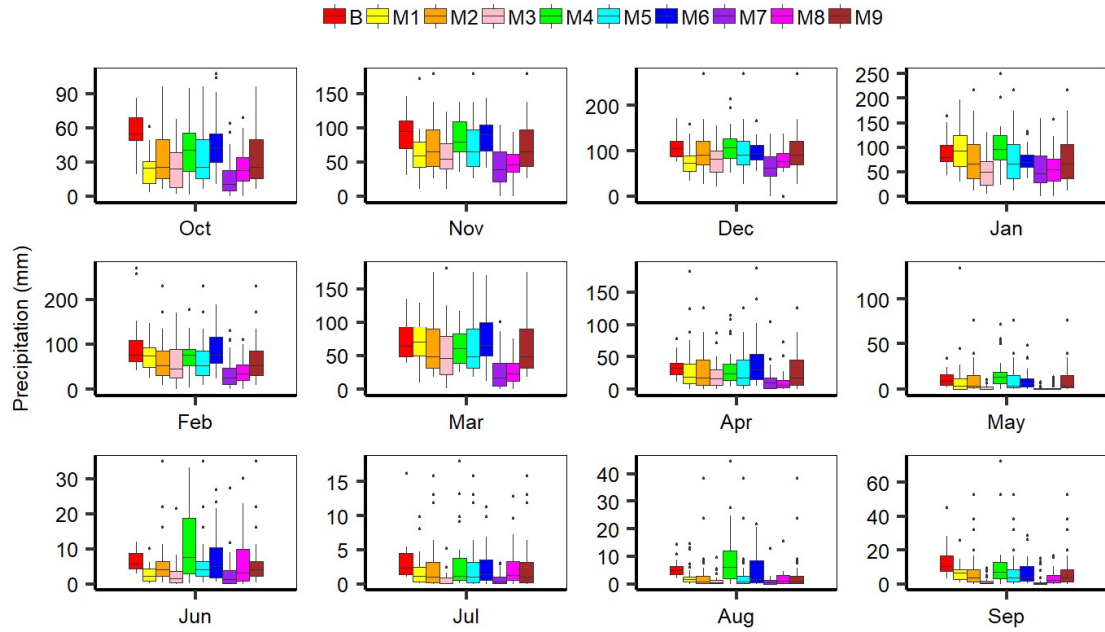


Fig. 4-14 Monthly mean precipitation comparison in the study area between base and end-century for rcp 4.5 scenario

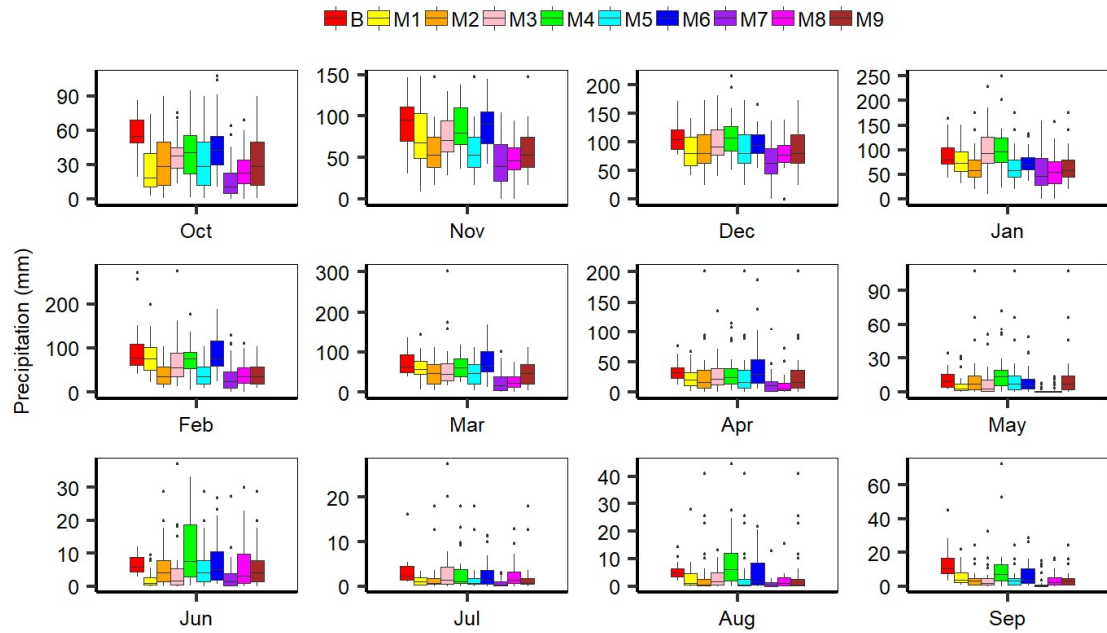


Fig. 4-15 Monthly mean precipitation comparison in the study area between base and mid-century rcp 8.5 scenario

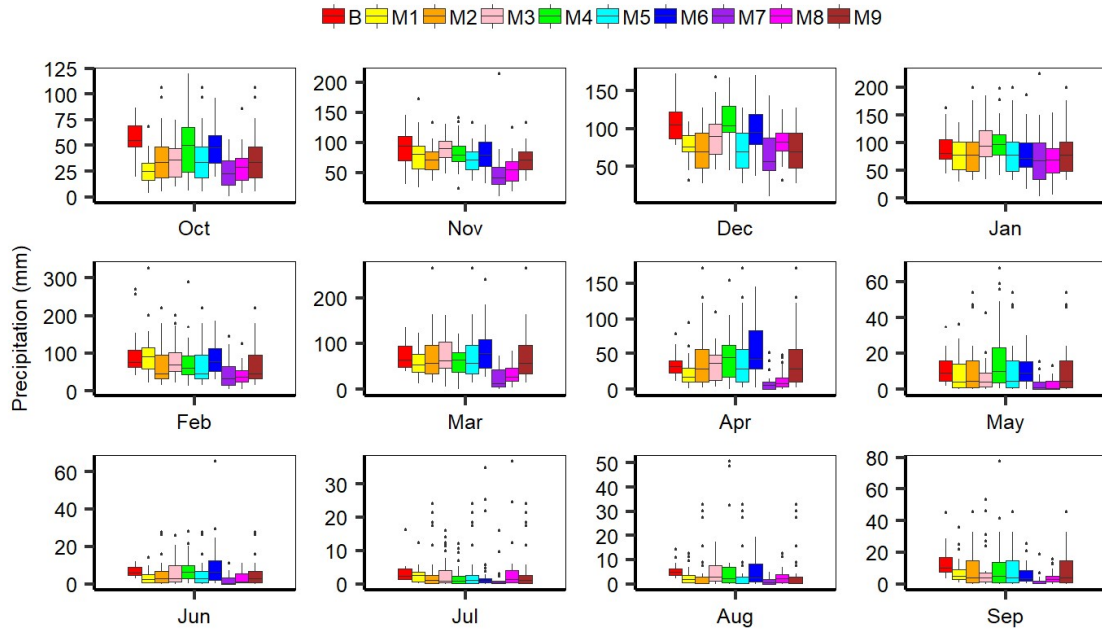


Fig. 4-16 Monthly mean precipitation comparison in the study area between base and end-century for rcp 8.5 scenario

4.7.2 Temperature Projection

Comparisons of the daily maximum temperature (t_{\max}) and daily minimum temperature (t_{\min}) have been carried out at monthly time step between the base period and two future time slots namely (a) mid-century, and (b) end-century for the rcp4.5 and rcp8.5 scenarios (Fig. 4-17 and Fig. 4-18). The results showed that both t_{\max} and t_{\min} are projected to increase in the future with respect to the base period. Moreover, the higher rate of increase in temperature is found in rcp8.5 compared to rcp4.5 for the chosen time periods. The highest temperature rise is projected under rcp8.5 at the end century. The average annual temperature is projected to increase 1.7 °C to 2.6 °C at mid-century while 2.1 °C to 4.6 °C by the 21st century. Moreover, the maximum rise in t_{\max} is projected in summer, while the maximum rise in t_{\min} is projected in the winter (Table 4-5 and 4-6). The projected rate of temperature increase in the Olifants River basin is 0.28 °C to 0.51 °C per decade which is higher than the global average 0.17 °C per decade.

Furthermore, the trend analysis has been performed using well known Mann-Kendall (M-K) test along with Sen's slope (β_1) estimation for both t_{\max} and t_{\min} (Fig. 4-19 and Fig. 4-20). The results of the M-K test for the rcp8.5 mid-century and end-century for t_{\max} and t_{\min} confirm the existence of significant increasing trend (Table 4-9 and Table 4-10). In all the

cases for the rcp8.5, the τ values are positive, and p-value falls under the 0.05 threshold. In case of t_{\max} mid-century, the strongest increasing trend is found in HADGEM RACMO22T(M8) having a β_1 value of 0.088 while for end-century the strongest rising trend has been found in ECEARTH RACMO22T (M4) with β_1 value of 0.103. Coincidentally, similar results with different magnitudes have been found in t_{\min} for the respective cases. Overall, for the rcp8.5 ECEARTH RACMO22T (M4) is exhibiting the highest increasing trend.

The M-K test and Sen’s slope estimation results for the rcp 4.5 mid-century and end-century for t_{\max} and t_{\min} concurred on the increasing trend but differ in the strength of the trend (Table 4-7 and Table 4-8). For instance, only ECEARTH CCLM (M2) and HADGEM CCLM (M7) showed significant trend with p and β_1 values are respectively, 0.007, 0.029 and 0.003, 0.033 in case of the t_{\min} for mid-century and no significant trend has been observed in the rest seven ensembles. Moreover, for the end century no significant trend in t_{\min} has been found among the climate ensembles. Similar phenomenon has been observed for t_{\max} where no significant trend exists for the end-century and during mid-century; only HADGEM CCLM (M7), HADGEM RACMO22T (M8) and HADGEM RACMO22T (M9) are showing significant increasing trend.

Table 4-5: Changes in maximum temperature during future period when compared to those of base period in °C

Scenario	Mid-century			End-century		
	Summer	Winter	Annual	Summer	Winter	Annual
rcp4.5	2.12	1.74	1.96	2.49	1.96	2.27
rcp8.5	2.79	2.32	2.59	4.82	4.16	4.55

Table 4-6: Change in minimum temperature during future period when compared to those of base period in °C

Scenario	Mid-century			End-century		
	Summer	Winter	Annual	Summer	Winter	Annual
rcp4.5	1.81	1.62	1.73	2.14	2.12	2.13
rcp8.5	2.26	2.28	2.27	4.10	4.12	4.11

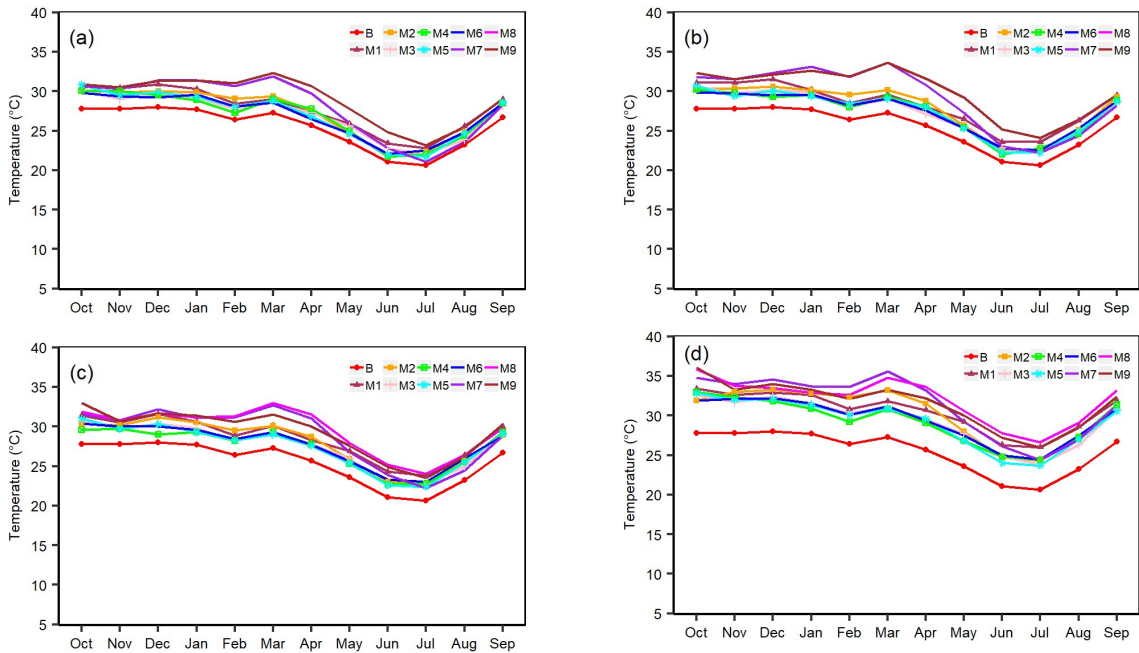


Fig. 4-17 Daily maximum temperature comparison at monthly time step between base and future periods for (a) rcp 4.5 mid-century, (b) rcp 4.5 end-century, (c) rcp 8.5 mid-century and iv) rcp 8.5 end-century

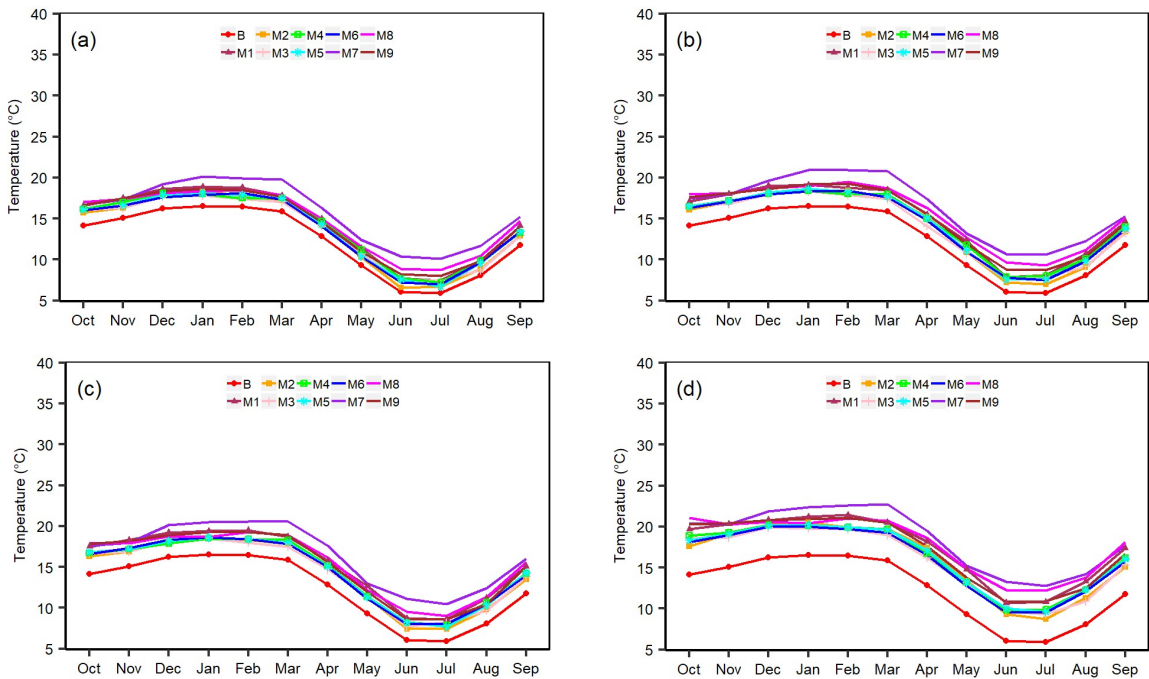


Fig. 4-18 Daily minimum temperature comparison at monthly time step between base and future periods for (a) rcp 4.5 mid-century, (b) rcp 4.5 end-century, (c) rcp 8.5 mid-century and iv) rcp 8.5 end-century

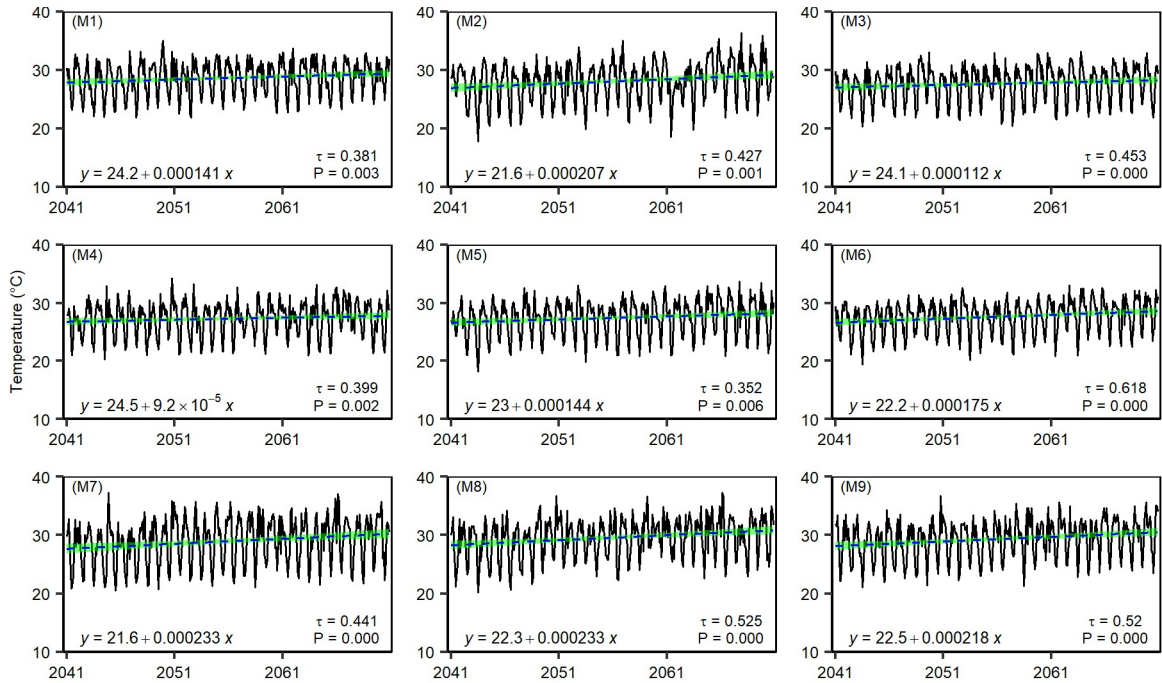


Fig. 4-19 Monthly timeseries, linear regression analysis and annual Mann-Kendall statistics of daily maximum temperature for rcp 8.5 mid-century for the study area.

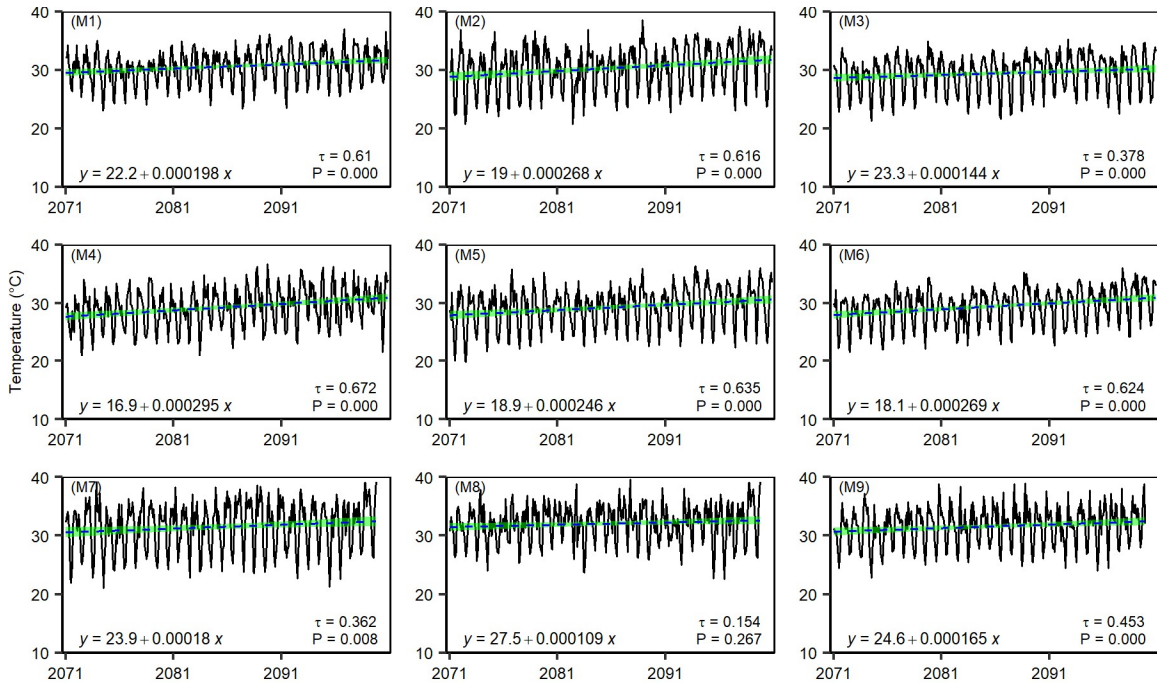


Fig. 4-20 Monthly timeseries, linear regression analysis and annual Mann-Kendall statistics of daily maximum temperature for rcp 8.5 end-century for the study area. The black solid line, the blue dashed line and the green patch are representing the monthly temperature timeseries, linear regression line and ranges, respectively.

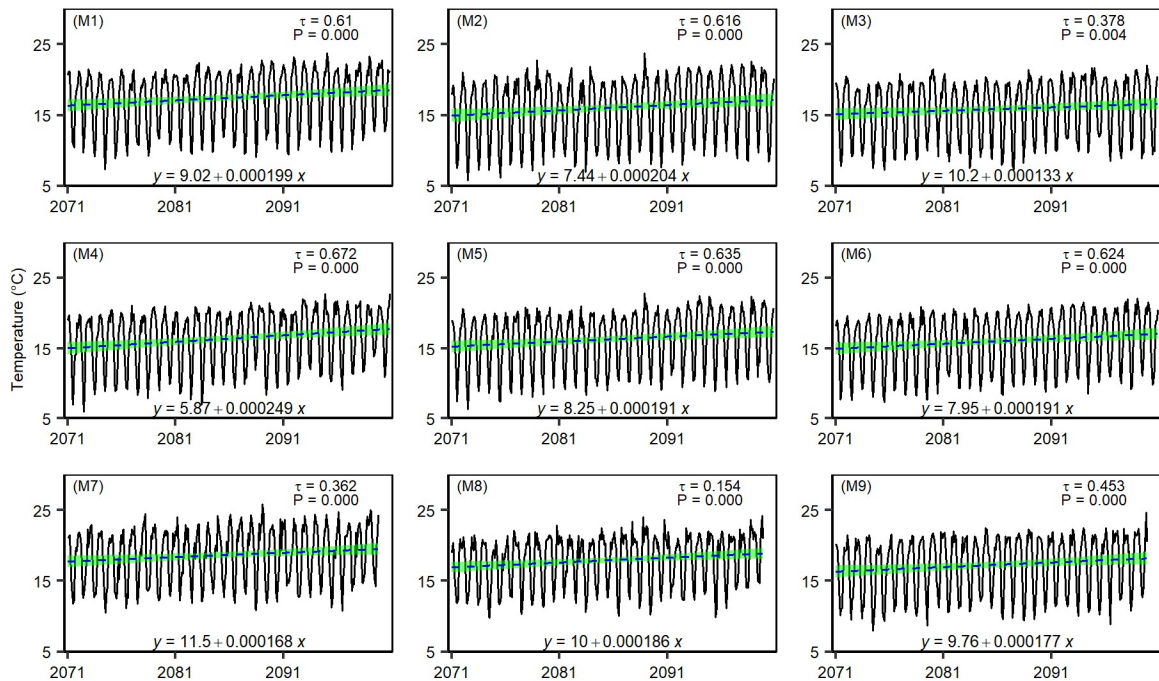


Fig. 4-21 Monthly timeseries, linear regression analysis and annual Mann-Kendall statistics of daily maximum temperature for rcp 8.5 mid-century for the study area.

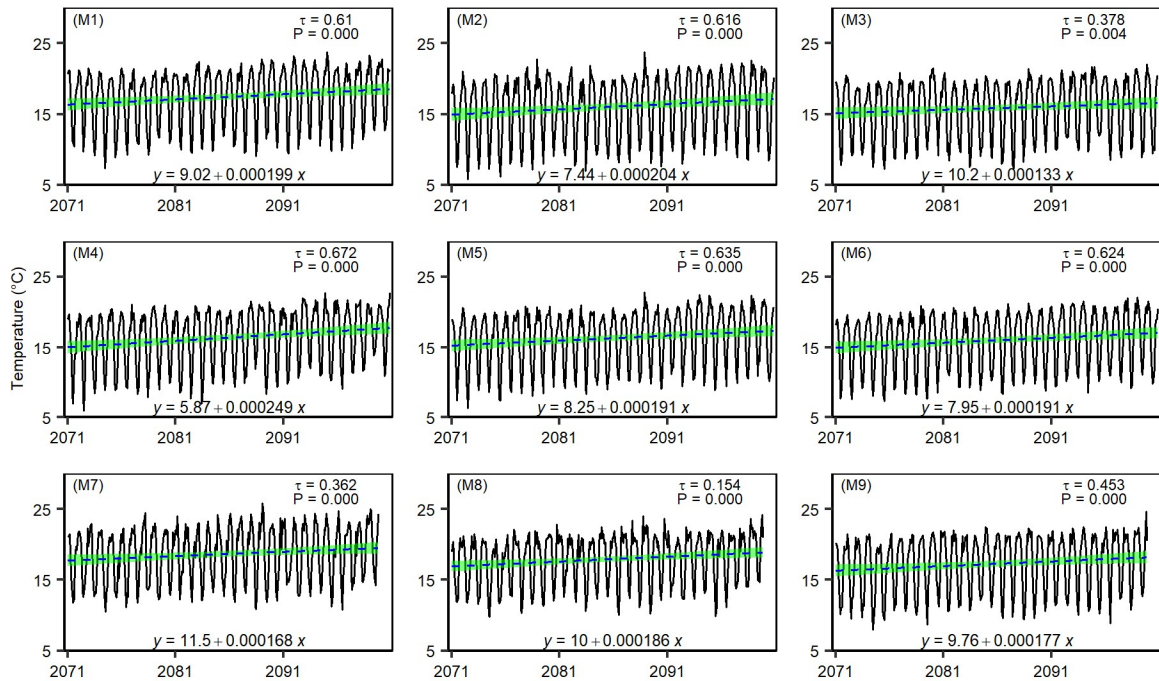


Fig. 4-22 Monthly timeseries, linear regression analysis and annual Mann-Kendall statistics of daily maximum temperature for rcp 8.5 end-century for the study area. The black solid line, the blue dashed line and the green patch are representing the monthly temperature timeseries, linear regression line and ranges, respectively.

Table 4-7: Statistics of Mann-Kendall analysis (τ and P) and Sen’s slope (β_1) of daily minimum temperature at annual time step during the future periods for the rcp 4.5 scenario

Ensemble	t_{\min} mid-century			t_{\min} end-century		
	τ	P	β_1	τ	P	β_1
M1	0.048	0.720	0.005	0.138	0.312	0.006
M2	0.348	0.007	0.029	0.258	0.054	0.014
M3	0.190	0.150	0.009	0.066	0.628	0.000
M4	0.132	0.321	0.008	0.210	0.120	0.010
M5	0.329	0.012	0.023	0.277	0.040	0.014
M6	0.327	0.011	0.025	0.169	0.214	0.006
M7	0.382	0.003	0.033	0.032	0.827	0.000
M8	0.337	0.010	0.025	0.047	0.750	0.000
M9	0.298	0.023	0.018	0.107	0.445	0.008

Table 4-8: Statistics of Mann-Kendall analysis (τ and P) and Sen’s slope (β_1) of daily maximum temperature at annual time step during the future periods for the rcp 4.5 scenario

Ensemble	t_{\max} mid-century			t_{\max} end-century		
	τ	P	β_1	τ	P	β_1
M1	0.207	0.109	0.025	0.021	0.886	0.000
M2	0.175	0.174	0.029	0.191	0.147	0.039
M3	0.042	0.759	0.000	0.024	0.990	0.000
M4	0.075	0.574	0.011	0.064	0.640	0.004
M5	0.221	0.088	0.029	0.130	0.330	0.013
M6	0.166	0.201	0.016	0.146	0.274	0.017
M7	0.331	0.010	0.053	0.059	0.160	0.006
M8	0.301	0.020	0.037	0.193	0.677	0.029
M9	0.301	0.020	0.037	0.193	0.160	0.017

Table 4-9: Statistics of Mann-Kendall analysis (τ and P) and Sen’s slope (β_1) of daily minimum temperature at annual time step during the future periods for the rcp 8.5 scenario

Ensemble	t_{\min} mid-century			t_{\min} end-century		
	τ	P	β_1	τ	P	β_1
M1	0.497	0.0E+00	0.050	0.660	5.9E-07	0.075
M2	0.451	4.0E-04	0.050	0.647	8.3E-07	0.080
M3	0.426	9.0E-04	0.030	0.433	1.0E-03	0.053
M4	0.543	2.7E-05	0.038	0.723	2.2E-16	0.088
M5	0.526	5.2E-05	0.038	0.717	1.2E-07	0.074
M6	0.525	6.5E-05	0.041	0.769	2.3E-16	0.067
M7	0.617	2.1E-06	0.071	0.539	8.2E-05	0.050
M8	0.558	1.5E-05	0.067	0.560	2.6E-05	0.071
M9	0.574	8.1E-06	0.064	0.677	4.8E-07	0.055

Table 4-10: Statistics of Mann-Kendall analysis (τ and P) and Sen’s slope (β_1) of daily maximum temperature at annual time step during the future periods for the rcp 8.5 scenario

Ensemble	t_{\max} mid-century			t_{\max} end-century		
	τ	P	β_1	τ	P	β_1
M1	0.381	3.2E-03	0.042	0.610	3.4E-06	0.074
M2	0.427	9.0E-04	0.089	0.616	2.4E-06	0.100
M3	0.453	4.0E-04	0.050	0.378	3.8E-03	0.050
M4	0.399	2.0E-03	0.033	0.672	2.4E-07	0.103
M5	0.352	6.4E-03	0.041	0.635	1.3E-06	0.088
M6	0.618	1.8E-06	0.067	0.624	1.8E-06	0.095
M7	0.441	5.0E-04	0.080	0.362	8.0E-03	0.037
M8	0.525	4.4E-05	0.088	0.154	2.7E-01	0.017
M9	0.520	5.4E-05	0.071	0.453	7.0E-04	0.045

4.7.3 Flow Projection

The monthly average flow comparison at B7H015 between the base period and two future time horizons (a) mid-century and (b) end-century for rcp4.5 and rcp8.5 is presented in Fig. 4-23 as a truncated boxplot to better capture the quartiles. However, detailed boxplots for each month are compared for rcp4.5 mid-century (Fig. 4-24), rcp4.5 end-century (Fig. 4-25), rcp8.5 mid-century (Fig.4-26), and rcp8.5 end-century (Fig.4-27) to complement the comparison. Overall, the decrease in the mean annual flow is projected with significant fluctuations at monthly step. For instance, in case of rcp4.5 mid-century fluctuations in the simulated flows are found throughout the year except decrease in the November and December. The seasonal flow distribution during the future periods are found similar to the base period with varying magnitudes. The highest number of extreme events i.e. floods are projected to occur during February and March.

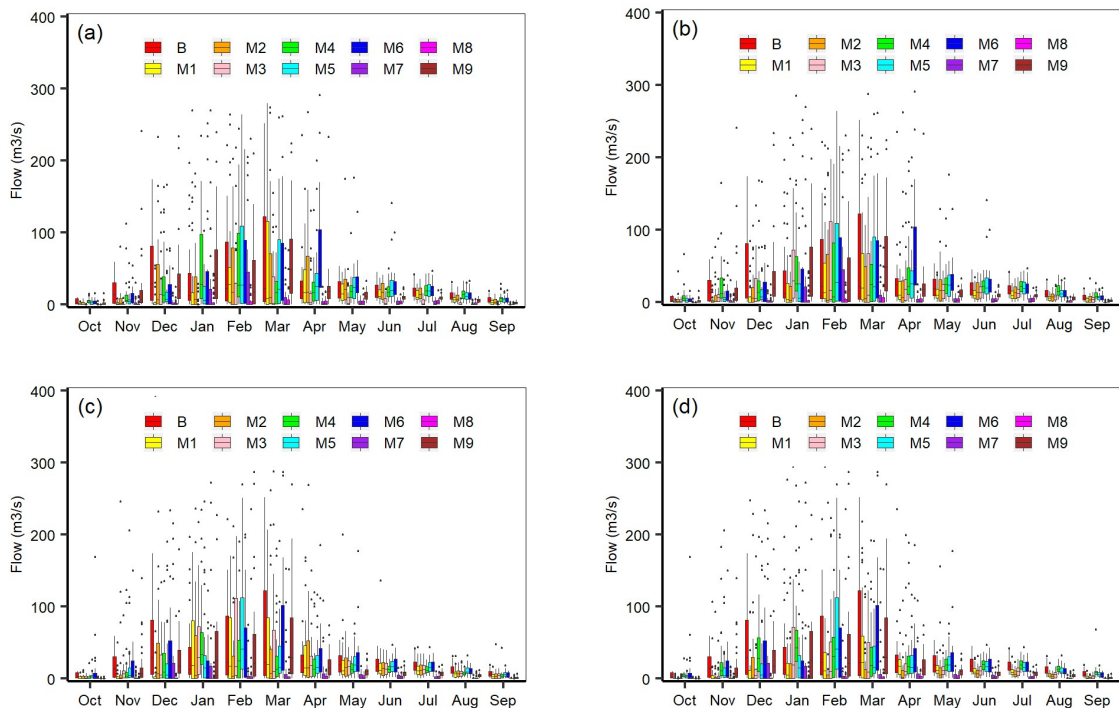


Fig. 4-23 Monthly mean flow comparison between base and future periods at Mamba (B7H015); (a) rcp 4.5 mid-century, (b) rcp 4.5 end-century, (c) rcp 8.5 mid-century, and (d) rcp 8.5 end-century

In case of rcp4.5 end-century, the mean monthly flow is projected to decrease throughout the year except in the case of M4 (ECEARTH RACMO22T) climate ensemble in January. More frequent extreme events are projected during the summer compare to winter. Similar phenomenon like rcp 4.5 is found during the mid-century and end-century of rcp8.5. A wider range of flow is projected in the summer compare to the winter thus the uncertainty in the summer flow will be higher. In general, more frequent extreme events i.e. floods are predicted in the future compared to the historical period.

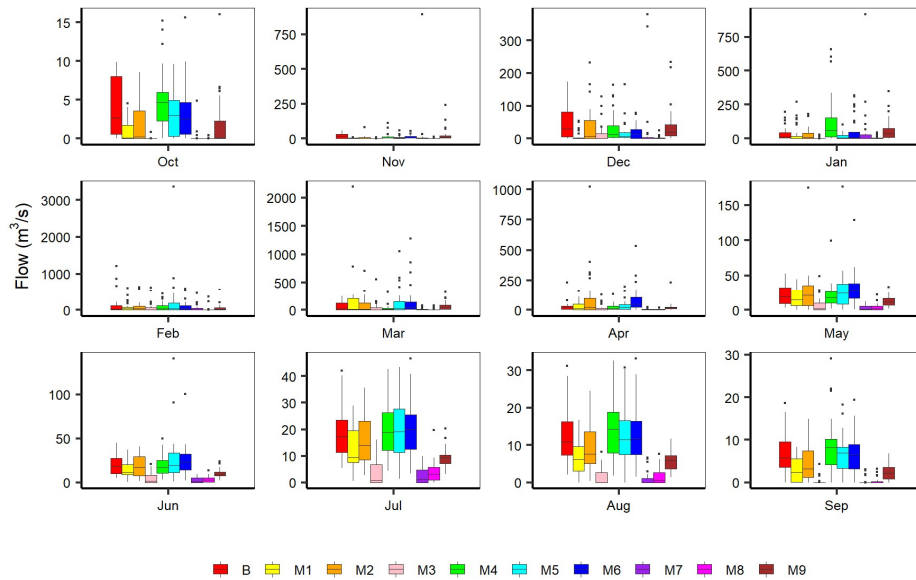


Fig. 4-24 Boxplot of monthly mean flow comparison at Mamba for rcp4.5 mid-century

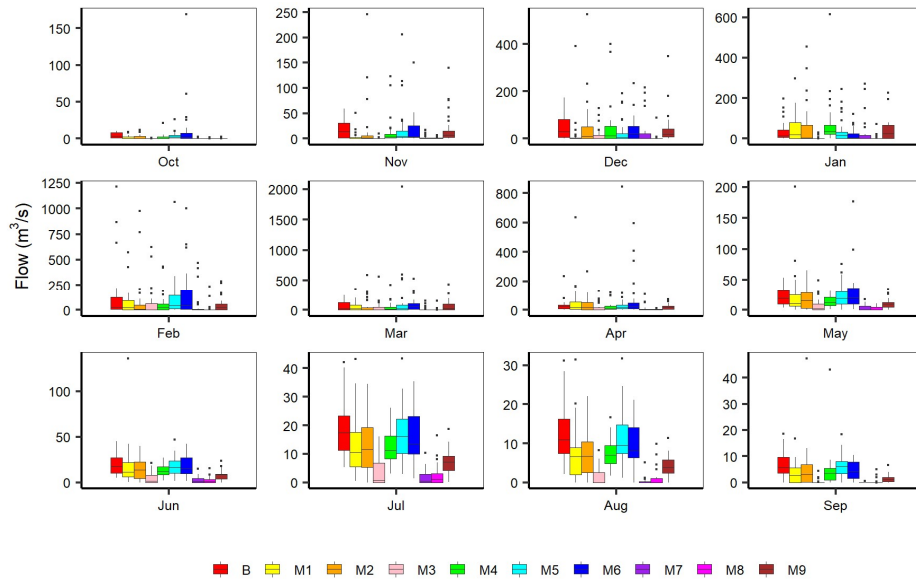


Fig. 4-25 Boxplot of monthly mean flow comparison at Mamba for rcp4.5 end-century

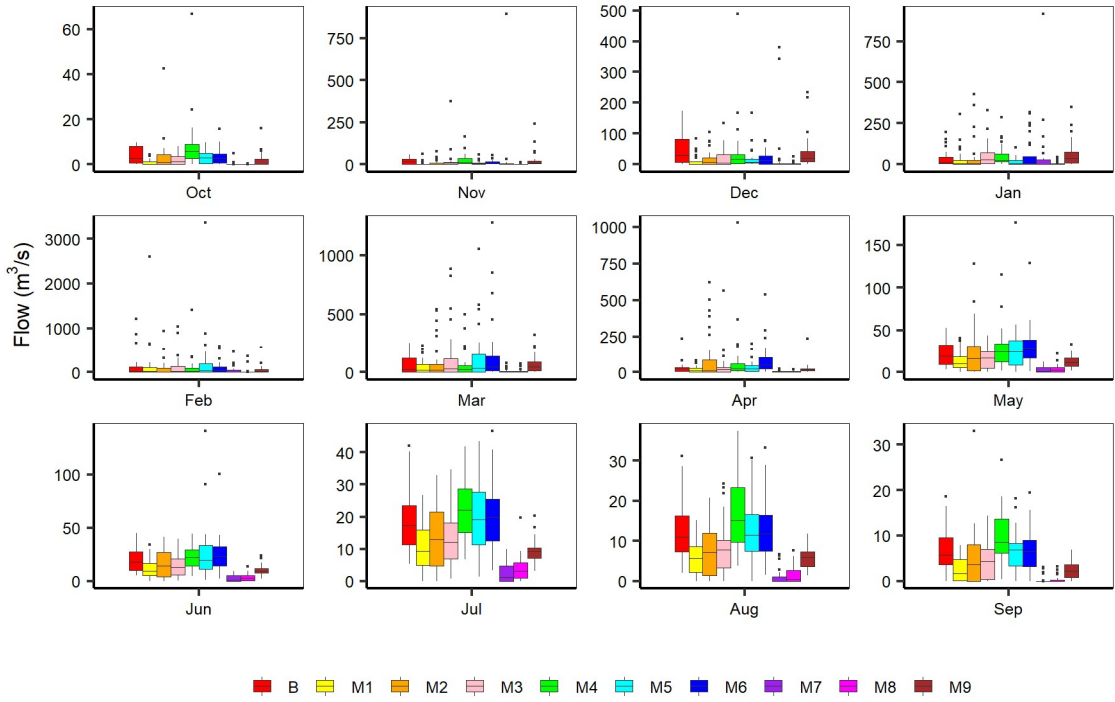


Fig. 4-26 Boxplot of monthly mean flow comparison at Mamba for rcp8.5 mid-century

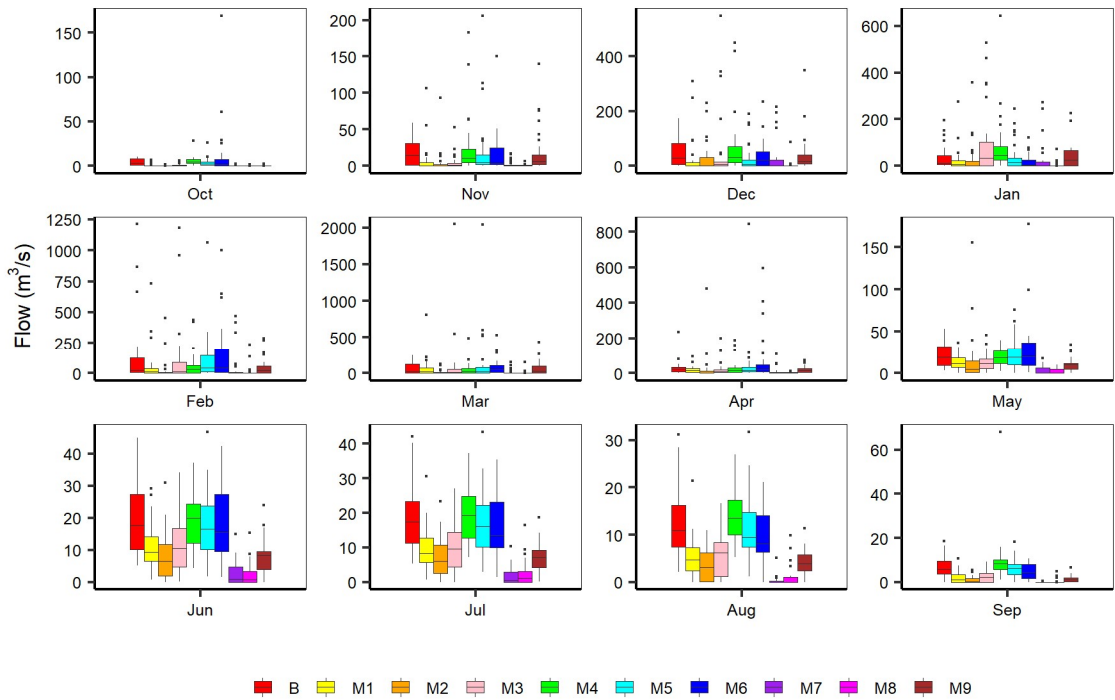


Fig. 4-27 Boxplot of monthly mean flow comparison at Mamba for rcp8.5 end-century

4.7.4 Hydrograph Comparison

The hydrograph is compared between the base period and two future periods a) mid-century and b) end century for two different scenarios rcp4.5 and rcp8.5 (Fig. 4-28) at Mamba station (B7H015). The historical flow computed from the average value of the base period. The median future flow is calculated from the median of average values of nine different climate ensembles. The future flow band is determined from the minimum and maximum value of nine different climate ensembles for that month. It is apparent from the Fig. 4-28 that the summer flow uncertainty is higher than that of winter. Moreover, the flow uncertainty is lower at the end century period compared to mid-century period. In addition, the peak flow is expected to shift towards March from February at the end century.

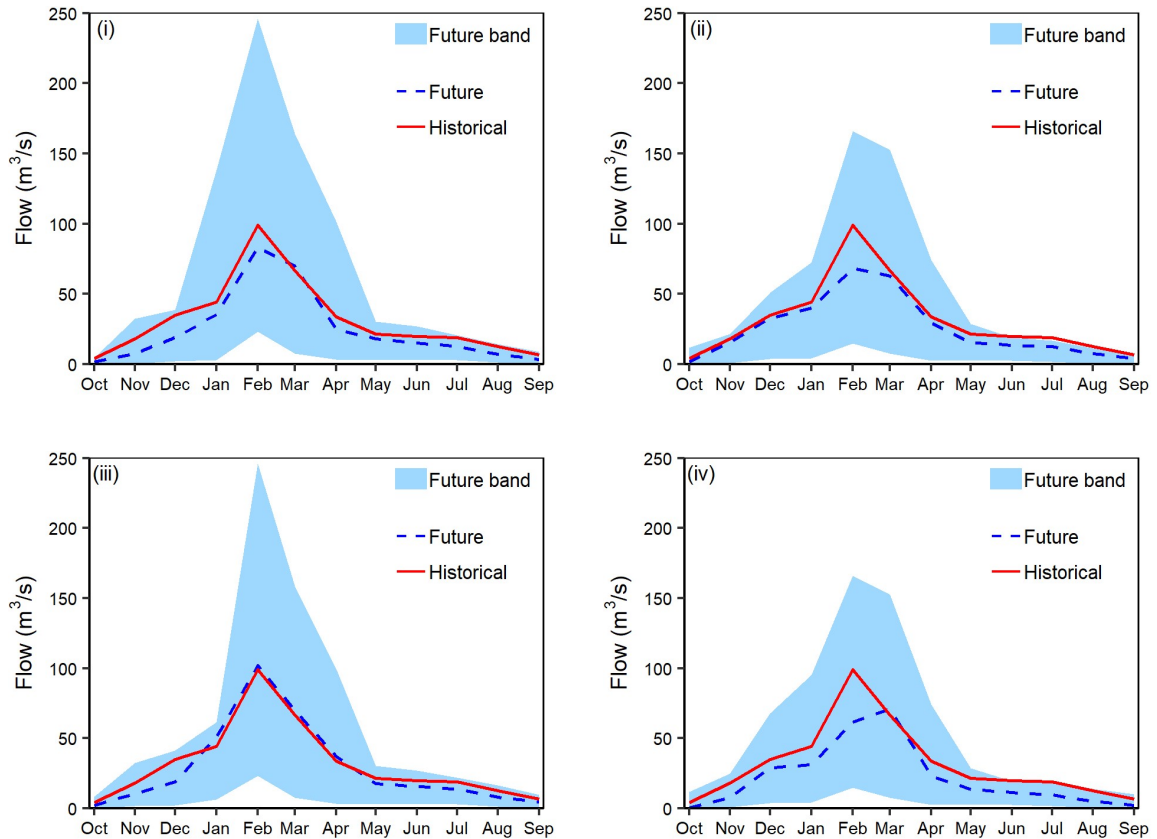


Fig. 4-28 Historical and future flow hydrographs with ranges for, (i) rcp 4.5 mid-century, (ii) rcp 4.5 end-century, (iii) rcp 8.5 mid-century, and (iv) rcp 8.5 end-century at Mamba

4.7.5 Flow Duration Curve (FDC) Comparison

In 1998, South Africa promulgated the National Water Act which introduced the term “ecological reserve” to meet basic human needs and environmental sustainability. Kruger National Park (KNP) is located at the downstream of the Olifants river and a minimum flow $0.5 \text{ m}^3/\text{s}$ is set at B7H015 station for ensuring the ecological reserve of the KNP (Aurecon, 2011). The FDC is compared between the base period and two future periods i.e. (a) mid-century and b) end-century for two different scenarios rcp4.5 and rcp8.5 (Fig. 4-29) at B7H015. The historical flow computed from the average value of the base period. The median future flow is calculated from the median of average values of nine different climate ensembles. The future flow band is determined from the minimum and maximum value of nine different climate ensembles for that month. The FDC’s indicate that the unavailability of the minimum flow for ecological reverse will increase by 2 to 12 percent (Table 4-11)

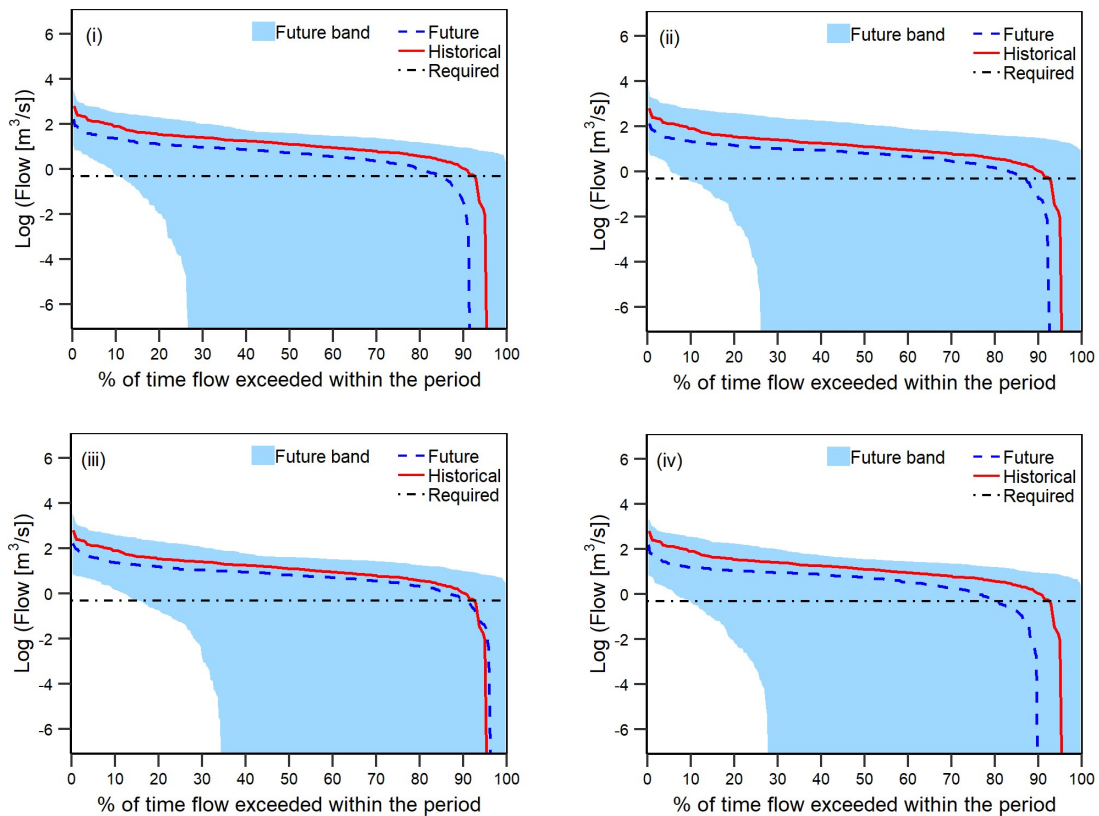


Fig. 4-29 Historical and future Flow Duration Curves (FDC’s) for (i) rcp 4.5 mid-century, (ii) rcp 4.5 end-century, (iii) rcp 8.5 mid-century, and (iv) rcp 8.5 end-century at Mamba

Table 4-11: Flow exceedance for minimum flow (0.5 m³/s) at Mamba

Period	Base	Rcp4.5	Rcp8.5
Base-period	92%	-	-
Mid-century	-	84%	90%
End-century	-	87%	80%

4.8 Spatial Distribution of Precipitation Change

Spatial distribution of Mean Annual Precipitation (MAP) changes in each subbasin between the base and future periods are analyzed for two different scenarios rcp4.5 and rcp8.5 (Fig. 4-30). The MAP is projected to decrease over the Olifants River basin with some exceptions in the mid veld area near the escarpment. The difference is computed by subtracting MAP observed from median value of annual average precipitation of nine climate ensembles thus a negative value indicates a decrease in the future and vice versa. The values indicate that on the average a decrease of 20, 23, 17.6 and 24 percent decrease in MAP are likely to occur for rcp4.5 during mid-century, rcp4.5 end-century, rcp8.5 mid-century and rcp8.5 end-century, respectively with respect to the base period. The difference in projected precipitation varied significantly across the basin. For instance, for rcp4.5 mid-century the variation ranges from -1.6 to 49.0 percent with -25.0 percent average in the lowveld region, -54.8 to 24.9 percent with -16.5 percent average in the mid-veld region and -5.8 to -29.1 percent with -18.0 percent average in the highveld region. The similar phenomenon observed for the rcp4.5 end-century, rcp8.5 mid-century, and rcp8.5 end-century. Spatial distribution of projected precipitation for different climate ensembles, periods and emission scenarios are presented in the annexure 3. In general, high spatial variation in the precipitation similar to historical will remain in the future.

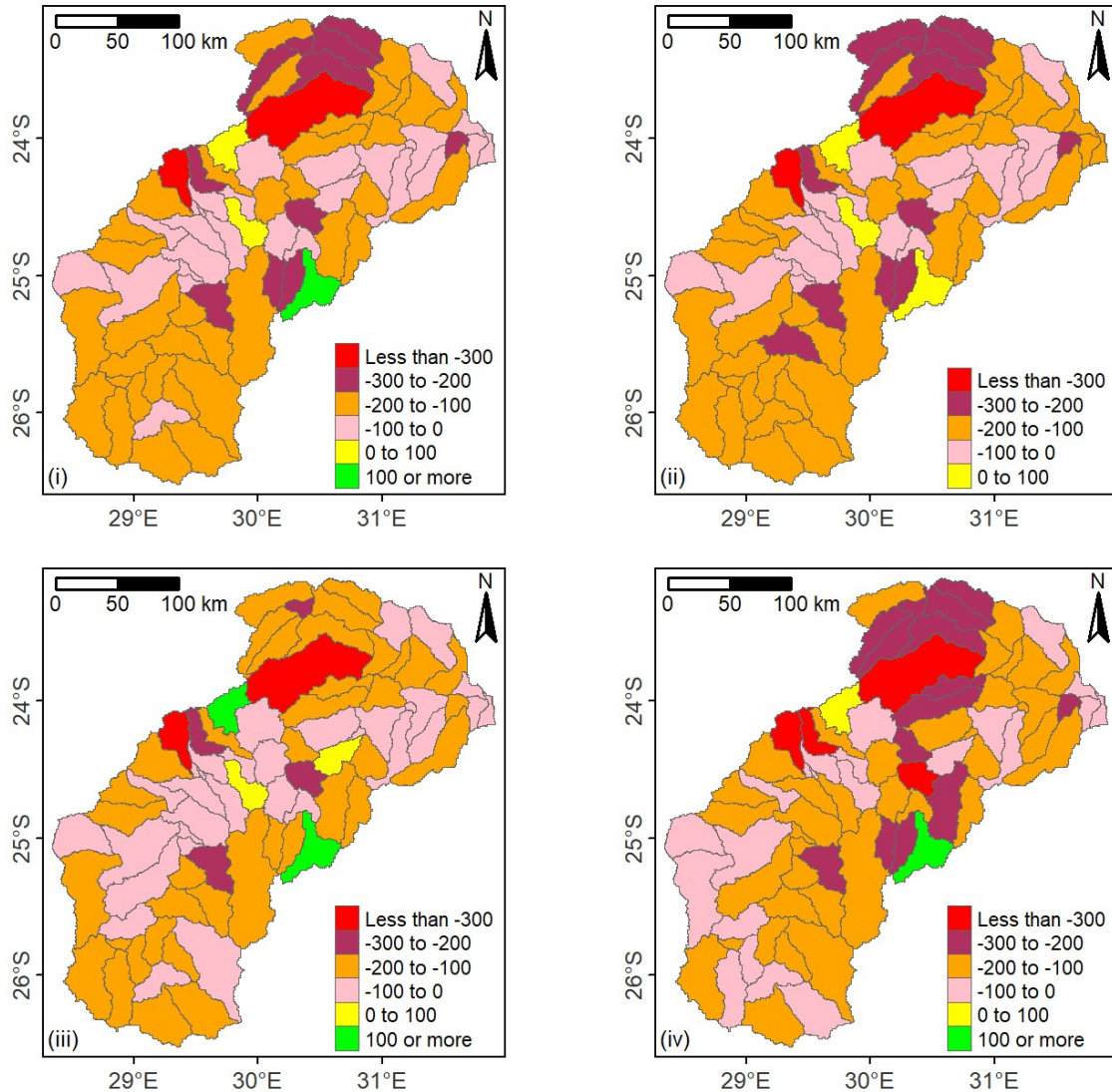


Fig. 4-30 Change in precipitation across the Olifants River basin from base to (i) rcp 4.5 mid-century, (ii) rcp 4.5 end-century, (iii) rcp 8.5 mid-century, and (iv) rcp 8.5 end-century

4.9 Spatial Distribution of Potential Evapotranspiration Change

The difference between mean annual Potential Evapotranspiration (PET) in each of the subbasins between the base and future periods are plotted for rcp4.5 and rcp8.5 (Fig. 4-31). The PET is projected to increase over the Olifants River basin with some exceptions and the highest increase is projected at the end-century under rcp8.5. The difference is computed by subtracting base period value from median value of annual average PET of nine climate ensembles thus a positive value indicates an increase in the future. The

difference in mean annual PET varied gently across the basin. For instance, for rcp4.5 mid-century the variation ranges from -1.4 to 13.0 percent with 6.9 percent average in the lowveld region, -1.5 to 14.4 percent with 5.7 percent average in the mid-velde region and -1.1 to 11.4 percent with 5.4 percent average in the highveld region. The similar phenomenon observed for the rcp4.5 end-century, rcp8.5 mid-century and rcp8.5 end-century. Spatial distribution of projected PET for different climate ensembles, periods and emission scenarios are presented in Annexure 5.

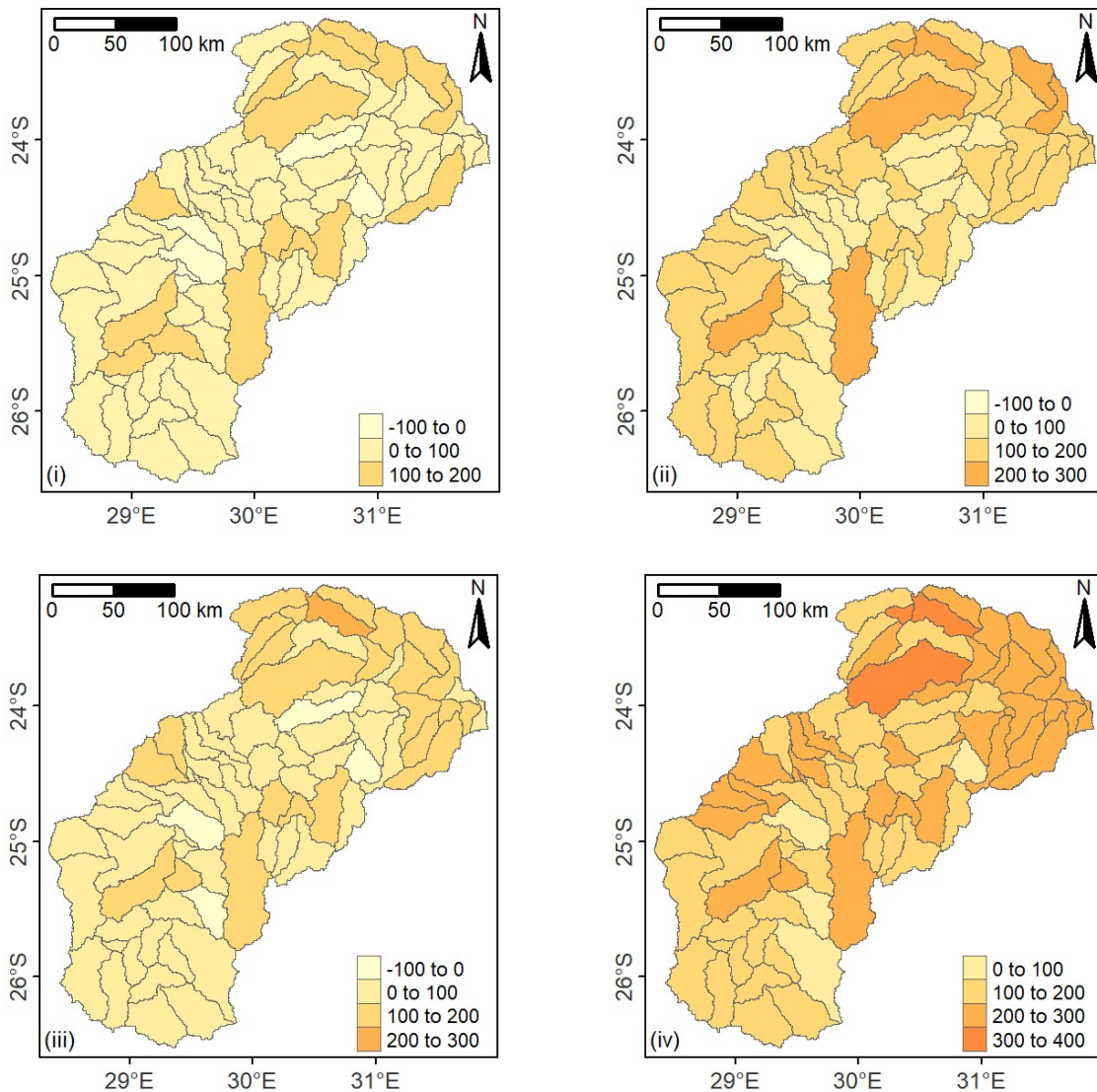


Fig. 4-31 Change in PET across the Olifants River Basin from base to (i) rcp 4.5 mid-century, (ii) rcp 4.5 end-century, (iii) rcp 8.5 mid-century, and (iv) rcp 8.5 end-century

4.10 Spatial Distribution of Water Yield Change

Water yield changes in each subbasin between the base and future periods are plotted for rcp4.5 and rcp8.5 (Fig. 4-32). The water yield is projected to decrease over the Olifants River basin with some exceptions and the highest decrease is projected at the end-century under rcp8.5. The difference is computed by subtracting the base period value from median value of annual average water yield of nine climate ensembles for each subbasin. Like precipitation, the water yield varied significantly across the basin.

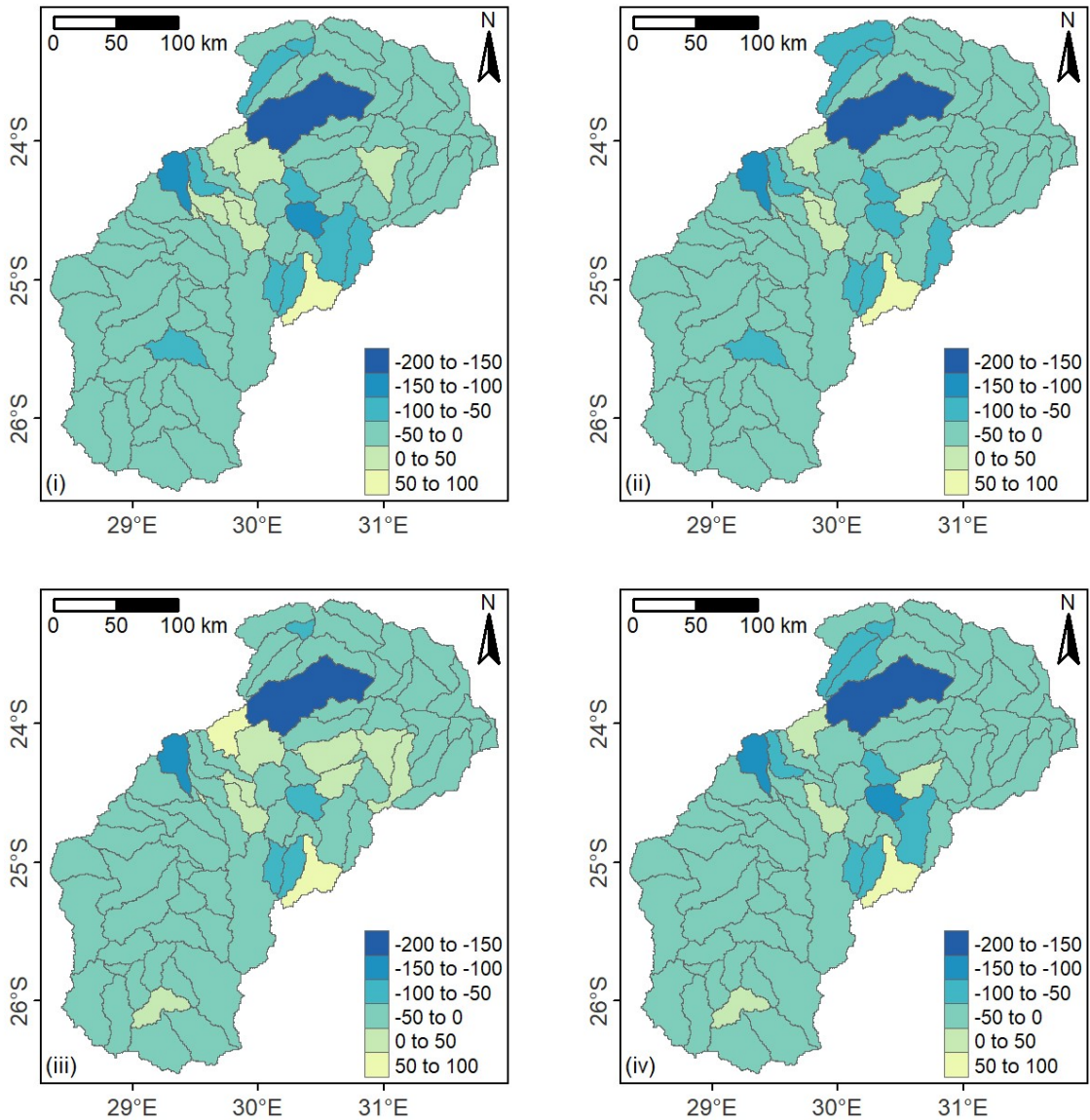


Fig. 4-32 Change in water yield across the Olifants River Basin from base to (i) rcp 4.5 mid-century, (ii) rcp 4.5 end-century, (iii) rcp 8.5 mid-century, and (iv) rcp 8.5 end-century

On an average, the water yield will decrease 43, 18 and 34 percent in the lowveld, mid-veld and high veld region, respectively for rcp4.5 mid-century. Similar phenomena observed for other cases. Spatial distribution of projected yield for different climate ensembles, periods and emission scenarios are presented in the Annexure 6.

CHAPTER V

CONCLUSIONS AND RECOMMENDATIONS

5.1 Conclusions

Understanding the impact of climate change on hydrological regime at watershed scale is very important for sustainable development of water resources. A hydrological model was developed using Soil and Water Assessment Tool (SWAT) to investigate the impact of climate change in the Olifants River basin, South Africa. The model was calibrated and validated using monthly observed streamflow data for the period 2003-2008 and 2009-2012 respectively at two different locations. The calibrated model was forced with the bias corrected future climate data to predict the impact of climate change under rcp4.5 and rcp8.5 for mid-century (2041-2070) and end-century (2071-2100) period. Finally, the predicted streamflow for various climate ensembles are compared with the established minimum flow requirement for Kruger National Park (KNP).

Widely accepted model performance indices like Nash Sutcliffe Efficiency (NSE), Kling-Gupta Efficiency (KGE) and Percent Bias (PBIAS) are used to determine the SWAT model performance. NSE values are found to be 0.60 and 0.56 during the calibration and validation periods, respectively at Mamba (B7H015) station. KGE values are calculated to be 0.80 and 0.63, whereas PBIAS are found to be -2.21% and -0.47% during the calibration and validation period, respectively. At Blyde (B6H005) station, NSE values are found to be 0.52 and 0.74 during the calibration and validation period, respectively and KGE values are 0.65 and 0.81 for the respective periods. The PBIAS are found to be 19.26% and 8.82% during the calibration and validation period, respectively. These statistical indices demonstrate that the SWAT model realistically represents the basin hydrology.

The water budget analysis showed that the Evapotranspiration (ET) is the largest component (76%) and Potential Evapotranspiration (PET) is approximately 3 times higher than ET which indicate the necessity of irrigation for cropping. The surface flow and baseflow are 77% and 23% of the total flow, respectively. Monthly and seasonal water yield varied significantly due to the seasonal variation of the precipitation. Most of the

water yield (70%-90%) observed during the summer months (October to April). These values fall within the range of the reported values for the Olifants basin.

Nine different climate model ensembles were analysed in this study and significant temperature rise (0.28 °C to 0.51 °C per decade) was found from the base period. The predicted temperature would rise at a higher rate than the global average. The mean annual precipitation would decrease for both summer and winter period. However, the seasonal distribution pattern for precipitation would remain similar, which means most of the rainfall would occur during October to April period. Moreover, reduction in the surface runoff was found in the future period compared to base period. In addition, frequent extreme flow events were predicted which indicate there will be frequent severe flood and drought in the future.

The predicted flows were compared to the benchmark flow (0.5 m³/s) at Mamba station to assess the availability of minimum flow to maintain environmental flow for Kruger National Park (KNP). The results indicate that the benchmark minimum flow would not be available for a range of 2%-12% time for the future period.

5.2 Recommendations

Plausible scenarios of socioeconomic and emission changes are used as the inputs of the climate models to generate the future climatic variables. Abrupt changes in the climate model inputs, such as energy usage, landuse pattern, air pollution and greenhouse gas emission from the predicted plausible scenarios will invalidate the climate change projections and consequently the present study results. Moreover, the consumptive water use has profound effect on the streamflow simulation. Drastic changes in the elements like demographic pattern, landuse, etc., which could lead to the abrupt changes in the water use pattern will necessitate the revision of the findings. Therefore, periodic update of the water usage pattern and emission scenarios are recommended.

Hydrological models are useful tools for planning, operation and management of water resources. The uncertainty of the present model is not investigated at depth due to the time constraints; therefore, the results should be used with caution. Further studies can include

uncertainty analysis of hydrological model, groundwater-surfacewater interaction and water quality modelling.

REFERENCES

- Abbaspour, K.C., Rouholahnejad, E., Vaghefi, S., Srinivasan, R., Yang, H., Kløve, B., 2015. A continental-scale hydrology and water quality model for Europe: Calibration and uncertainty of a high-resolution large-scale SWAT model. *Journal of Hydrology* 524, 733–752. <https://doi.org/10.1016/j.jhydrol.2015.03.027>
- Abbott, M.B., Bathurst, J.C., Cunge, J.A., O’Connell, P.E., Rasmussen, J., 1986. An introduction to the European Hydrological System — Systeme Hydrologique European, “SHE”, 1: History and philosophy of a physically-based, distributed modelling system. *Journal of Hydrology* 87, 45–59. [https://doi.org/10.1016/0022-1694\(86\)90114-9](https://doi.org/10.1016/0022-1694(86)90114-9)
- Akpalu, W., Rashid, H.M., Ringler, C., 2011. Climate variability and maize yield in the Limpopo region of South Africa: Results from GME and MELE methods. *Climate and Development* 3, 114–122. <https://doi.org/10.1080/17565529.2011.582269>
- Al-Amin, S., Abdul-Aziz, O.I., 2013. Challenges in mechanistic and empirical modelling of stormwater: review and perspectives: mechanistic and empirical modelling of stormwater. *Irrigation and Drainage* 62, 20–28. <https://doi.org/10.1002/ird.1804>
- Annandale, J.G., Jovanovic, N.Z., Pretorius, J.J.B., Lorentz, S.A., Rethman, N.F.G., Tanner, P.D., 2001. Gypsiferous mine water use in irrigation on rehabilitated open-cast mine land: Crop Production, soil water and salt balance. *Ecological Engineering* 17, 153–164. [https://doi.org/10.1016/S0925-8574\(00\)00155-5](https://doi.org/10.1016/S0925-8574(00)00155-5)
- Arnell, N., 1999. Climate change and global water resources. *Global Environmental Change* 9, S31–S49. [https://doi.org/10.1016/S0959-3780\(99\)00017-5](https://doi.org/10.1016/S0959-3780(99)00017-5)
- Arnold, J.G., Fohrer, N., 2005. SWAT2000: current capabilities and research opportunities in applied watershed modelling. *Hydrological Processes* 19, 563–572. <https://doi.org/10.1002/hyp.5611>
- Arnold, J.G., Moriasi, D.N., Gassman, P.W., Abbaspour, K.C., White, M.J., Srinivasan, R., ..., Van Liew, M.W., 2012. SWAT: Model use, calibration, and validation. *Transactions of the ASABE* 55, 1491–1508.
- Arnold, J.G., Srinivasan, R., Muttiah, R.S., Williams, J.R., 1998a. Large Area Hydrologic Modeling And Assessment Part I: Model Development. *Journal of the American*

- Water Resources Association 34, 73–89. <https://doi.org/10.1111/j.1752-1688.1998.tb05961.x>
- Arnold, J.G., Srinivasan, R., Muttiah, R.S., Williams, J.R., 1998b. Large area hydrologic modeling and assessment part i: model development 1. JAWRA Journal of the American Water Resources Association 34, 73–89. <https://doi.org/10.1111/j.1752-1688.1998.tb05961.x>
- Arranz, R, J., McCartney, M., 2007. International Water Management Institute, in: Finlayson, C.M., Everard, M., Irvine, K., McInnes, R.J., Middleton, B.A., van Dam, A.A., Davidson, N.C. (Eds.), *The Wetland Book*. Springer Netherlands, Dordrecht, pp. 681–685. https://doi.org/10.1007/978-90-481-9659-3_142
- Aurecon, 2011. Development of a reconciliation strategy for the Olifants river water supply system. Report number: P WMA 04/B50/00/8310/6
- Barnett, T.P., Adam, J.C., Lettenmaier, D.P., 2005. Potential impacts of a warming climate on water availability in snow-dominated regions. *Nature* 438, 303–309. <https://doi.org/10.1038/nature04141>
- Bates, B., Kundzewicz, Z.W., IPCC (Eds.), 2008. *Climate Change and Water*. Technical Paper of the Intergovernmental Panel on Climate Change, IPCC Secretariat, Geneva, 210 pp, IPCC Technical Paper; 6.
- Bedient, P.B., Huber, W.C., Vieux, B.E., 2008. *Hydrology and floodplain analysis*.
- Benhin, J.K.A., 2006. *Climate change and South African Agriculture*. CEEPA Discussion Paper No. 21 Centre for Environmental Economics and Policy in Africa, University of Pretoria.
- Beven, K.J., Kirkby, M.J., 1979. A physically based, variable contributing area model of basin hydrology / Un modèle à base physique de zone d'appel variable de l'hydrologie du bassin versant. *Hydrological Sciences Bulletin* 24, 43–69. <https://doi.org/10.1080/02626667909491834>
- Brutsaert, W., 2005. *Hydrology: an introduction*. Cambridge University Press.
- Callaway, J.M., 2004. Adaptation benefits and costs: are they important in the global policy picture and how can we estimate them? *Global Environmental Change* 14, 273–282. <https://doi.org/10.1016/j.gloenvcha.2004.04.002>

- Canadell, J.G., Le Quere, C., Raupach, M.R., Field, C.B., Buitenhuis, E.T., Ciais, P., Conway, T.J., Gillett, N.P., Houghton, R.A., Marland, G., 2007. Contributions to accelerating atmospheric CO₂ growth from economic activity, carbon intensity, and efficiency of natural sinks. *Proceedings of the National Academy of Sciences* 104, 18866–18870. <https://doi.org/10.1073/pnas.0702737104>
- Caparoci Nogueira, S., Moreira, M., Lordelo Volpato, M., 2018. Evaluating Precipitation Estimates from Eta, TRMM and CHRIPS Data in the South-Southeast Region of Minas Gerais State—Brazil. *Remote Sensing* 10, 313. <https://doi.org/10.3390/rs10020313>
- Chilkoti, V., Bolisetti, T., Balachandar, R., 2017. Climate change impact assessment on hydropower generation using multi-model climate ensemble. *Renewable Energy* 109, 510–517. <https://doi.org/10.1016/j.renene.2017.02.041>
- Conservation Ontario, 2001. *The Importance of Watershed Management in Protecting Ontario's Drinking Water Supplies.*
- Crutzen, P.J., 2006. The “anthropocene” (pp. 13–18). *Earth system science in the anthropocene.* Springer Berlin Germany.
- Cullis, J., Strzepek, K., Tadross, M., Sami, K., Havenga, B., Gildenhuis, B., Smith, J., 2011. Incorporating climate change into water resources planning for the town of Polokwane, South Africa. *Climatic Change* 108, 437–456. <https://doi.org/10.1007/s10584-010-9891-9>
- Dabrowski, J.M., 2014. Applying SWAT to predict ortho-phosphate loads and trophic status in four reservoirs in the upper Olifants catchment, South Africa. *Hydrology and Earth System Sciences* 18, 2629–2643. <https://doi.org/10.5194/hess-18-2629-2014>
- Dai, A., 2013. Erratum: Increasing drought under global warming in observations and models. *Nature Climate Change* 3, 171–171. <https://doi.org/10.1038/nclimate1811>
- DAFF, 2018. Area estimate and fifth production forecast of winter crops (2018). Department of Agriculture and Forestry, South Africa. Date of accessed 4 July 2019. <https://www.daff.gov.za/daffweb3/Home/Crop-Estimates>

- DAFF, 2019. Area planted and fifth production forecast: 2019. Department of Agriculture and Forestry, South Africa. Accessed 4 July 2019. <https://www.daff.gov.za/daffweb3/Home/Crop-Estimates>
- Dennis, I., Dennis, R., 2012. Climate change vulnerability index for South African aquifers. *Water SA* 38. <https://doi.org/10.4314/wsa.v38i3.7>
- Devia, G.K., Ganasri, B.P., Dwarakish, G.S., 2015. A Review on Hydrological Models. *Aquatic Procedia* 4, 1001–1007. <https://doi.org/10.1016/j.aqpro.2015.02.126>
- Donnelly, C., Greuell, W., Andersson, J., Gerten, D., Pisacane, G., Roudier, P., Ludwig, F., 2017. Impacts of climate change on European hydrology at 1.5, 2 and 3 degrees mean global warming above preindustrial level. *Climatic Change* 143, 13–26. <https://doi.org/10.1007/s10584-017-1971-7>
- Engel, B., Storm, D., White, M., Arnold, J., Arabi, M., 2007. A Hydrologic/Water Quality Model Application. *Journal of the American Water Resources Association* 43, 1223–1236. <https://doi.org/10.1111/j.1752-1688.2007.00105.x>
- Fang, G.H., Yang, J., Chen, Y.N., Zammit, C., 2015. Comparing bias correction methods in downscaling meteorological variables for a hydrologic impact study in an arid area in China. *Hydrology and Earth System Sciences* 19, 2547–2559. <https://doi.org/10.5194/hess-19-2547-2015>
- Fischlin, A., Midgley, G. F., Price, J. T., Leemans, R., Gopal, B., Turley, C., ... Velichko, A. A., 2007. Ecosystems, their properties, goods and services.
- Fowler, H.J., Blenkinsop, S., Tebaldi, C., 2007. Linking climate change modelling to impacts studies: recent advances in downscaling techniques for hydrological modelling. *International Journal of Climatology* 27, 1547–1578. <https://doi.org/10.1002/joc.1556>
- Funk, C., Peterson, P., Landsfeld, M., Pedreros, D., Verdin, J., Shukla, S., Husak, G., Rowland, J., Harrison, L., Hoell, A., Michaelsen, J., 2015. The climate hazards infrared precipitation with stations—a new environmental record for monitoring extremes. *Scientific Data* 2, 150066. <https://doi.org/10.1038/sdata.2015.66>
- Gallego-Ayala, J., Juárez, D., 2011. Strategic implementation of integrated water resources management in Mozambique: An A’WOT analysis. *Physics and Chemistry of the Earth, Parts A/B/C* 36, 1103–1111. <https://doi.org/10.1016/j.pce.2011.07.040>

- Gassman, M. R. Reyes, C. H. Green, J. G. Arnold, 2007. The Soil and Water Assessment Tool: Historical Development, Applications, and Future Research Directions. *Transactions of the ASABE* 50, 1211–1250. <https://doi.org/10.13031/2013.23637>
- Gassman, P.W., Huang, F., Arnold, J.G., White, M., Griensven, A.V., Srinivasan, R.,... Watson, B., 2010. The Worldwide Use of the SWAT Model.
- Göhler, M., Mai, J., & Cuntz, M. (2013). Use of eigendecomposition in a parameter sensitivity analysis of the Community Land Model. *Journal of Geophysical Research: Biogeosciences*, 118(2), 904-921. <https://doi.org/10.1002/jgrg.20072>
- Gosain, A.K., Rao, S., Basuray, D., 2006. Climate change impact assessment on hydrology of Indian river basins. *Current Science*, 90(3), 346-353.
- Govender, M., & Everson, C. S. (2005). Modelling streamflow from two small South African experimental catchments using the SWAT model. *Hydrological Processes: An International Journal*, 19(3), 683-692. <https://doi.org/10.1002/hyp.5621>
- Green, W. H., & Ampt, G. A. (1911). Studies on Soil Physics. *The Journal of Agricultural Science*, 4(1), 1-24.
- Grotch, S.L., MacCracken, M.C., 1991. The use of general circulation models to predict regional climatic change. *Journal of Climate* 4, 286–303.
- Gupta, H.V., Kling, H., Yilmaz, K.K., Martinez, G.F., 2009. Decomposition of the mean squared error and NSE performance criteria: Implications for improving hydrological modelling. *Journal of Hydrology* 377, 80–91. <https://doi.org/10.1016/j.jhydrol.2009.08.003>
- Gyamfi, C., Ndambuki, J., Salim, R., 2016a. Simulation of Sediment Yield in a Semi-Arid River Basin under Changing Land Use: An Integrated Approach of Hydrologic Modelling and Principal Component Analysis. *Sustainability* 8, 1133. <https://doi.org/10.3390/su8111133>
- Gyamfi, C., Ndambuki, J., Salim, R., 2016b. Hydrological Responses to Land Use/Cover Changes in the Olifants Basin, South Africa. *Water* 8, 588. <https://doi.org/10.3390/w8120588>
- Hargreaves, G.L., Hargreaves, G.H., Riley, J.P., 1985. Agricultural Benefits for Senegal River Basin. *Journal of Irrigation and Drainage Engineering* 111, 113–124. [https://doi.org/10.1061/\(ASCE\)0733-9437\(1985\)111:2\(113\)](https://doi.org/10.1061/(ASCE)0733-9437(1985)111:2(113))

- Healy, R.W., Winter, T.C., LaBaugh, J.W., Franke, O.L., 2007. Water budgets: foundations for effective water-resources and environmental management. US Geological Survey Reston, Virginia.
- Helsel, D.R., Hirsch, R.M., 1992. Statistical methods in water resources. Elsevier.
- Hughes, D.A., 2006. Comparison of satellite rainfall data with observations from gauging station networks. *Journal of Hydrology* 327, 399–410. <https://doi.org/10.1016/j.jhydrol.2005.11.041>
- Hughes, W.S., Balling, R.C., 1996. Urban Influences on South African Temperature Trends. *International Journal of Climatology* 16, 935–940. [https://doi.org/10.1002/\(SICI\)1097-0088\(199608\)16:8<935::AID-JOC64>3.0.CO;2-V](https://doi.org/10.1002/(SICI)1097-0088(199608)16:8<935::AID-JOC64>3.0.CO;2-V)
- Immerzeel, W.W., van Beek, L.P.H., Bierkens, M.F.P., 2010. Climate Change Will Affect the Asian Water Towers. *Science* 328, 1382–1385. <https://doi.org/10.1126/science.1183188>
- IPCC, 2014. Climate Change 2014: Impacts, Adaptation, and Vulnerability. Part B: Regional Aspects. Contribution of Working Group II to the Fifth Assessment Report of the Intergovernmental Panel on Climate Change [Barros, V.R., C.B. Field, D.J. Dokken, M.D. Mastrandrea, K.J. Mach, T.E. Bilir, M. Chatterjee, K.L. Ebi, Y.O. Estrada, R.C. Genova, B. Girma, E.S. Kissel, A.N. Levy, S. MacCracken, P.R. Mastrandrea, and L.L. White (eds.)]. Cambridge University Press, Cambridge, United Kingdom and New York, NY, USA, pp. 688.
- IPCC, 2007. Climate Change 2007: The Physical Science Basis. Contribution of Working Group I to the Fourth Assessment Report of the Intergovernmental Panel on Climate Change [Solomon, S., D. Qin, M. Manning, Z. Chen, M. Marquis, K.B. Averyt, M. Tignor and H.L. Miller (eds.)]. Cambridge University Press, Cambridge, United Kingdom and New York, NY, USA, 996 pp. Cambridge University Press, Cambridge; New York.
- IPCC, 2001. Climate Change 2001: The Scientific Basis. Contribution of Working Group I to the Third Assessment Report of the Intergovernmental Panel on Climate Change [Houghton, J.T., Y. Ding, D.J. Griggs, M. Noguer, P.J. van der Linden, X. Dai, K. Maskell, and C.A. Johnson (eds.)]. Cambridge University Press,

- Cambridge, United Kingdom and New York, NY, USA, 881pp. Cambridge University Press, Cambridge; New York.
- Kasting, J.F., 1993. Earth's early atmosphere. *Science* 259, 920–926.
- Kasting, J.F., Toon, O.B., Pollack, J.B., 1988. How climate evolved on the terrestrial planets. *Scientific American* 258, 90–97.
- Kouwen, N. (1988). WATFLOOD: a micro-computer based flood forecasting system based on real-time weather radar. *Canadian Water Resources Journal*, 13(1), 62-77. 13:1, 62-77, DOI: 10.4296/cwrj1301062
- Kruger, A.C., Shongwe, S., 2004. Temperature trends in South Africa: 1960-2003. *International Journal of Climatology* 24, 1929–1945. <https://doi.org/10.1002/joc.1096>
- Kusangaya, S., Warburton, M.L., Archer van Garderen, E., Jewitt, G.P.W., 2014. Impacts of climate change on water resources in southern Africa: A review. *Physics and Chemistry of the Earth, Parts A/B/C* 67–69, 47–54. <https://doi.org/10.1016/j.pce.2013.09.014>
- Kwon, H.-H., Khalil, A.F., Siegfried, T., 2008. Analysis of Extreme Summer Rainfall Using Climate Teleconnections and Typhoon Characteristics in South Korea. *Journal of the American Water Resources Association (JAWRA)* 44(2): 436–448. <https://doi.org/10.1111/j.1752-1688.2008.00173.x>
- Lange, M. de, Merrey, D.J., Levite, H., Svendsen, M., 2005. Water resources planning and management in the Olifants Basin of South Africa: past, present and future., in: Svendsen, M. (Ed.), *Irrigation and River Basin Management: Options for Governance and Institutions*. CABI, Wallingford, pp. 145–168. <https://doi.org/10.1079/9780851996721.0145>
- Lashof, D.A., Ahuja, D.R., 1990. Relative contributions of greenhouse gas emissions to global warming. *Nature* 344, 529–531. <https://doi.org/10.1038/344529a0>
- Lenderink, G., Buishand, A., van Deursen, W., 2007. Estimates of future discharges of the river Rhine using two scenario methodologies: direct versus delta approach 15.
- Levitus, S., Antonov, J.I., Boyer, T.P., Baranova, O.K., Garcia, H.E., Locarnini, R.A.,... Zweng, M.M., 2012. World ocean heat content and thermocline sea level change

- (0-2000 m), 1955-2010: World Ocean Heat Content. *Geophys. Res. Lett.* 39, n/a-n/a. <https://doi.org/10.1029/2012GL051106>
- Liang, X., Xie, Z., & Huang, M., 2003. A new parameterization for surface and groundwater interactions and its impact on water budgets with the variable infiltration capacity (VIC) land surface model. *Journal of Geophysical Research: Atmospheres*, 108(D16). <https://doi.org/10.1029/2002JD003090>
- Lott, F. C., Christidis, N., & Stott, P. A., 2013. Can the 2011 East African drought be attributed to human-induced climate change?. *Geophysical Research Letters*, 40(6), 1177-1181. <https://doi.org/10.1002/grl.50235>
- Mai, J., Tolson, B.A., 2019. Model Variable Augmentation (MVA) for Diagnostic Assessment of Sensitivity Analysis Results. *Water Resources Research*, 55(4), 2631-2651. <https://doi.org/10.1029/2018WR023382>
- Masih, I., Maskey, S., Uhlenbrook, S., Smakhtin, V., 2011. Assessing the Impact of Areal Precipitation Input on Streamflow Simulations Using the SWAT Model 1. *Journal of the American Water Resources Association (JAWRA)* 47(1): 179–195. <https://doi.org/10.1111/j.1752-1688.2010.00502.x>
- Mathivha, F.I., Tshipala, N.N., Nkuna, Z., 2017. The relationship between drought and tourist arrivals: A case study of Kruger National Park, South Africa. *Jambá: Journal of Disaster Risk Studies* 9 (1), a471. <https://doi.org/10.4102/jamba.v9i1.471>
- Mausbach, M.J., Dedrick, A.R., 2004. The length we go: Measuring environmental benefits of conservation practices. *Journal of Soil and Water Conservation*, 59(5), 96A-103A.
- McCartney, M.P., 2004. Hydrology and water resources development in the Olifants River Catchment. International Water Management Institute, Colombo, Sri Lanka.
- Mckay, M.D., Beckman, R.J., Conover, W.J., 2000. A Comparison of Three Methods for Selecting Values of Input Variables in the Analysis of Output From a Computer Code. *Technometrics* 42, 55–61. <https://doi.org/10.1080/00401706.2000.10485979>
- Meinshausen, M., Meinshausen, N., Hare, W., Raper, S.C.B., Frieler, K., Knutti, R., Frame, D.J., Allen, M.R., 2009. Greenhouse-gas emission targets for limiting global warming to 2 °C. *Nature* 458, 1158–1162. <https://doi.org/10.1038/nature08017>

- Mekonnen, B.A., 2016. "Modeling and management of water quantity and quality in cold-climate prairie watersheds". Electronic Thesis and Dissertations. University of Saskatchewan.
- Merritt, W.S., Letcher, R.A., Jakeman, A.J., 2003. A review of erosion and sediment transport models. *Environmental Modelling & Software* 18, 761–799. [https://doi.org/10.1016/S1364-8152\(03\)00078-1](https://doi.org/10.1016/S1364-8152(03)00078-1)
- Moore, R.J., 2007. The PDM rainfall-runoff model. *Hydrology & Earth System Sciences*. 11(1), 483–499. <https://doi.org/10.5194/hess-11-483-2007>
- Moriasi, D. N., Arnold, J. G., Van Liew, M. W., Bingner, R. L., Harmel, R. D., Veith, T. L., 2007. Model Evaluation Guidelines for Systematic Quantification of Accuracy in Watershed Simulations. *Transactions of the ASABE* 50, 885–900. <https://doi.org/10.13031/2013.23153>
- Muttiah, R.S., Wurbs, R.A., 2002. Modeling the Impacts of Climate Change on Water Supply Reliabilities. *Water International* 27, 407–419. <https://doi.org/10.1080/02508060208687020>
- Navarro-Racines, C.E., Tarapues-Montenegro, J.E and Ramírez-Villegas, J.A. 2015. Bias-correction in the CCAFS-Climate Portal: A description of methodologies. Decision and Policy Analysis (DAPA) Research Area. International Center for Tropical Agriculture (CIAT). Cali, Colombia.
- Neitsch, S. L., Arnold, J. G., Kiniry, J. R., & Williams, J. R., 2011. Soil and water assessment tool theoretical documentation version 2009. Texas Water Resources Institute.
- Niang, I., Ruppel, O. C., Abdrabo, M. A., Essel, A., Lennard, C., Padgham, J., Urquhart, P., 2014. Africa Climate Change 2014: Impacts, Adaptation, and Vulnerability. Part B: Regional Aspects. Contribution of Working Group II to the Fifth Assessment Report of the Intergovernmental Panel on Climate Change.
- Nikulin, G., Jones, C., Giorgi, F., Asrar, G., Büchner, M., Cerezo-Mota, ... Sushama, L., 2012. Precipitation Climatology in an Ensemble of CORDEX-Africa Regional Climate Simulations. *Journal of Climate* 25, 6057–6078. <https://doi.org/10.1175/JCLI-D-11-00375.1>

- Nkhonjera, G.K., 2017. Understanding the impact of climate change on the dwindling water resources of South Africa, focusing mainly on Olifants River basin: A review. *Environmental Science & Policy* 71, 19–29. <https://doi.org/10.1016/j.envsci.2017.02.004>
- NOAA, 2019. Global Trend in CO₂ Predicted by National Oceanic and Atmospheric Administration (NOAA). Retrieved from URL <https://www.esrl.noaa.gov/gmd/ccgg/trends/global.html> (accessed 14 July 2019).
- Olivera, F., Valenzuela, M., Srinivasan, R., Choi J., 2006. ArcGIS-SWAT: A Geodata Model and GIS Interface for SWAT. *Journal of the American Water Resources Association (JAWRA)* 42(2):295-309.
- Orlowsky, B., Seneviratne, S.I., 2012. Global changes in extreme events: regional and seasonal dimension. *Climatic Change* 110, 669–696. <https://doi.org/10.1007/s10584-011-0122-9>
- Owen, C.R., 1995. Water budget and flow patterns in an urban wetland. *Journal of Hydrology* 169, 171–187. [https://doi.org/10.1016/0022-1694\(94\)02638-R](https://doi.org/10.1016/0022-1694(94)02638-R)
- Paredes-Trejo, F.J., Barbosa, H.A., Lakshmi Kumar, T.V., 2017. Validating CHIRPS-based satellite precipitation estimates in Northeast Brazil. *Journal of Arid Environments* 139, 26–40. <https://doi.org/10.1016/j.jaridenv.2016.12.009>
- Penman, Monteith, 1965. “Evaporation and environment.” *Symposia of the society for experimental biology*. Vol. 19. Cambridge University Press (CUP) Cambridge, 1965.
- Piani, C., Haerter, J.O., Coppola, E., 2010. Statistical bias correction for daily precipitation in regional climate models over Europe. *Theoretical and Applied Climatology*, 99(1-2), 187-192.
- Pomeroy, J.W., Gray, D.M., Brown, T., Hedstrom, N.R., Quinton, W.L., Granger, R.J., Carey, S.K., 2007. The cold regions hydrological model: a platform for basing process representation and model structure on physical evidence. *Hydrological Processes: An International Journal*, 21(19), 2650-2667. <https://doi.org/10.1002/hyp.6787>
- Priestley, B., Taylor, 1972. “On the assessment of surface heat flux and evaporation using large-scale parameters.” *Monthly weather review* 100 (2), 81-92.

- Pringle, C.M., 2001. Pringle, C. M. (2001). Hydrologic connectivity and the management of biological reserves: a global perspective. *Ecological Applications*, 11(4), 981-998. [https://doi.org/10.1890/1051-0761\(2001\)011\[0981:HCATMO\]2.0.CO;2](https://doi.org/10.1890/1051-0761(2001)011[0981:HCATMO]2.0.CO;2)
- Rahman, M., Bolisetti, T., Balachandar, R., 2012. Hydrologic modelling to assess the climate change impacts in a Southern Ontario watershed. *Canadian Journal of Civil Engineering* 39, 91–103. <https://doi.org/10.1139/l11-112>
- Rahman, M. M., 2008. "Hydrologic modelling of the Canard River watershed". *Electronic Theses and Dissertations*. University of Windsor.
- Ritchie, J.T., 1972. Model for predicting evaporation from a row crop with incomplete cover. *Water resources research*, 8(5), 1204–1213.
- Rodhe, H., 1990. A comparison of the contribution of various gases to the greenhouse effect. *Science* 248, 1217–1219.
- Rosenberg, N.J., Brown, R.A., Izaurralde, R.C., Thomson, A.M., 2003. Integrated assessment of Hadley Centre (HadCM2) climate change projections on agricultural productivity and irrigation water supply in the conterminous United States. *Agricultural and Forest Meteorology* 117, 73–96. [https://doi.org/10.1016/S0168-1923\(03\)00025-X](https://doi.org/10.1016/S0168-1923(03)00025-X)
- Rowell, D.P., 2012. Sources of uncertainty in future changes in local precipitation. *Climate dynamics*, 39(7-8), 1929-1950. <https://doi.org/10.1007/s00382-011-1210-2>
- Roy, E.L., 2005. A study of the development of water resources in the Olifants catchment, South Africa: Application of the WEAP model.
- Sahoo, A.K., Pan, M., Troy, T.J., Vinukollu, R.K., Sheffield, J., Wood, E.F., 2011. Reconciling the global terrestrial water budget using satellite remote sensing. *Remote Sensing of Environment* 115, 1850–1865. <https://doi.org/10.1016/j.rse.2011.03.009>
- Satterthwaite, D., 2008. Cities' contribution to global warming: notes on the allocation of greenhouse gas emissions. *Environment and Urbanization* 20, 539–549. <https://doi.org/10.1177/0956247808096127>
- Schulze, R., Meigh, J., Horan, M., 2001. Present and potential future vulnerability of eastern and southern Africa's hydrology and water resources: START Regional Syntheses. *South African Journal of Science* 97, 150–160.

- Schulze, R.E., 2000. Modelling hydrological responses to land use and climate change: a southern African perspective. *AMBIO: A Journal of the Human Environment*, 29(1), 12-23.
- Schulze, R.E., Maharaj, M., Warburton, M.L., Gers, C.J., Horan, M.J.C., Kunz, R.P., Clark, D.J., 2007. South African atlas of climatology and agrohydrology. Water Research Commission, Pretoria, RSA, WRC Report 1489, 06.
- Shoemaker, L., Dai, T., Koenig, J., 2005. TMDL model evaluation and research needs. National Risk Management Research Laboratory, US Environmental Protection Agency.
- Singh, R., van Werkhoven, K., Wagener, T., 2014. Hydrological impacts of climate change in gauged and ungauged watersheds of the Olifants basin: a trading-space-for-time approach. *Hydrological Sciences Journal* 59, 29–55. <https://doi.org/10.1080/02626667.2013.819431>
- Singh, V.P., Woolhiser, D.A., 2002. Mathematical Modeling of Watershed Hydrology. *Journal of Hydrologic Engineering* 7, 270–292. [https://doi.org/10.1061/\(ASCE\)1084-0699\(2002\)7:4\(270\)](https://doi.org/10.1061/(ASCE)1084-0699(2002)7:4(270))
- Sloan, P.G., Moore, I.D., Coltharp, G.B., Eigel, J.D., 1983. Modeling Surface and Subsurface Stormflow on Steeply-Sloping Forested Watersheds. <https://doi.org/10.13023/kwrri.rr.142>
- Sorooshian, S. (Ed.), 2008. Hydrological modelling and the water cycle: coupling the atmospheric and hydrological models, Water science and technology library. Springer, Berlin ; London.
- Stone, M.C., Hotchkiss, R.H., Hubbard, C.M., Fontaine, T.A., Mearns, L.O., Arnold, J.G., 2001. Impacts of climate change on Missouri river basin water yield. *JAWRA Journal of the American Water Resources Association*, 37(5), 1119–1129. <https://doi.org/10.1111/j.1752-1688.2001.tb03626.x>
- Stott, P.A., Stone, D.A., Allen, M.R., 2004. Human contribution to the European heatwave of 2003. *Nature* 432, 610–614. <https://doi.org/10.1038/nature03089>
- Tadross, M., Davis, C., Engelbrecht, F., Joubert, A., & Archer, E. R., 2011. Regional scenarios of future climate change over southern Africa. CSIR.

- Tett, S.F.B., Stott, P.A., Allen, M.R., Ingram, W.J., Mitchell, J.F.B., 1999. Causes of twentieth-century temperature change near the Earth's surface. *Nature* 399, 569–572. <https://doi.org/10.1038/21164>
- Teutschbein, C., Seibert, J., 2012. Bias correction of regional climate model simulations for hydrological climate-change impact studies: Review and evaluation of different methods. *Journal of Hydrology* 456–457, 12–29. <https://doi.org/10.1016/j.jhydrol.2012.05.052>
- Trenberth, K., 2011. Changes in precipitation with climate change. *Climate Research* 47, 123–138. <https://doi.org/10.3354/cr00953>
- Tuo, Y., Duan, Z., Disse, M., Chiogna, G., 2016. Evaluation of precipitation input for SWAT modeling in Alpine catchment: A case study in the Adige river basin (Italy). *Science of The Total Environment* 573, 66–82. <https://doi.org/10.1016/j.scitotenv.2016.08.034>
- USDA Soil Conservation Service, 1972. National engineering handbook section 4 hydrology. Chapters 4–10. Washington, DC: U.S. Government Printing Office. 127.
- Van der Merwe, P., Saayman, M., 2008. Travel motivations of tourists visiting Kruger National Park. *Koedoe* 50, 154–159. <https://doi.org/10.4102/koedoe.v50i1.140>
- Vancutsem, C., Ceccato, P., Dinku, T., Connor, S.J., 2010. Evaluation of MODIS land surface temperature data to estimate air temperature in different ecosystems over Africa. *Remote Sensing of Environment* 114, 449–465. <https://doi.org/10.1016/j.rse.2009.10.002>
- Wan, Z., Hook, S., Hulley, G. (2015). MOD11A1 MODIS/Terra Land Surface Temperature/Emissivity Daily L3 Global 1km SIN Grid V006. NASA EOSDIS LP DAAC. doi: 10.5067/MODIS/MOD11A1.006. Accessed January 7, 2019.
- Warren, W., Parkinson, C., 2005. An Introduction to Three-Dimensional Climate Modeling. Second Edition, National Center for Atmospheric Research and NASA Goddard Space Flight Center. University Science Books, California. Herndon VA. 368 pp.

- Whitehead, P.G., Wilby, R.L., Battarbee, R.W., Kernan, M., Wade, A.J., 2009. A review of the potential impacts of climate change on surface water quality. *Hydrological Sciences Journal* 54, 101–123. <https://doi.org/10.1623/hysj.54.1.101>
- Wilby, R.L., Wigley, T.M.L., 1997. Downscaling general circulation model output: a review of methods and limitations. *Progress in Physical Geography: Earth and Environment* 21, 530–548. <https://doi.org/10.1177/030913339702100403>
- Wilcke, R.A.I., Mendlik, T., Gobiet, A., 2013. Multi-variable error correction of regional climate models. *Climatic Change* 120, 871–887. <https://doi.org/10.1007/s10584-013-0845-x>
- Wood, A.W., Leung, L.R., Sridhar, V., Lettenmaier, D.P., 2004. Hydrologic Implications of Dynamical and Statistical Approaches to Downscaling Climate Model Outputs. *Climatic Change* 62, 189–216. <https://doi.org/10.1023/B:CLIM.0000013685.99609.9e>
- Zhang, X., Srinivasan, R., & Hao, F. (2007). Predicting hydrologic response to climate change in the Luohe River basin using the SWAT model. *Transactions of the ASABE*, 50(3), 901-910. <https://doi.org/10.13031/2013.23154>
- Yew Gan, T., Dlamini, E.M., Biftu, G.F., 1997. Effects of model complexity and structure, data quality, and objective functions on hydrologic modeling. *Journal of Hydrology* 192, 81–103. [https://doi.org/10.1016/S0022-1694\(96\)03114-9](https://doi.org/10.1016/S0022-1694(96)03114-9)
- Yilmaz, K.K., Yazicigil, H., 2011. Potential impacts of climate change on Turkish water resources: a review. In *Climate change and its effects on water resources* (pp. 105-114). Springer, Dordrecht. https://doi.org/10.1007/978-94-007-1143-3_12
- Yue, S., Pilon, P., Cavadias, G., 2002. Power of the Mann–Kendall and Spearman’s rho tests for detecting monotonic trends in hydrological series. *Journal of Hydrology* 259, 254–271. [https://doi.org/10.1016/S0022-1694\(01\)00594-7](https://doi.org/10.1016/S0022-1694(01)00594-7)
- Zhu, T., Ringler, C., 2010. Climate change implications for water resources in the Limpopo River Basin (No. 961). International Food Policy Research Institute (IFPRI).
- Ziervogel, G., New, M., Archer van Garderen, E., Midgley, G., Taylor, A., Hamann, R., ..., Warburton, M., 2014. Climate change impacts and adaptation in South Africa: Climate change impacts in South Africa. *Wiley Interdisciplinary Reviews: Climate Change*, 5(5), 605–620. <https://doi.org/10.1002/wcc.295>

ANNEXURES

Annexure 1: List of available precipitation stations

SL	Station	Location	Data Period	Source
1	B1E001	Witbank @ Witbank Dam	1964-2009	DWA
2	B1E003	Rondebosch @ Middelburg Dam	1979-2008	DWA
3	B2E001	Groenfontein @ Bronkhorstsp. Dam	1967-2017	DWA
4	B3E003	Loskop Nat. Res. @ Loskop Dam	1935-2017	DWA
5	B3E007	Rhenosterkop @ Rhenosterkop Dam	1980-2017	DWA
6	B4E003	Buffelskloof @ Buffelskloof Dam	1971-2017	DWA
7	B4E004	Roosenekal	1971-2017	DWA
8	B5E004	Tambotieboom @ Arabie Dam	1990-2017	DWA
9	B6E003	Blyderiv.Poortnatres @ Blyderiv.Poort Dam	1971-2017	DWA
10	B7E004	Sheila @ Phalaborwa Barrage	1967-2007	DWA
11	Witbank	Witbank	1993-2018	SAWS
12	Hoedspruit	Hoedspruit	1996-2008	SAWS
13	Phalaborwa	Phalaborwa Airport AWS	2008-2014	SAWS

Annexure 2: List of climate model ensembles

SL	GCM	RCM
a	CanESM2	RCA4
b	ECEARTH	CCLM4-8-17
c	ECEARTH	HIRHAM5
d	ECEARTH	RACMO22T
e	ECEARTH	RCA4
f	ECEARTH	REMO2009
g	HadGEM2	CCLM4-8-17
h	HadGEM2	CRCM5
i	HadGEM2	RCA4

The SL is used to define the climate ensemble in the subsequent maps

Annexure 3: Projected precipitation maps for the future periods

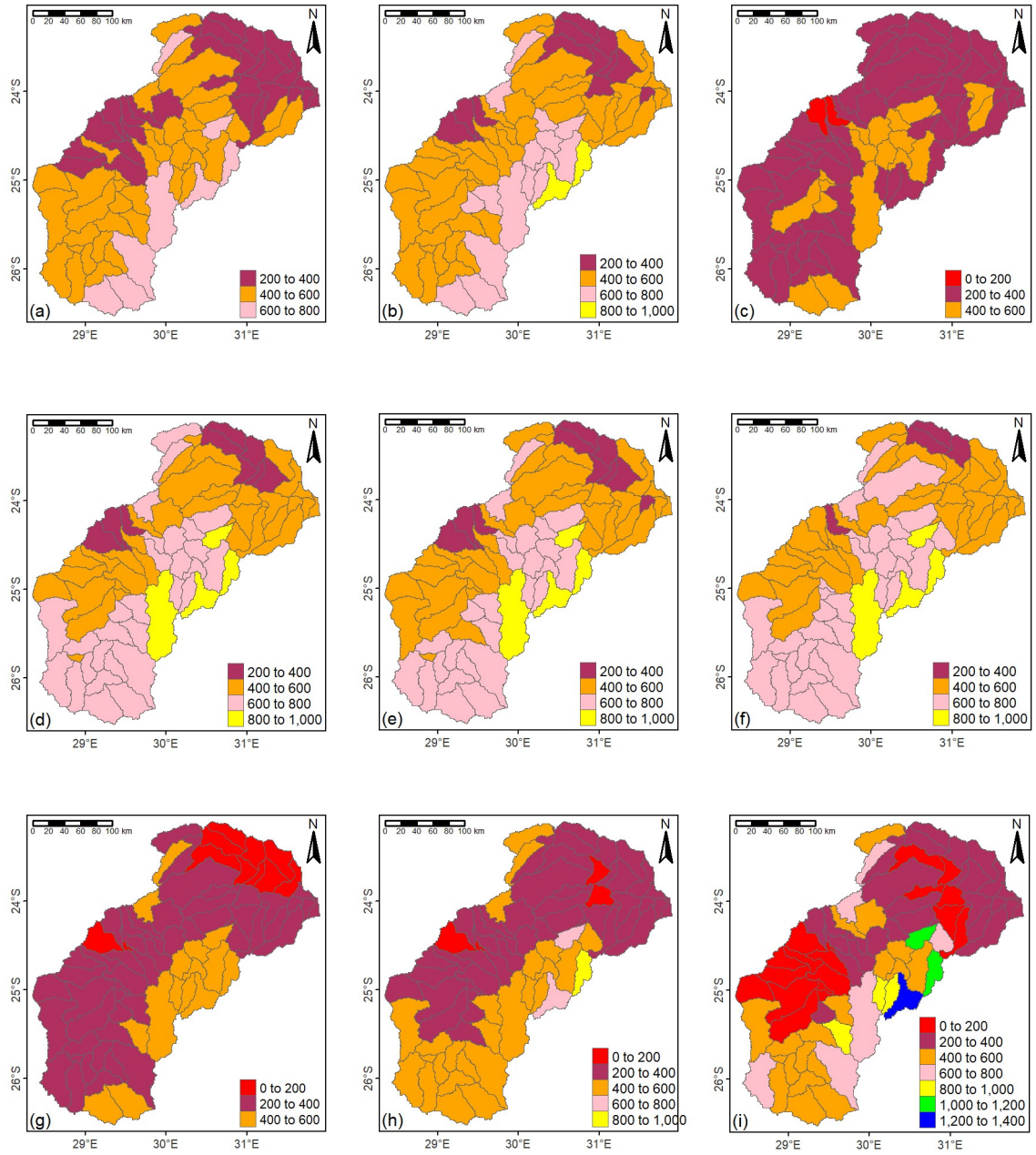


Figure A3-1: Projected annual precipitation in the Olifants River basin for mid-century under rep 4.5 climate projections. (The units are in mm).

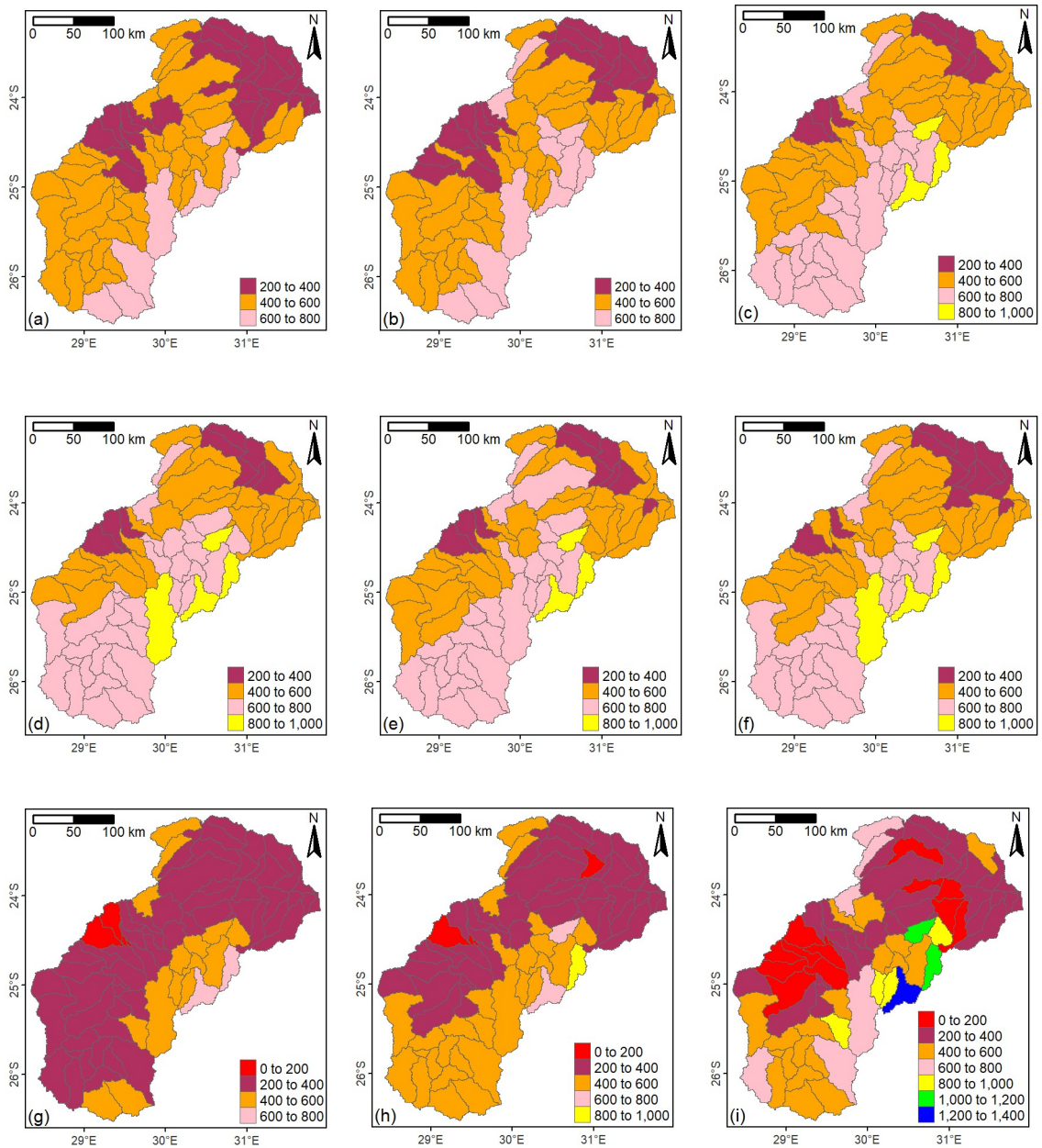


Figure A3-2: Projected annual precipitation in the Olifants River basin for mid-century under rcp 8.5 climate projections (The units are in mm).

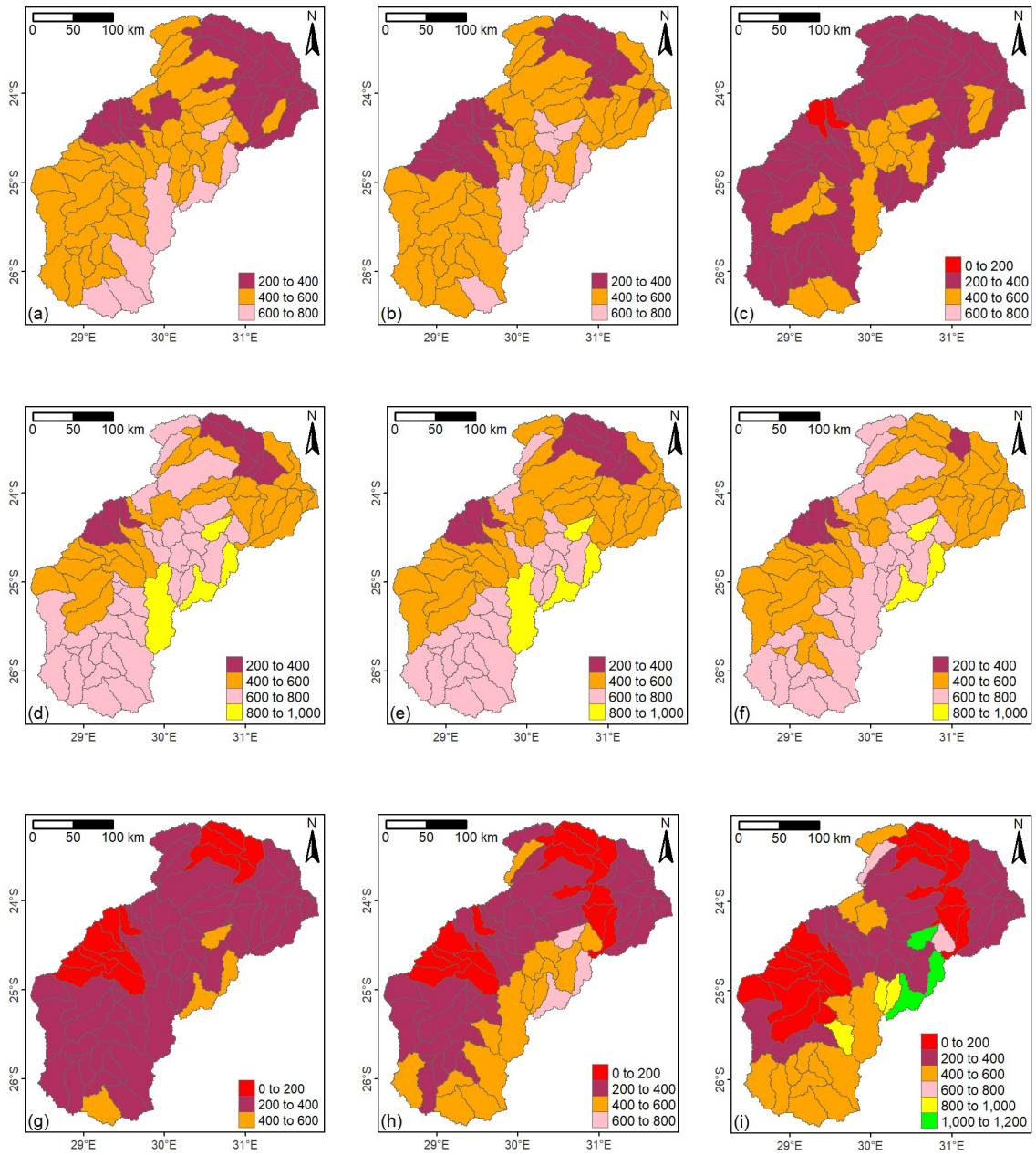


Figure A3-3: Projected annual precipitation in the Olifants River basin for end-century under rcp 4.5 climate projections (The units are in mm).

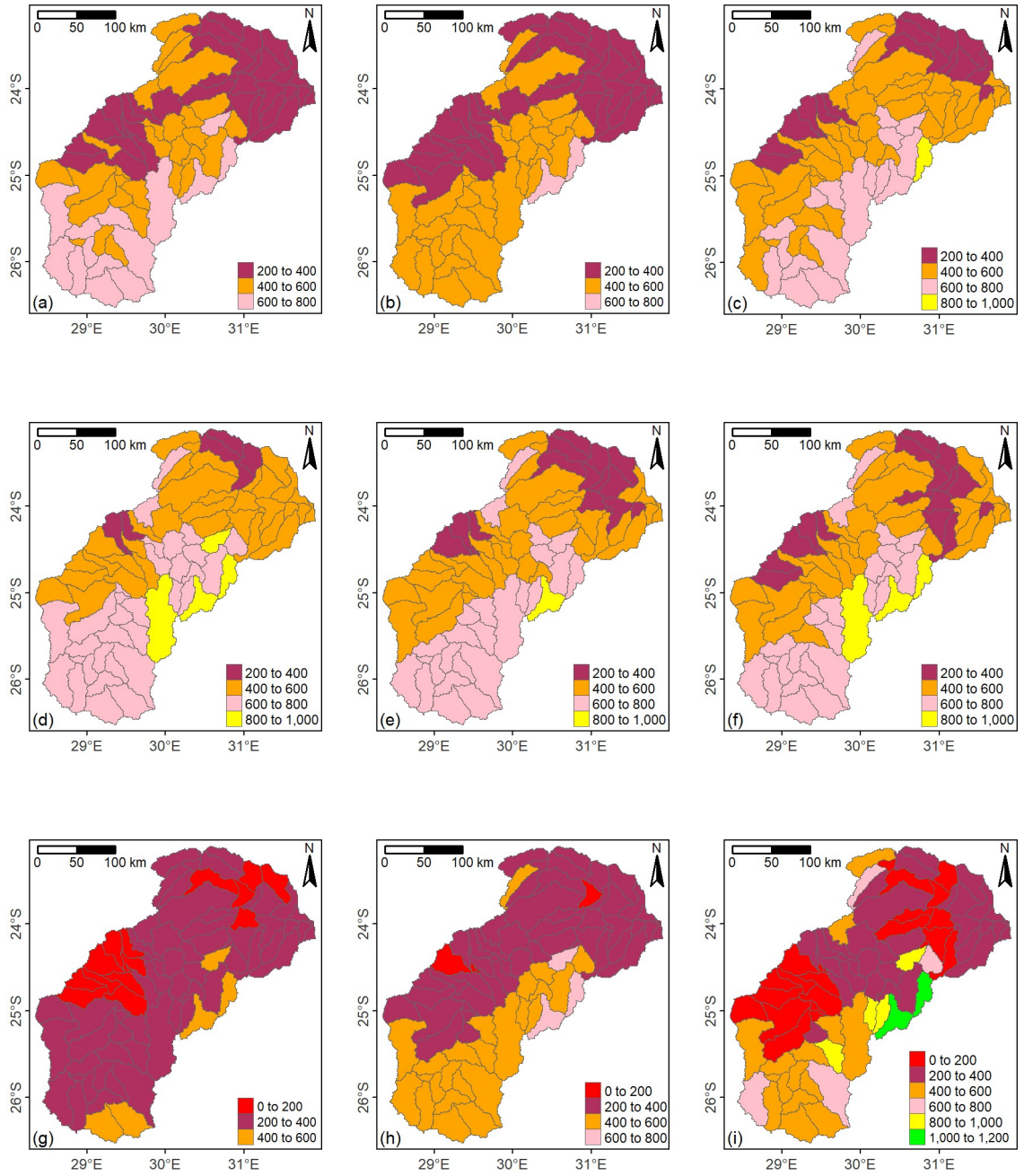


Figure A3-4: Projected annual precipitation in the Olifants River basin for end-century under rcp 8.5 climate projections (The units are in mm).

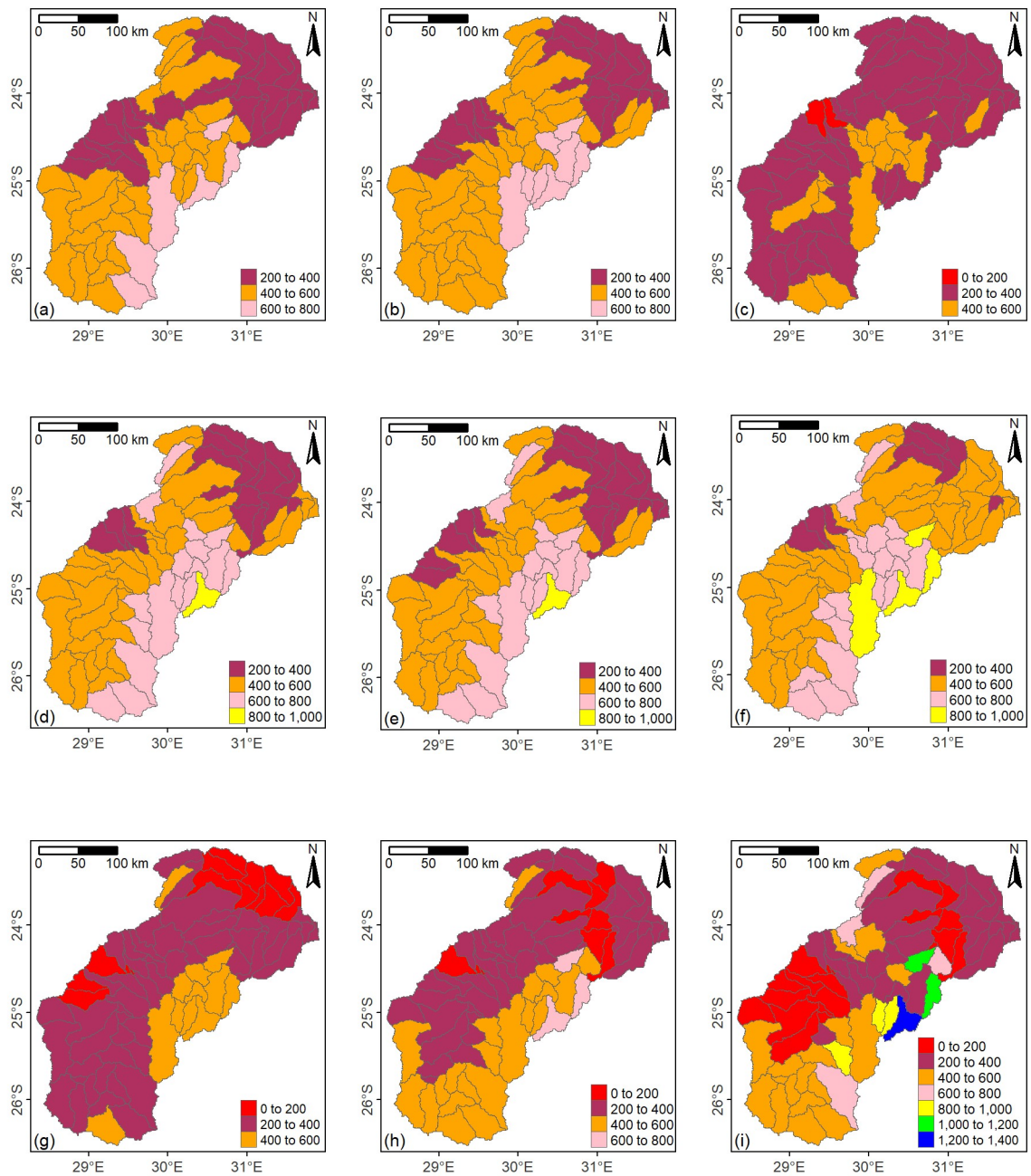


Figure A3-5: Projected summer precipitation in the Olifants River basin for mid-century under rcp 4.5 climate projections (The units are in mm).

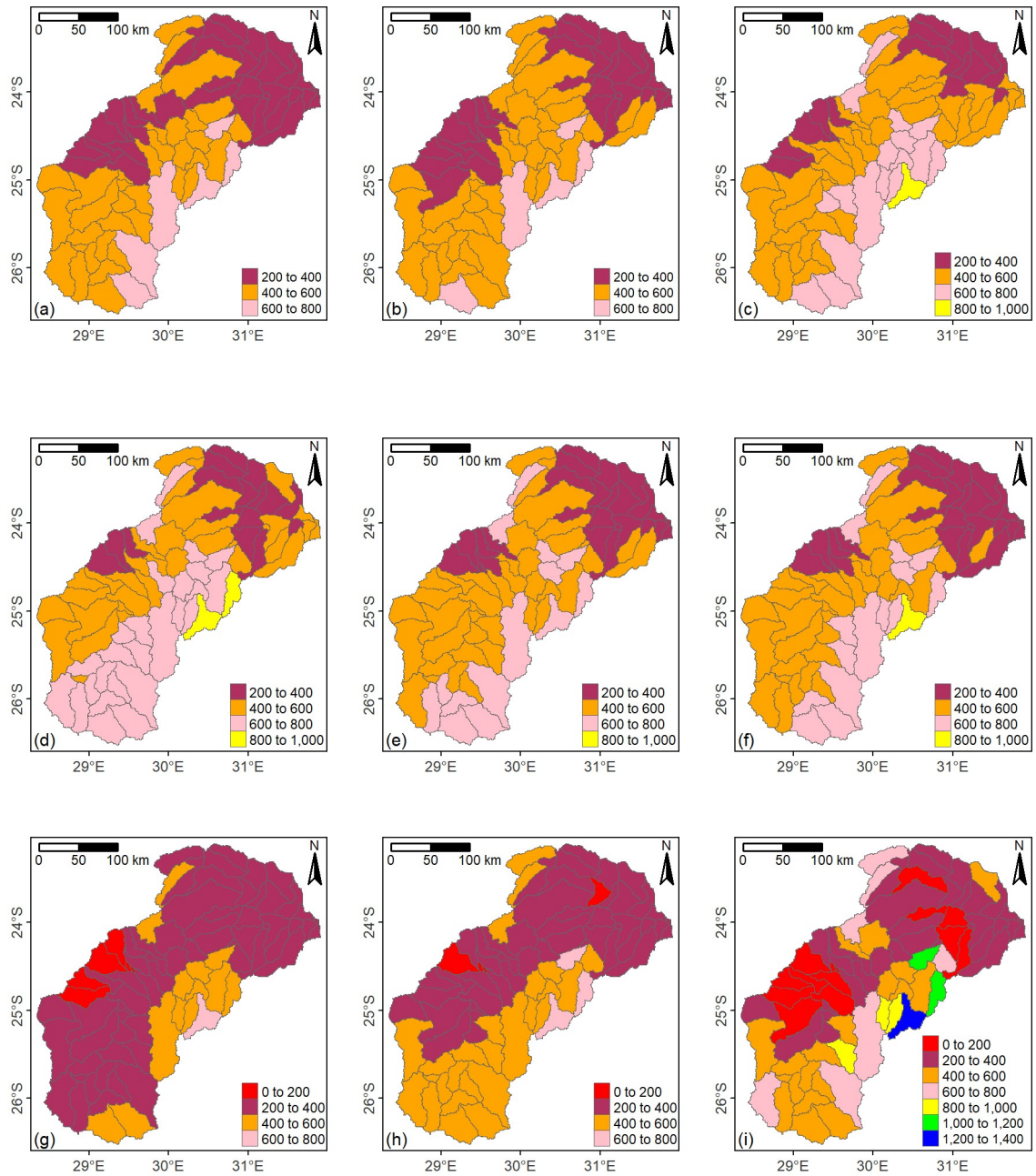


Figure A3-6: Projected summer precipitation in the Olifants River basin for mid-century under rcp 8.5 climate projections (The units are in mm).

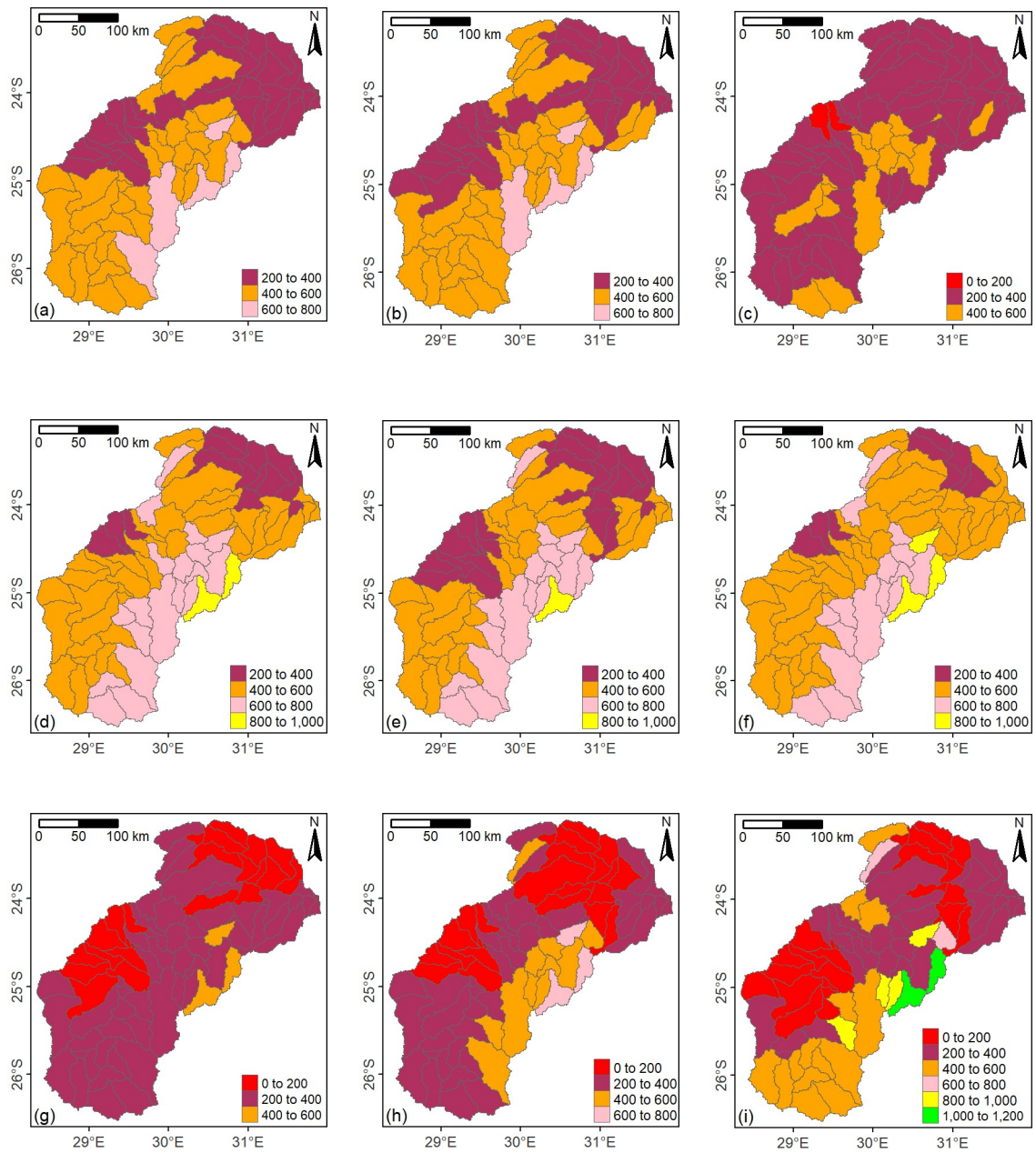


Figure A3-7: Projected summer precipitation in the Olifants River basin for end-century under rcp 4.5 climate projections (The units are in mm).

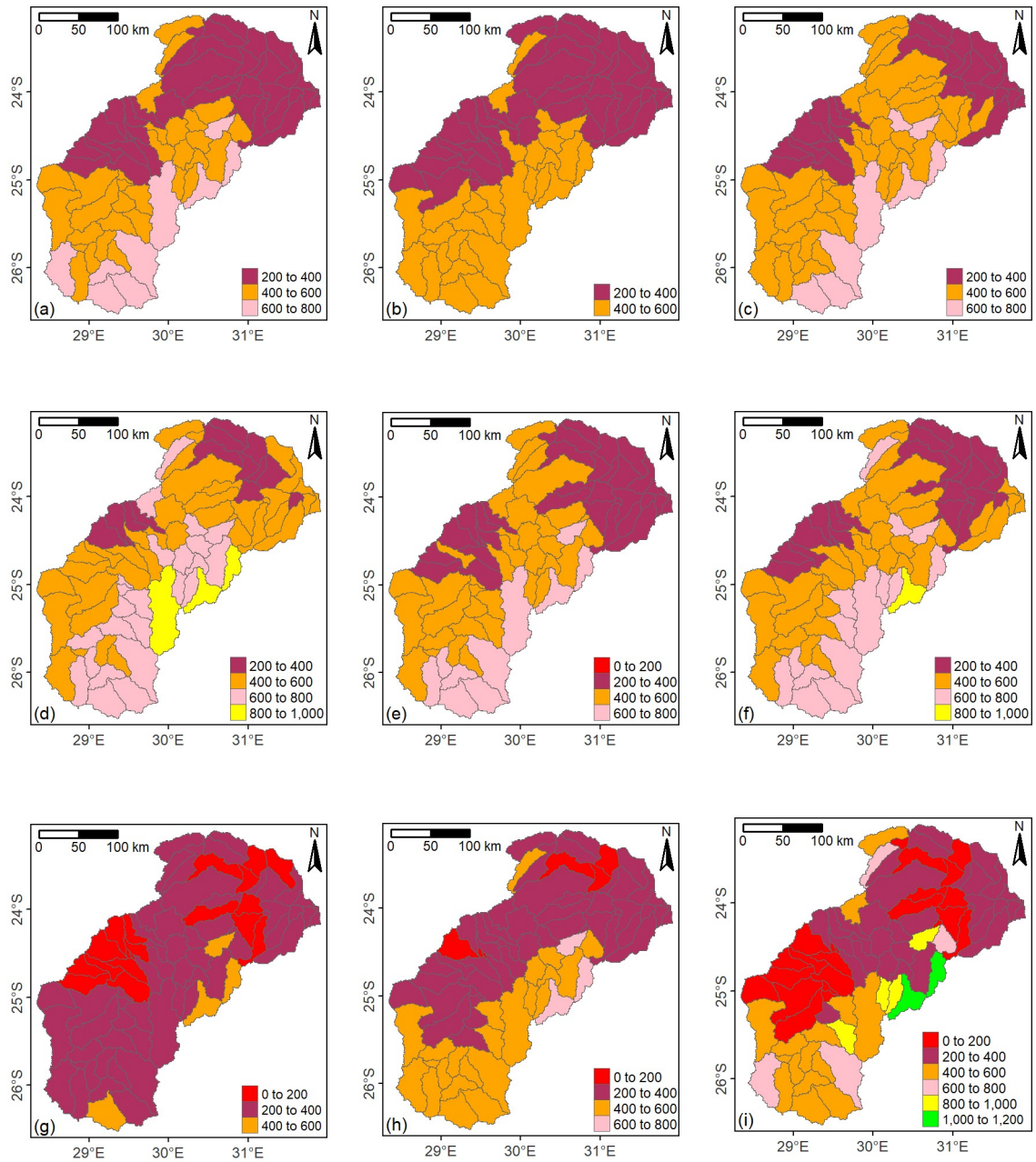


Figure A3-8: Projected summer precipitation in the Olifants River basin for end-century under rcp 8.5 climate projections (The units are in mm).

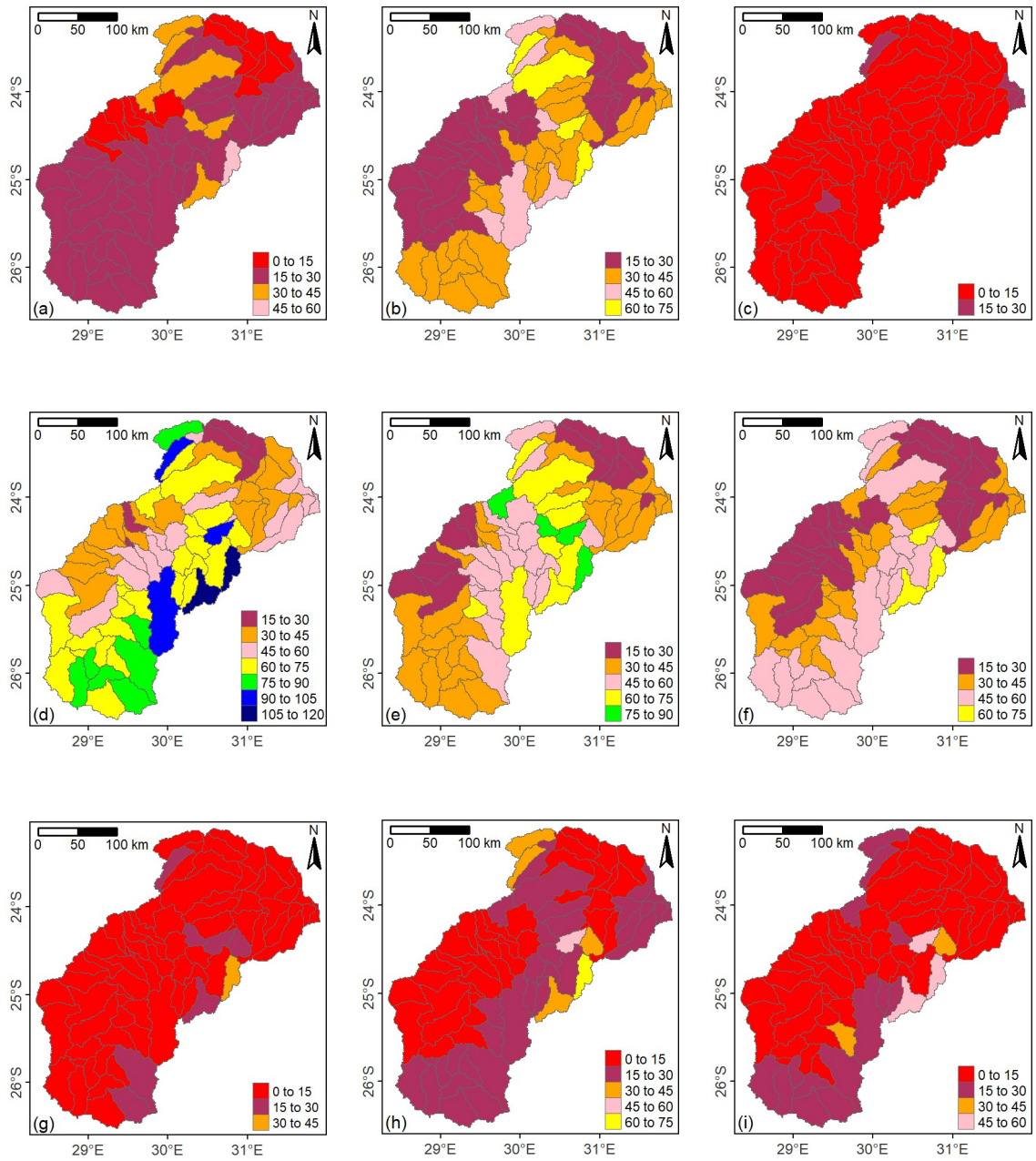


Figure A3-9: Projected winter precipitation in the Olifants River basin for mid-century under rcp 4.5 climate projections (The units are in mm).

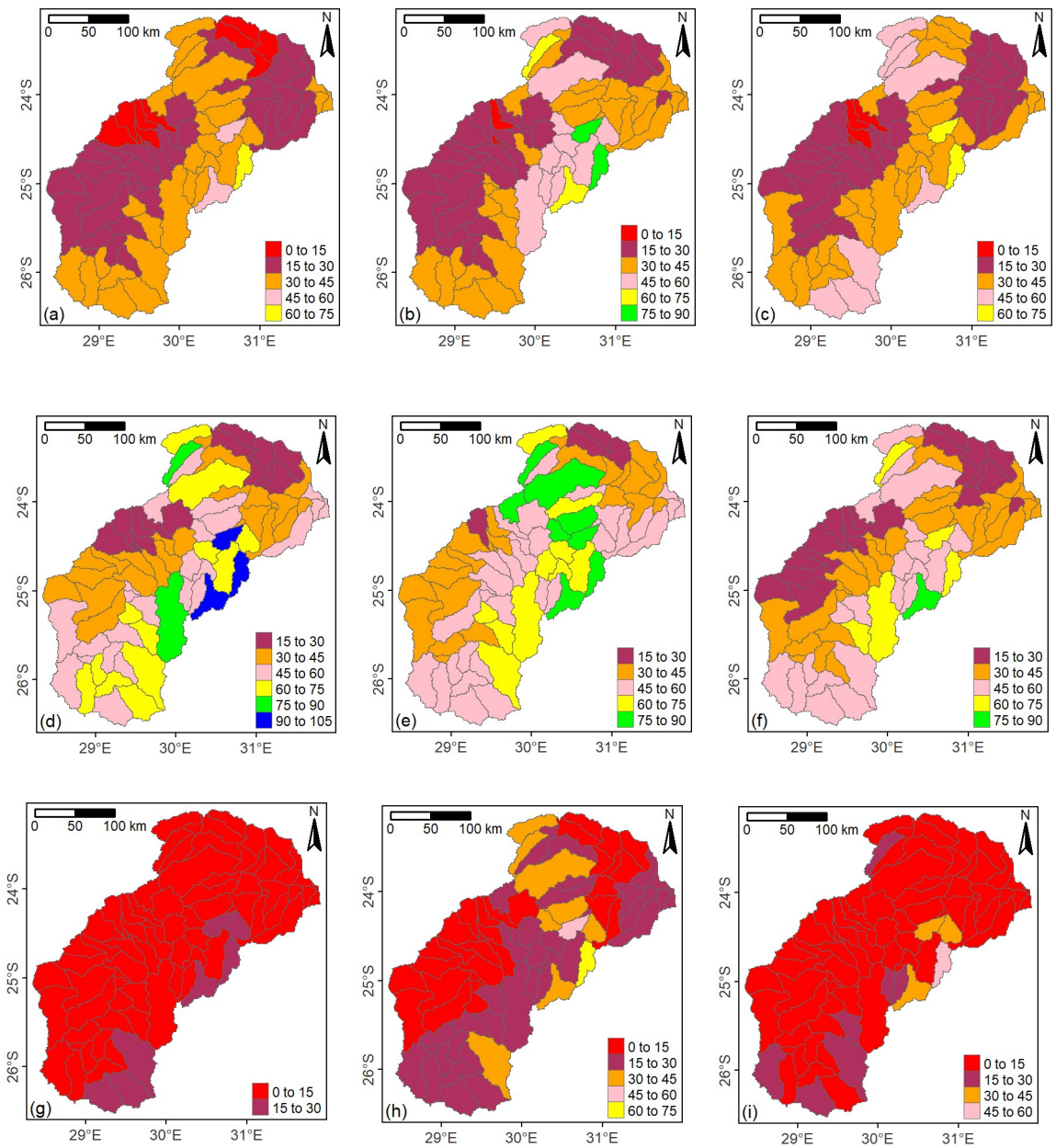


Figure A3-10: Projected winter precipitation in the Olifants River basin for mid-century under rcp 8.5 climate projections (The units are in mm).

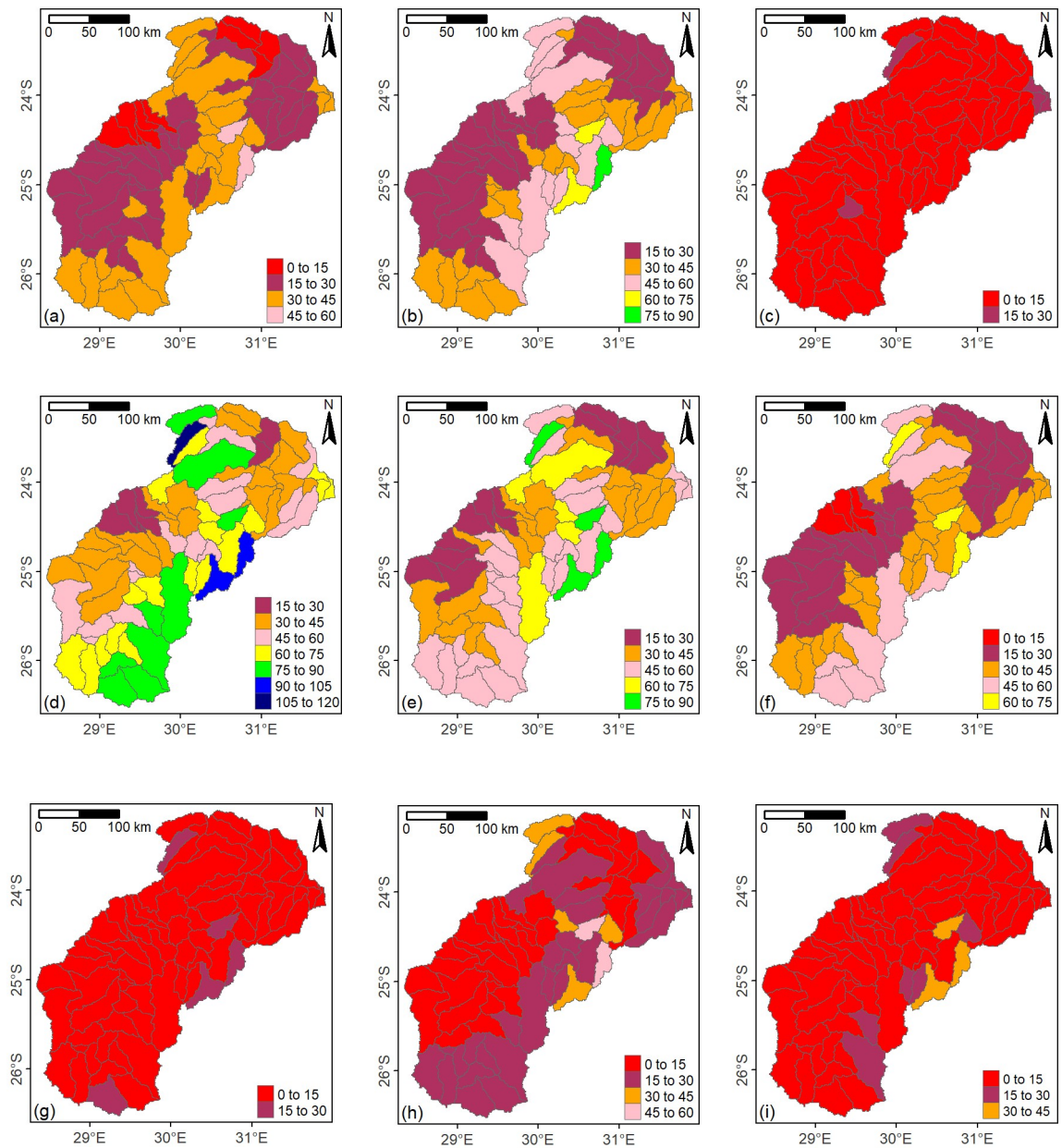


Figure A3-11: Projected winter precipitation in the Olifants River basin for end-century under rep 4.5 climate projections (The units are in mm).

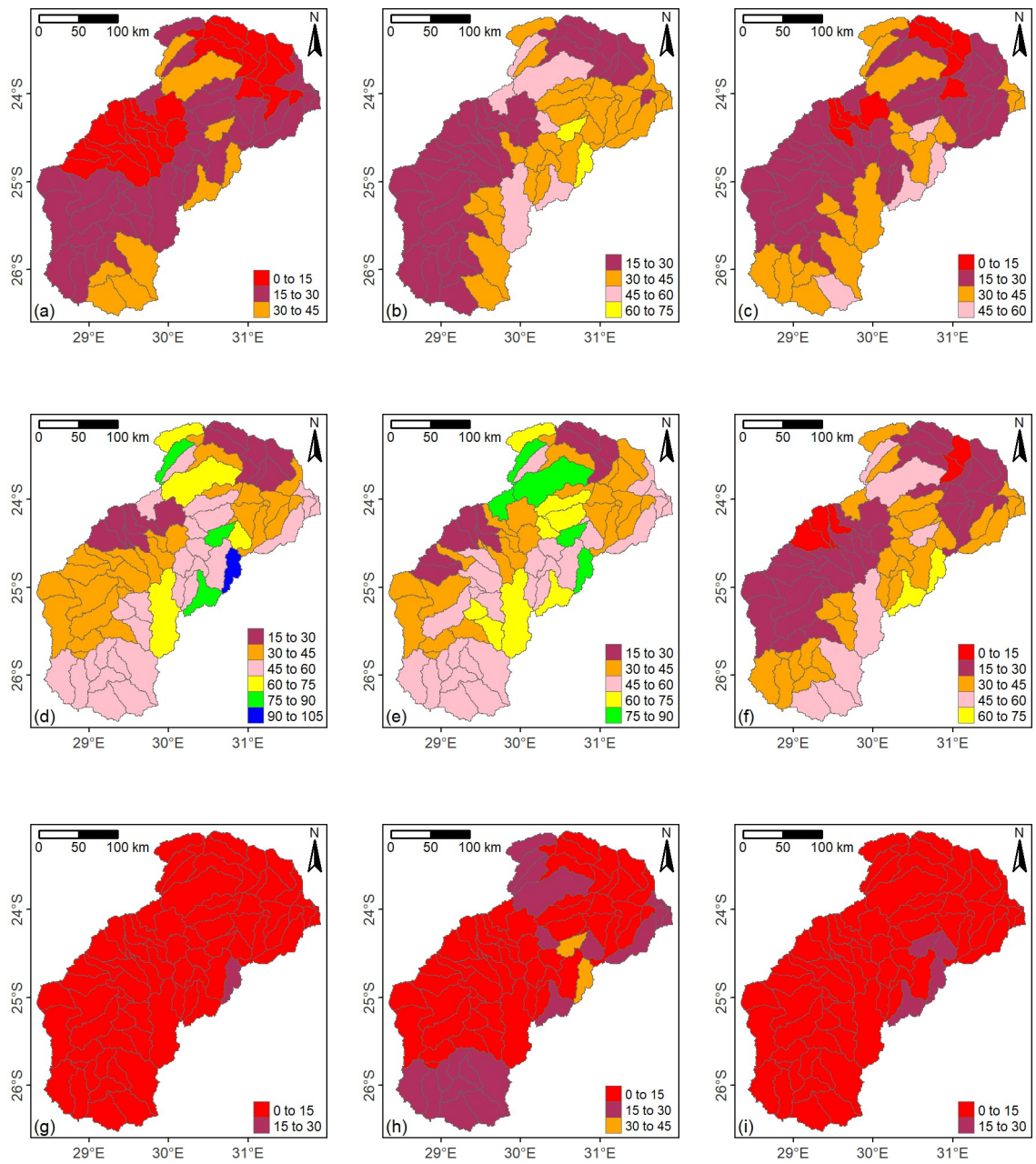


Figure A3-12: Projected winter precipitation in the Olifants River basin for end-century under rcp 8.5 climate projections (The units are in mm).

Annexure 4: Projected temperature maps for the future periods

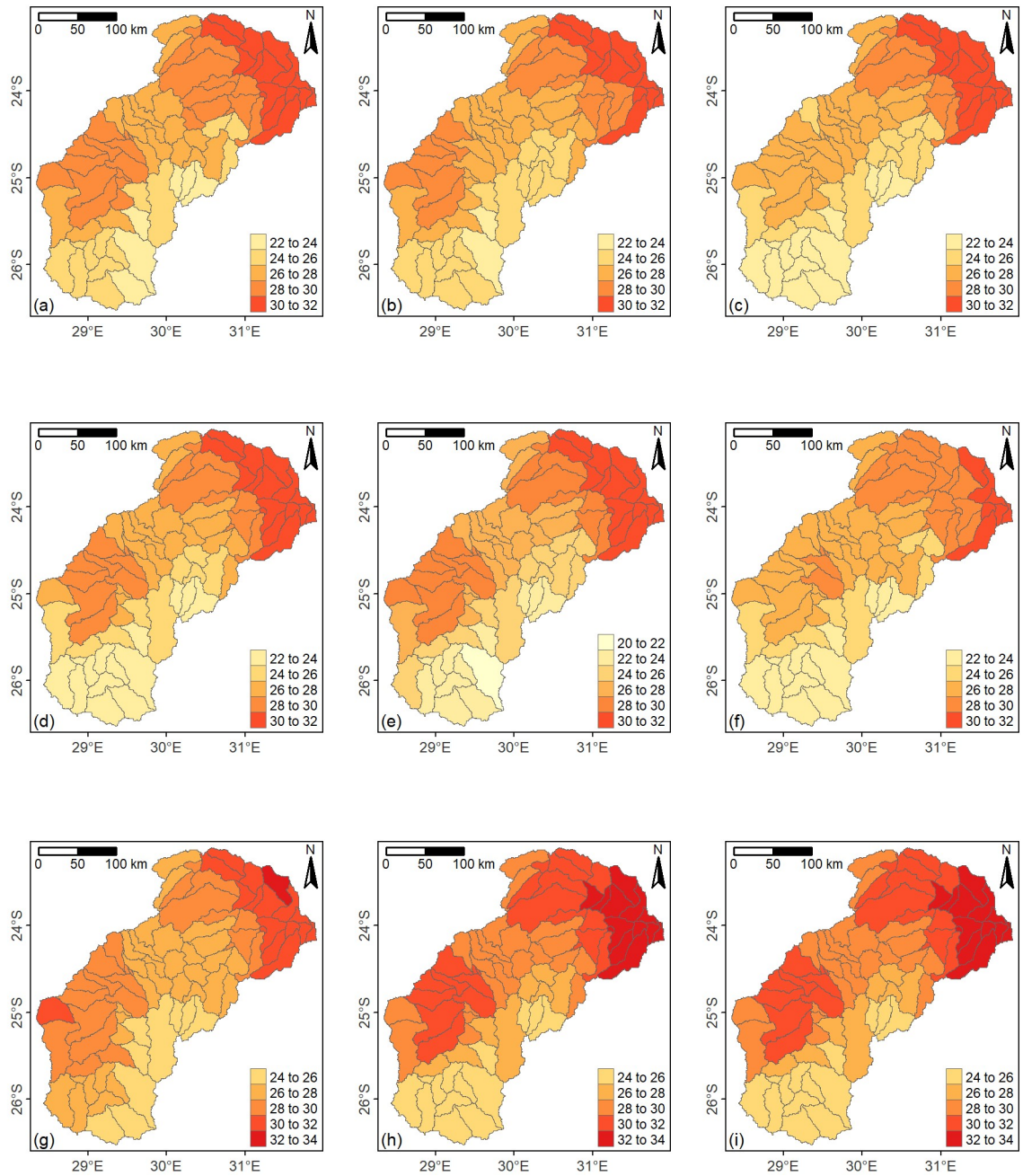


Figure A4-1: Projected maximum annual temperature in the Olifants River basin for mid-century under rcp 4.5 climate projections (The units are in $^{\circ}\text{C}$).

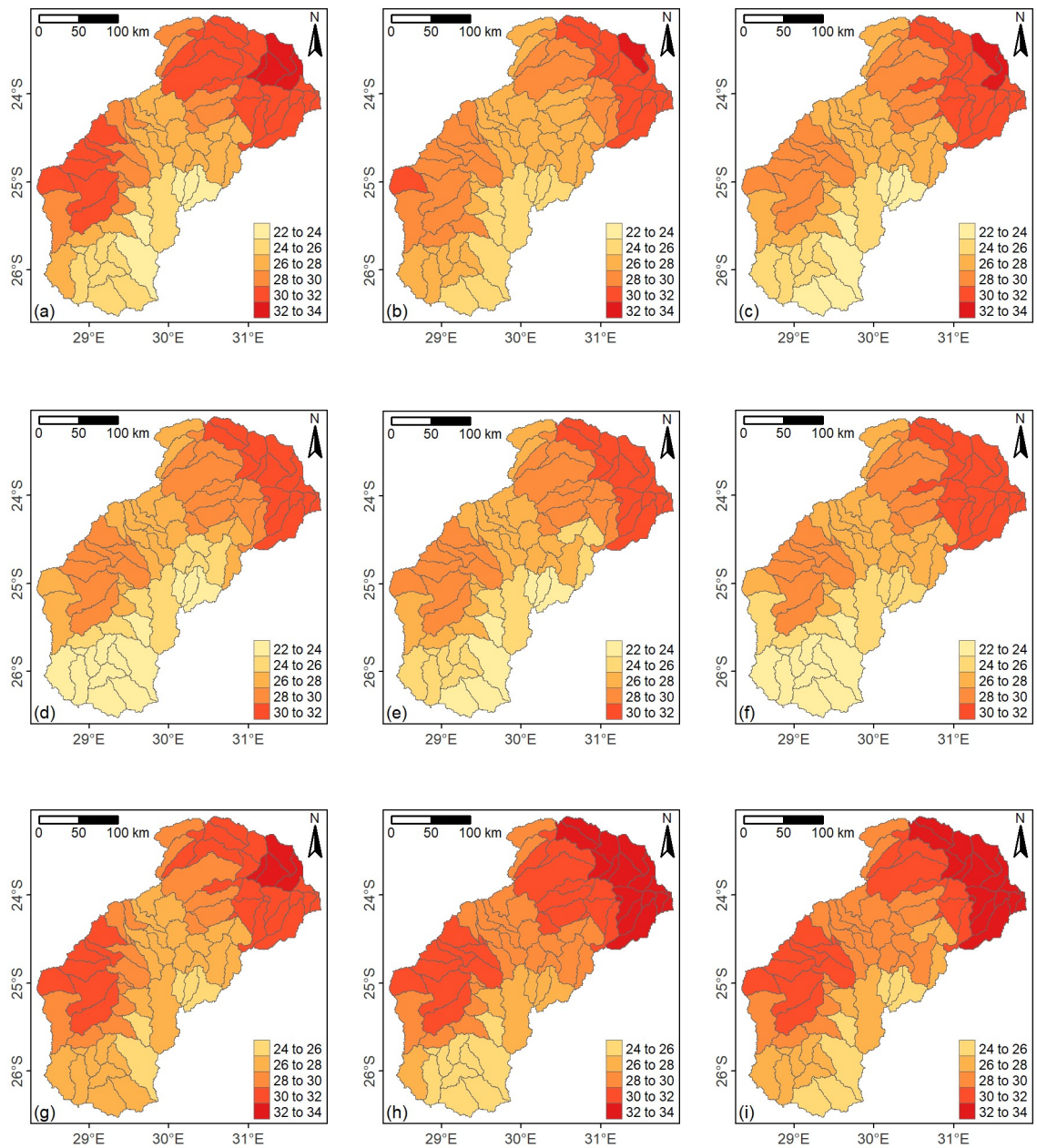


Figure A4-2: Projected maximum annual temperature in the Olifants River basin for mid-century under rcp 8.5 climate projections (The units are in $^{\circ}\text{C}$).

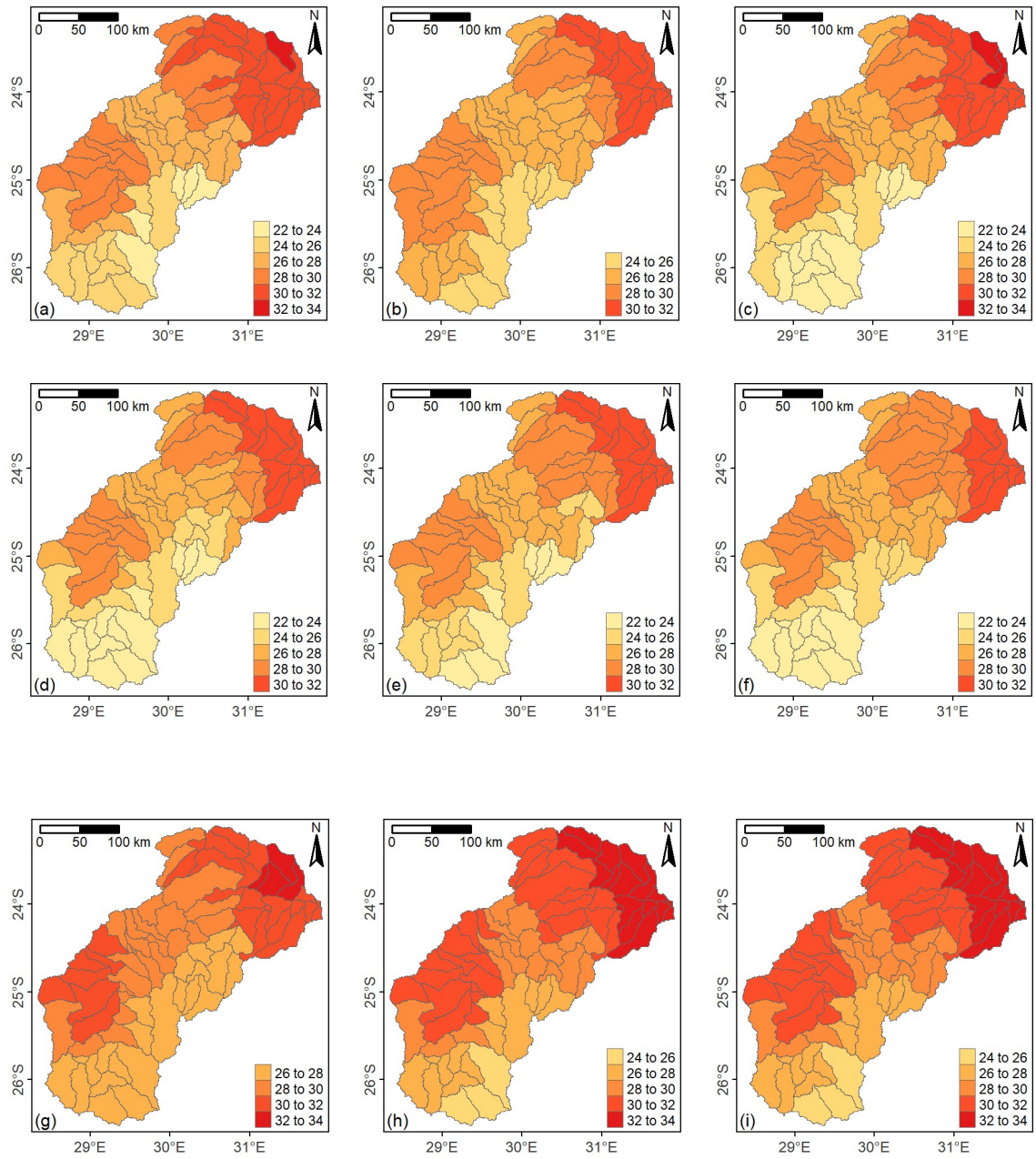


Figure A4-3: Projected maximum annual temperature in the Olifants River basin for end-century under rcp 4.5 climate projections (The units are in $^{\circ}\text{C}$).

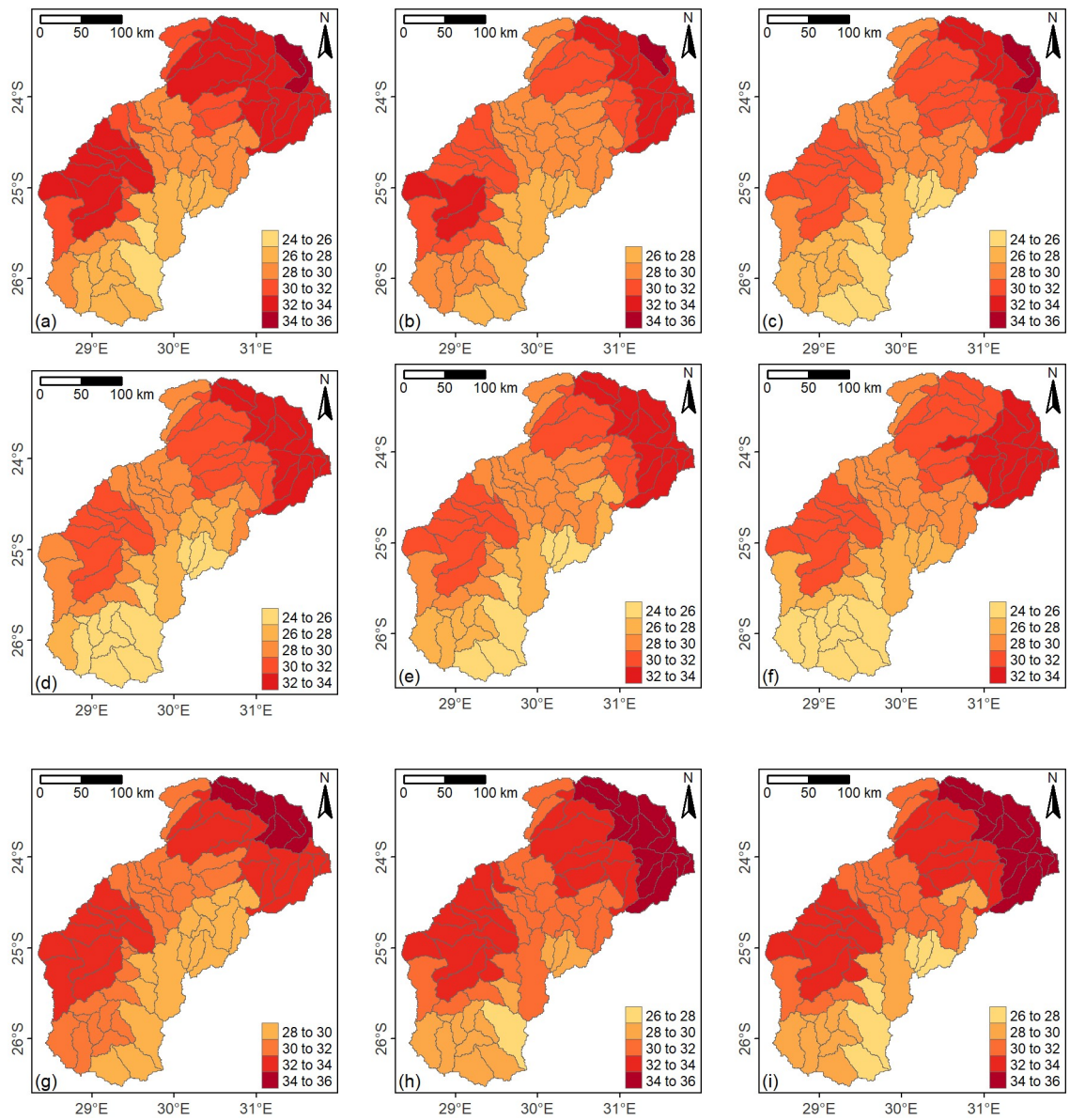


Figure A4-4: Projected maximum annual temperature in the Olifants River basin for end-century under rcp 8.5 climate projections (The units are in $^{\circ}\text{C}$).

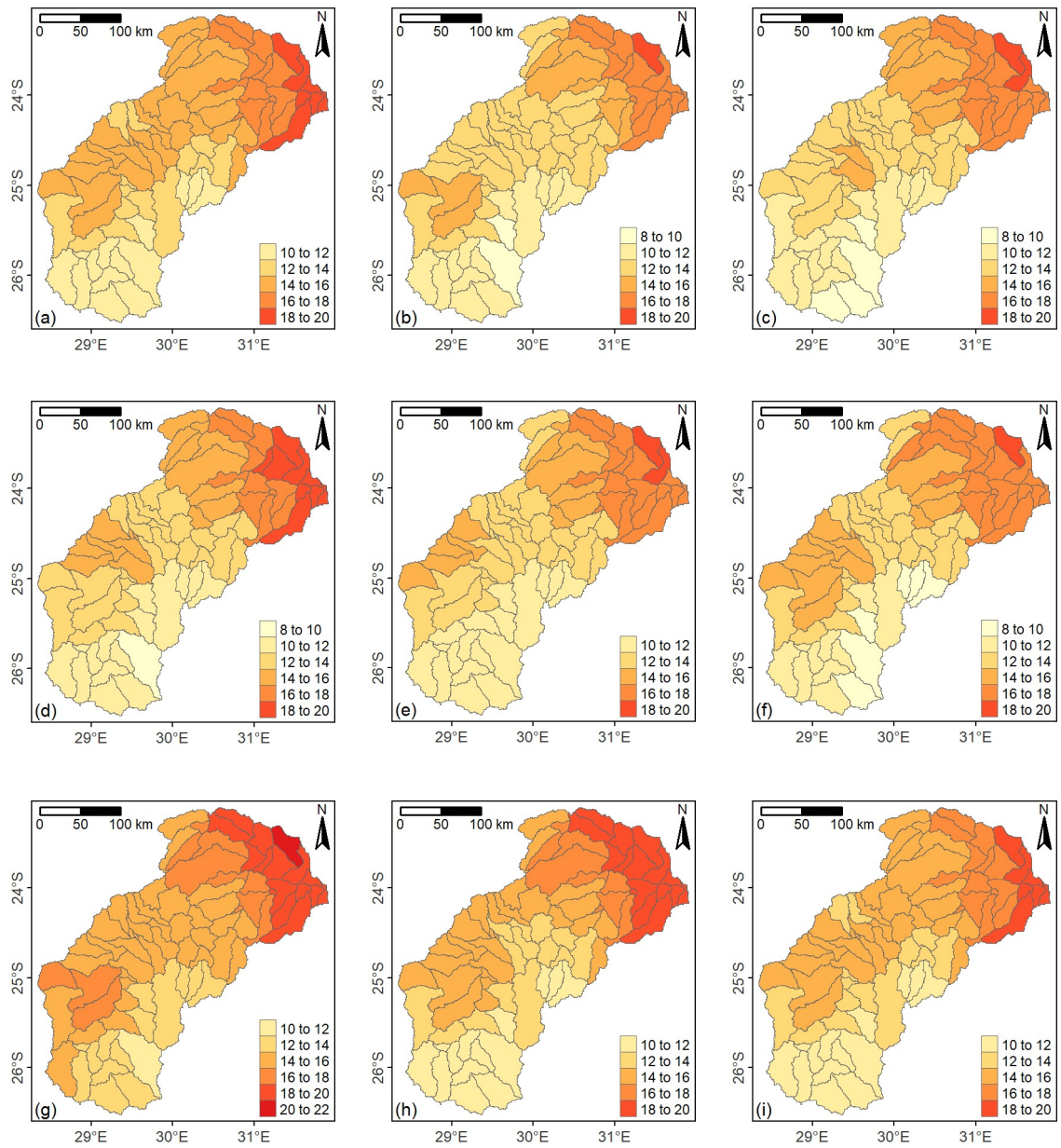


Figure A4-5: Projected minimum annual temperature in the Olifants River basin for mid-century under rcp 4.5 climate projections (The units are in $^{\circ}\text{C}$).

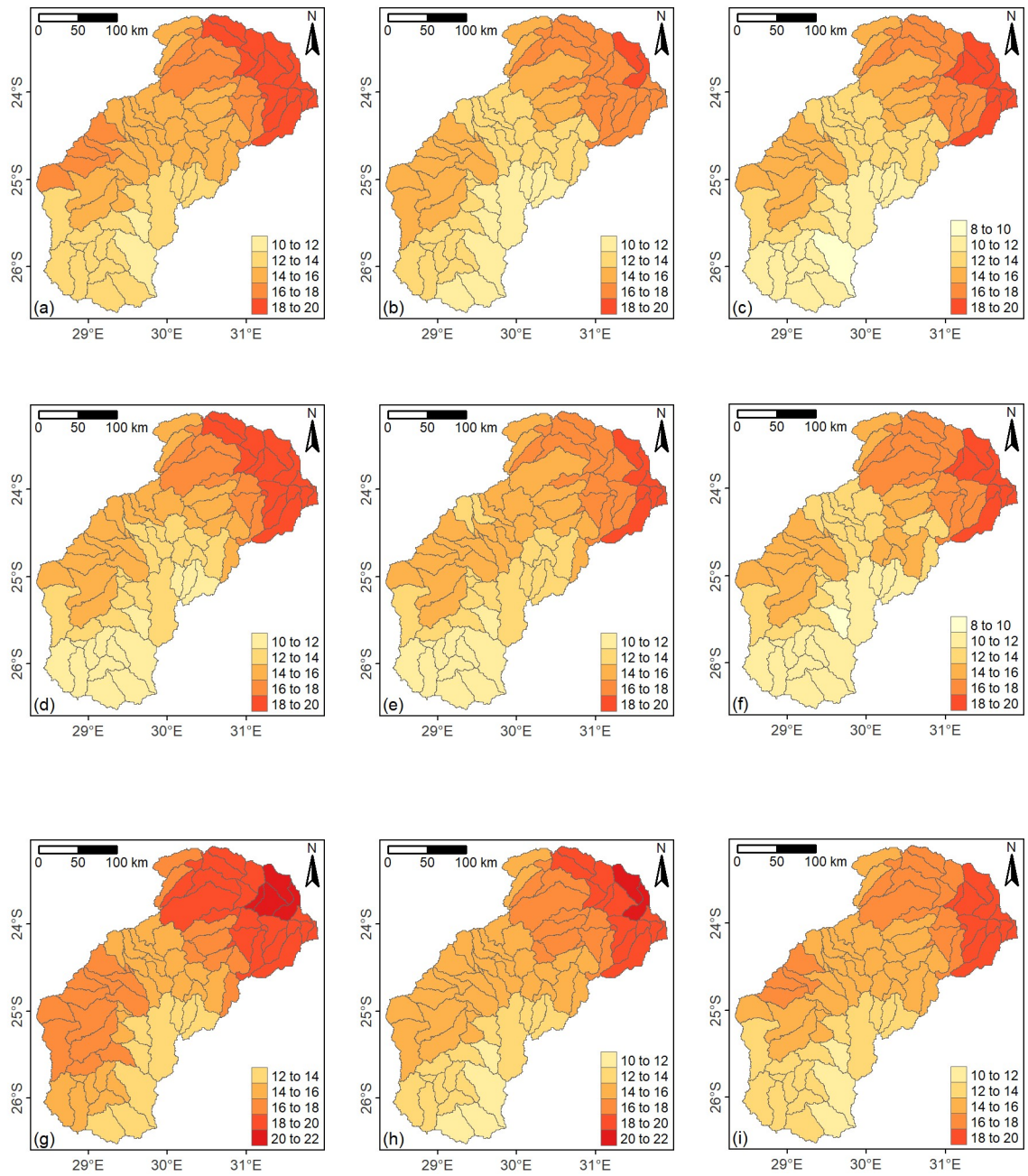


Figure A4-6: Projected minimum annual temperature in the Olifants River basin for mid-century under rcp 8.5 climate projections (The units are in $^{\circ}\text{C}$).

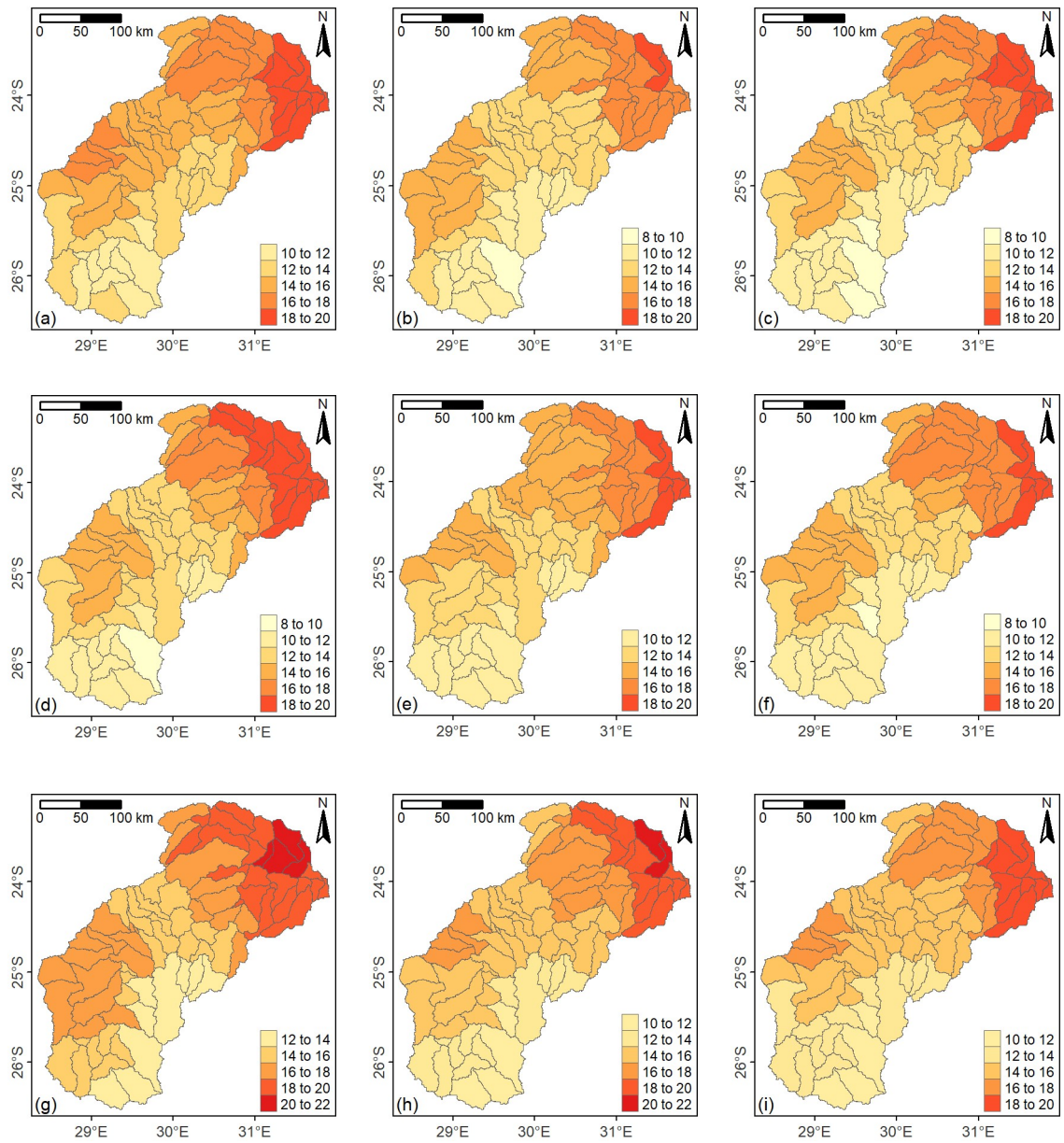


Figure A4-7: Projected minimum annual temperature in the Olifants River basin for end-century under rcp 4.5 climate projections. (The units are in $^{\circ}\text{C}$).

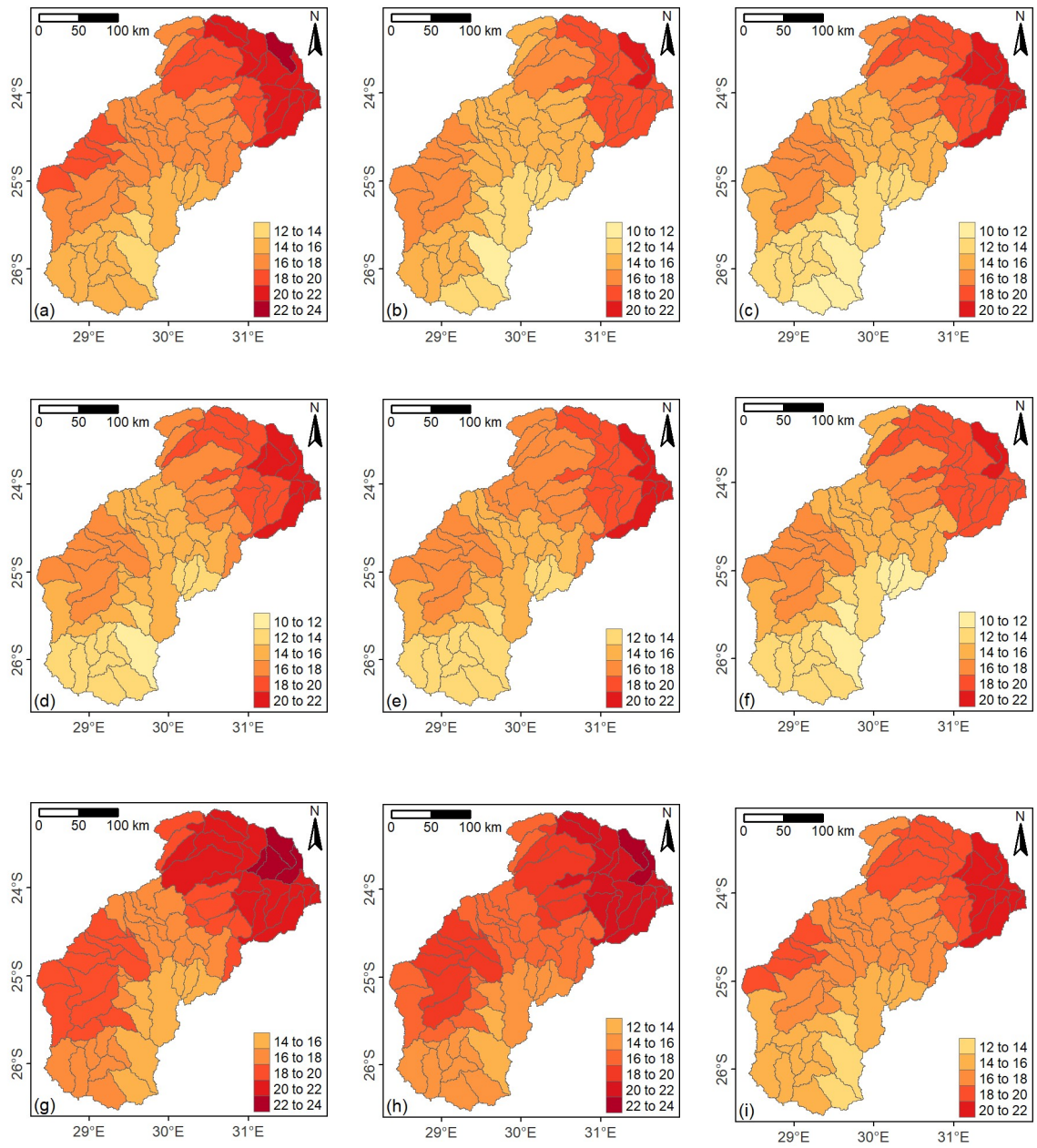


Figure A4-8: Projected minimum annual temperature in the Olifants River basin for end-century under rcp 8.5 climate projections (The units are in $^{\circ}\text{C}$).

Annexure 5: Projected PET maps for the future periods

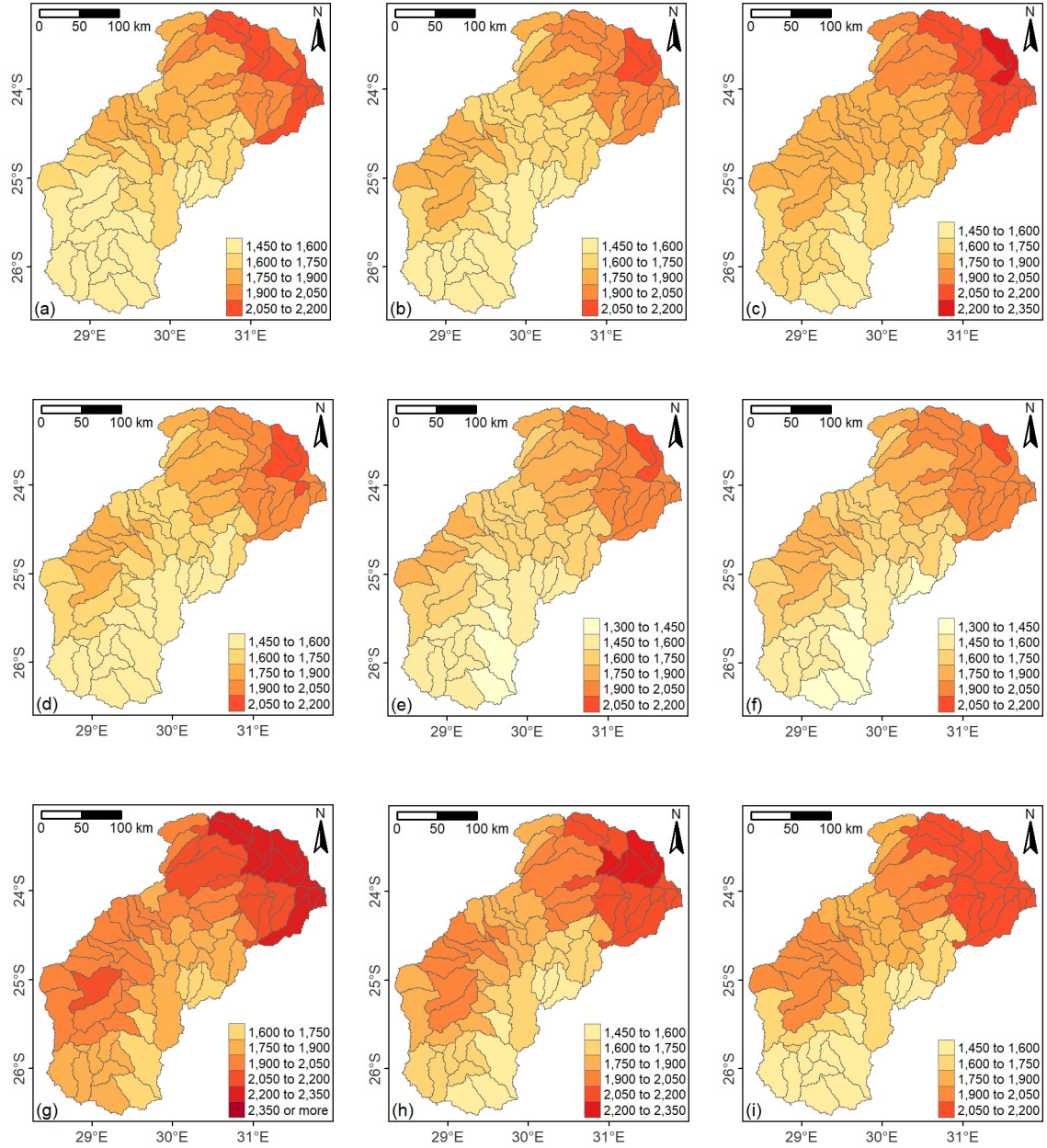


Figure A5-1: Projected annual potential evapotranspiration in the Olifants River basin for mid-century under rcp 4.5 climate projections (The units are in mm).

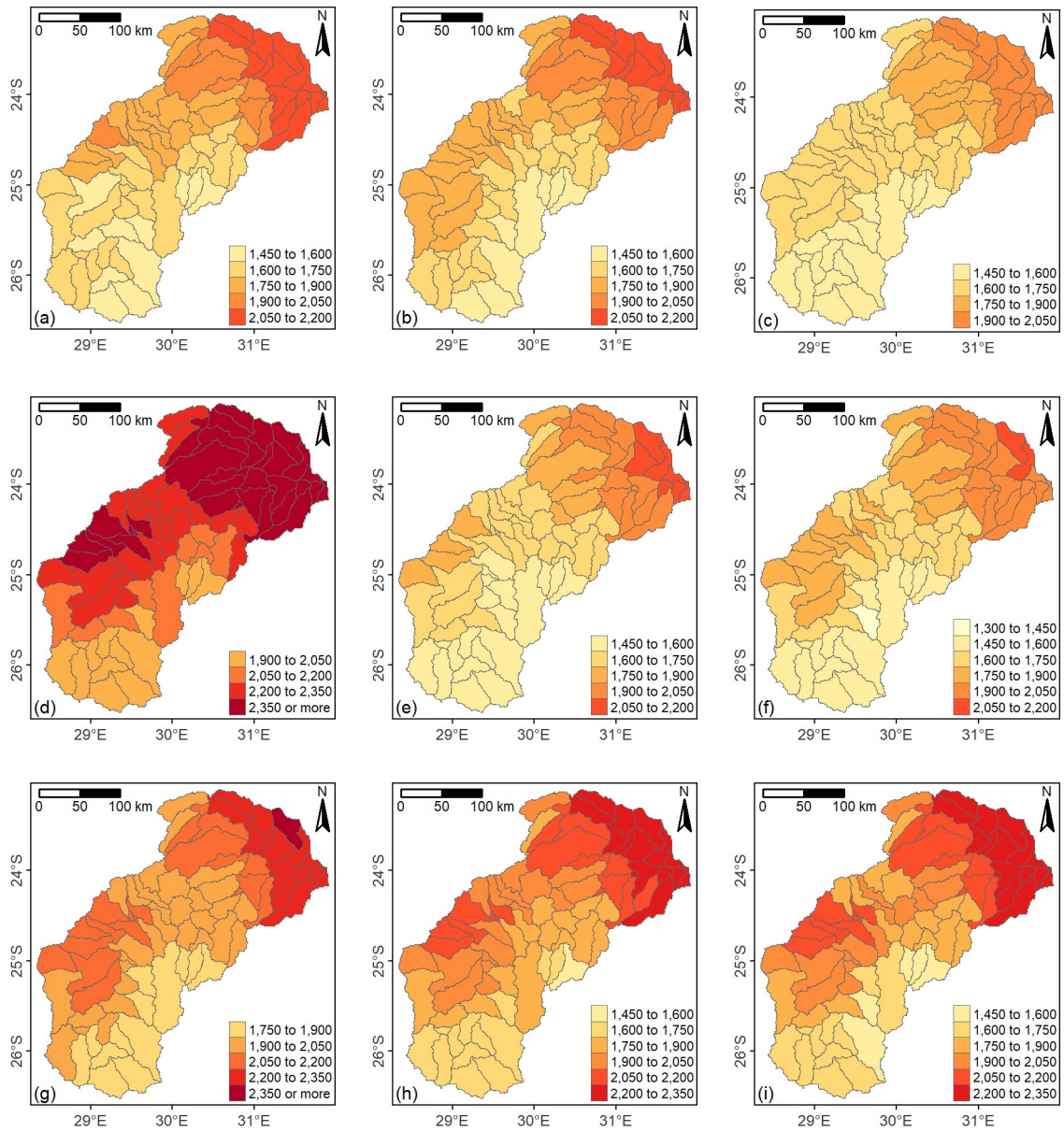


Figure A5-2: Projected annual potential evapotranspiration in the Olifants River basin for end-century under rcp 4.5 climate projections (The units are in mm).

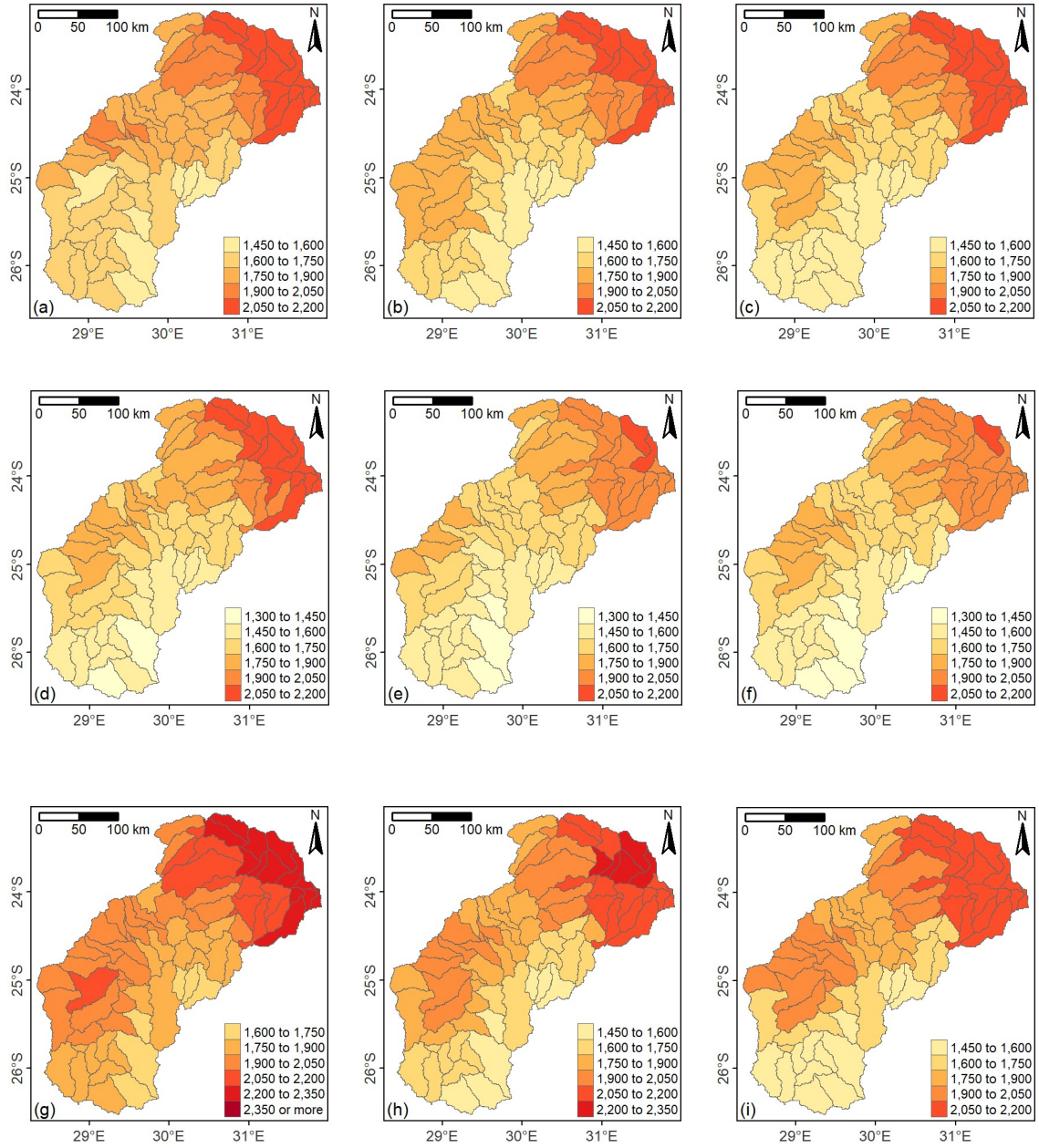


Figure A5-3: Projected annual potential evapotranspiration in the Olifants River basin for mid-century under rcp 8.5 climate projections (The units are in mm).

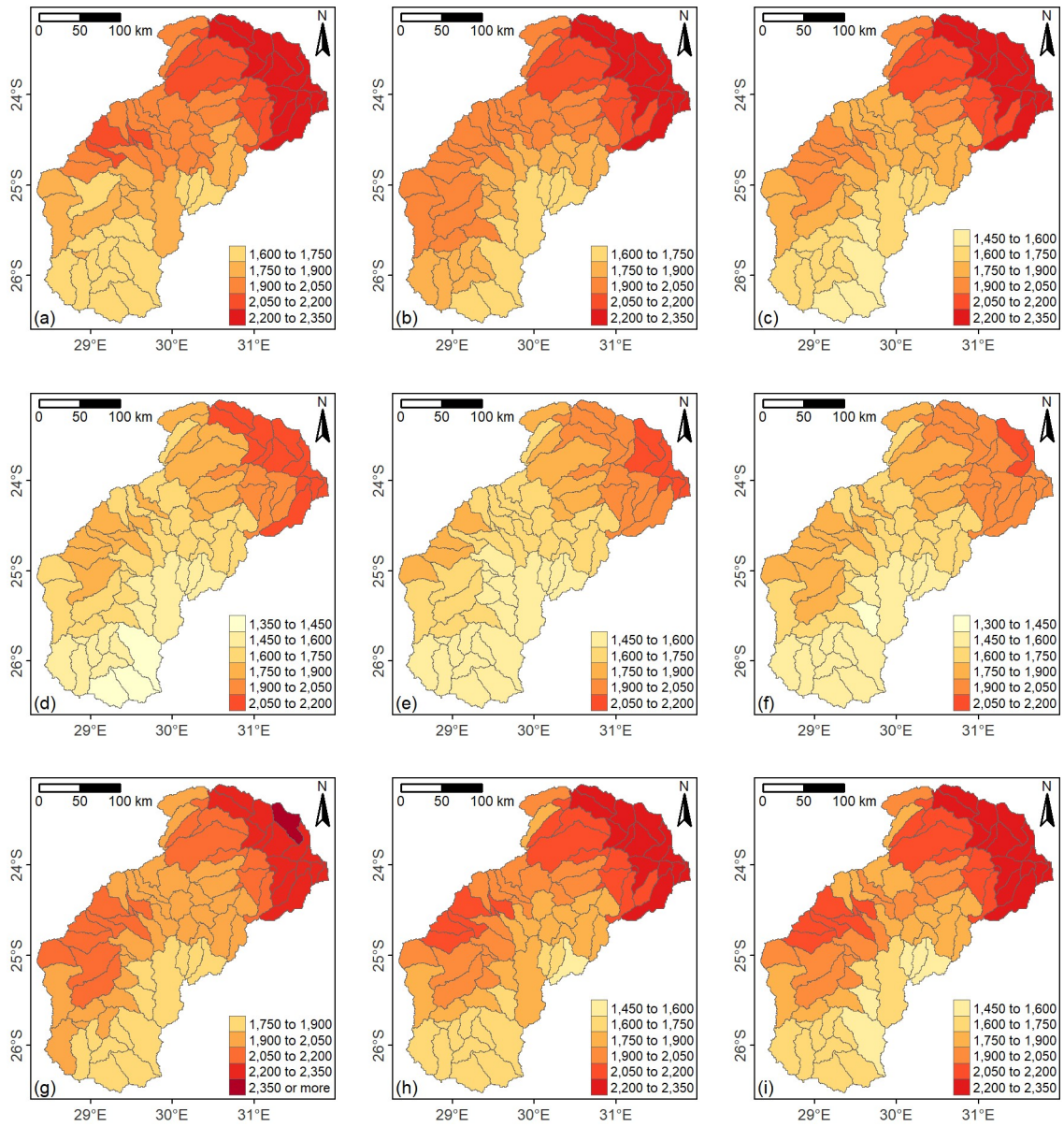


Figure A5-4: Projected annual potential evapotranspiration in the Olifants River basin for end-century under rcp 8.5 climate projections (The units are in mm).

Annexure 6: Projected water yield maps for the future periods

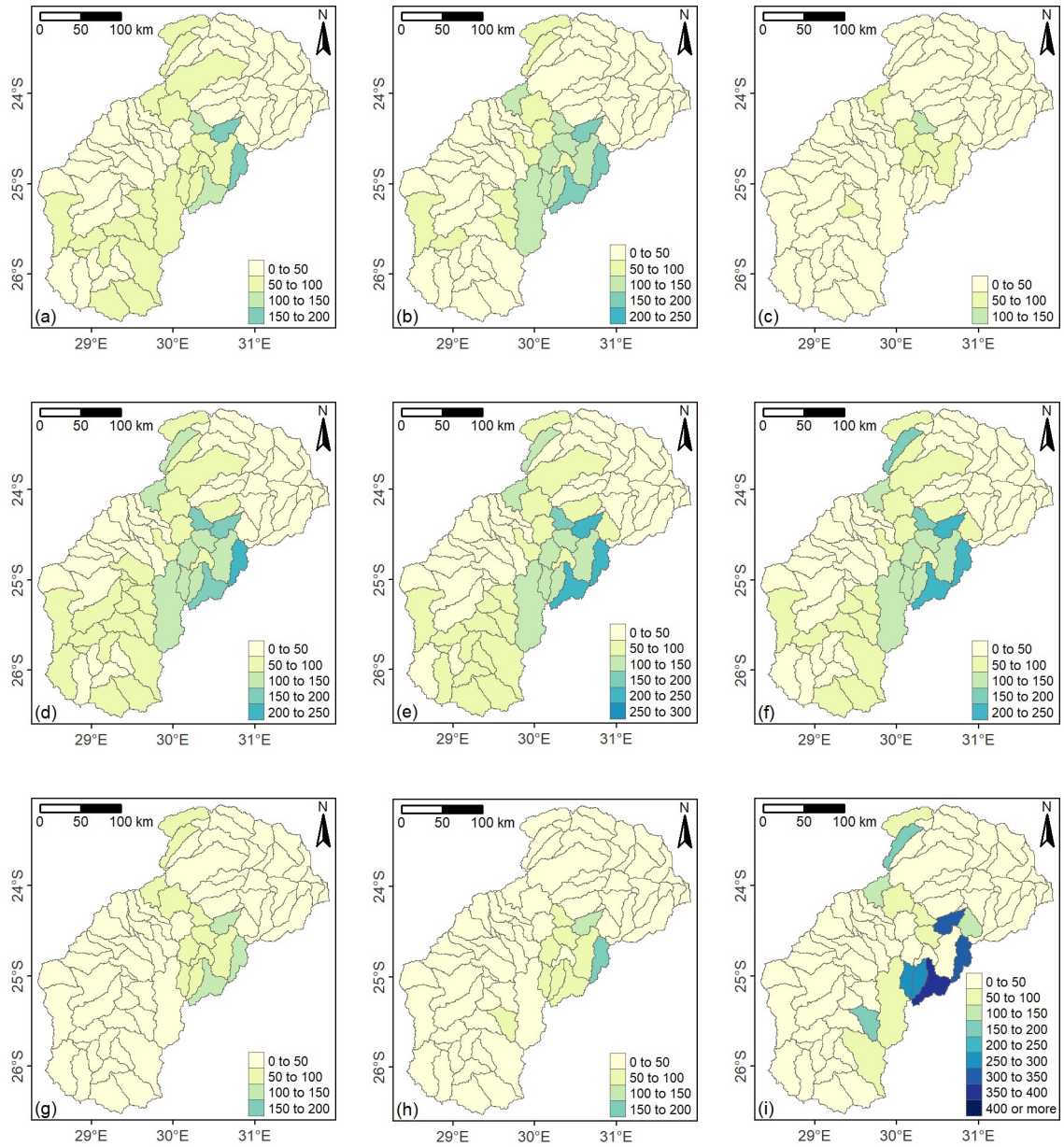


Figure A6-1: Projected annual water yield in the Olifants River basin for mid-century under rcp 4.5 climate projections (The units are in mm).

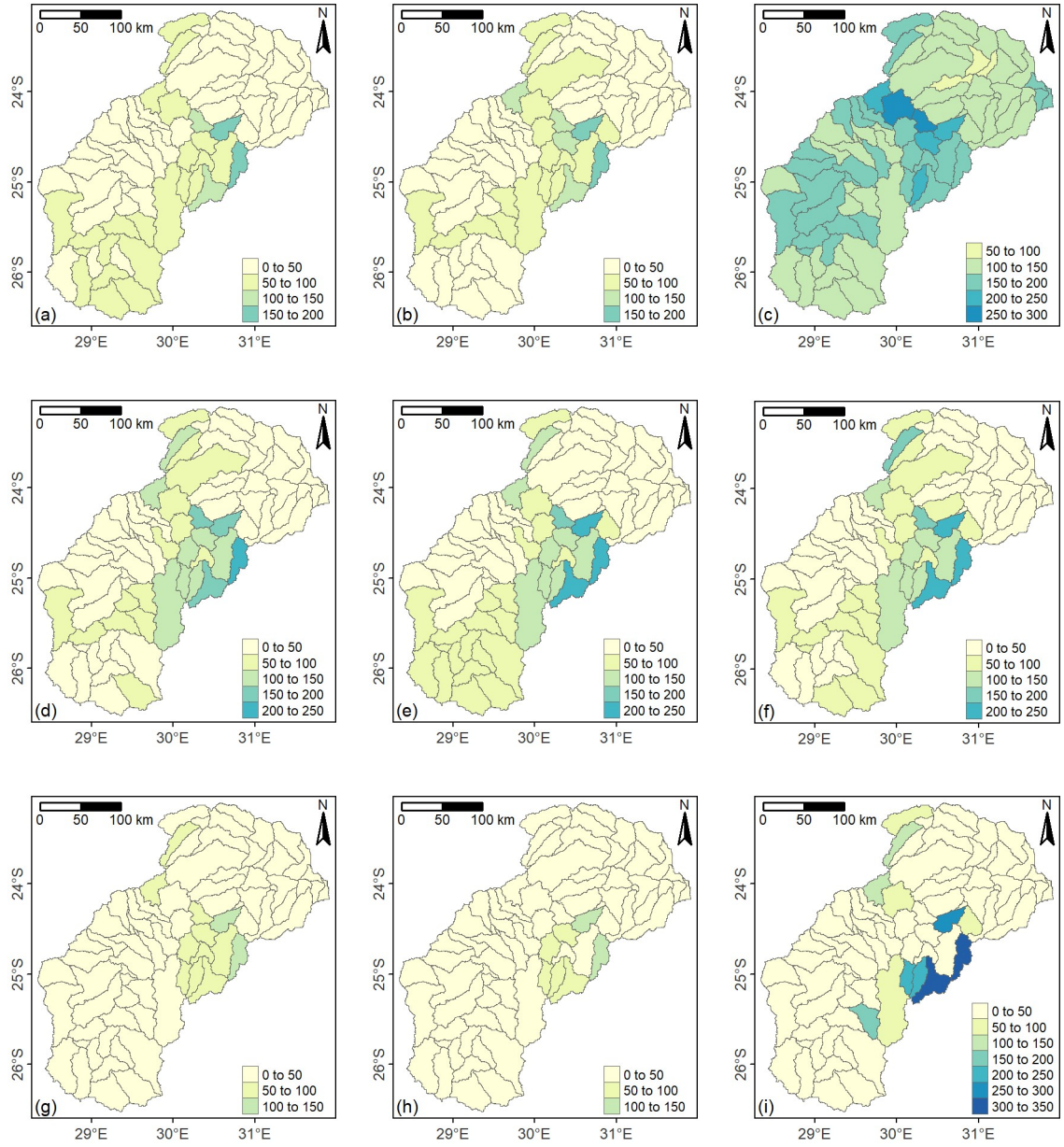


Figure A6-2: Projected annual water yield in the Olifants River basin for end-century under rcp 4.5 climate projections (The units are in mm).

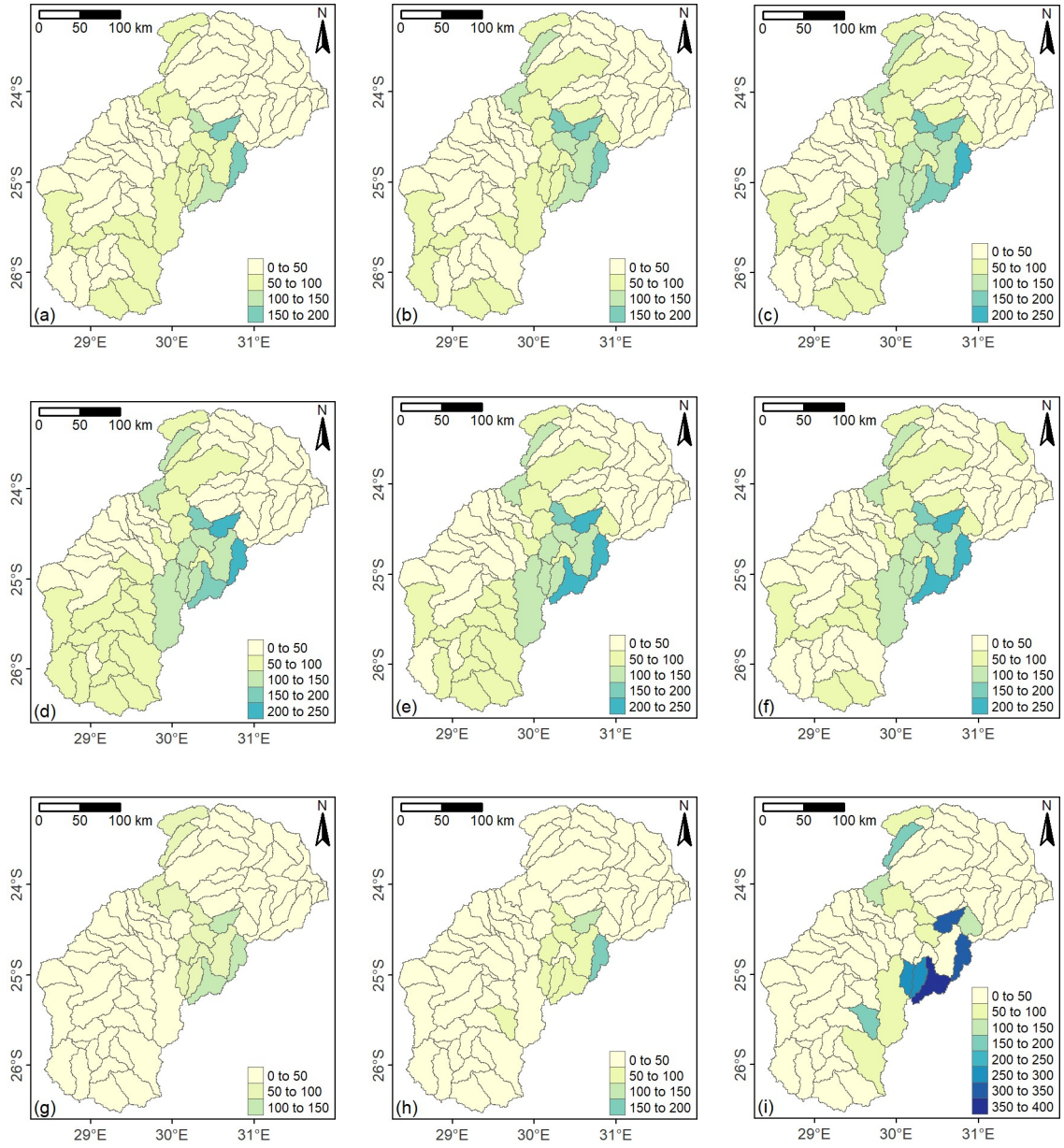


Figure A6-3: Projected annual water yield in the Olifants River basin for mid-century under rcp 8.5 climate projections (The units are in mm).

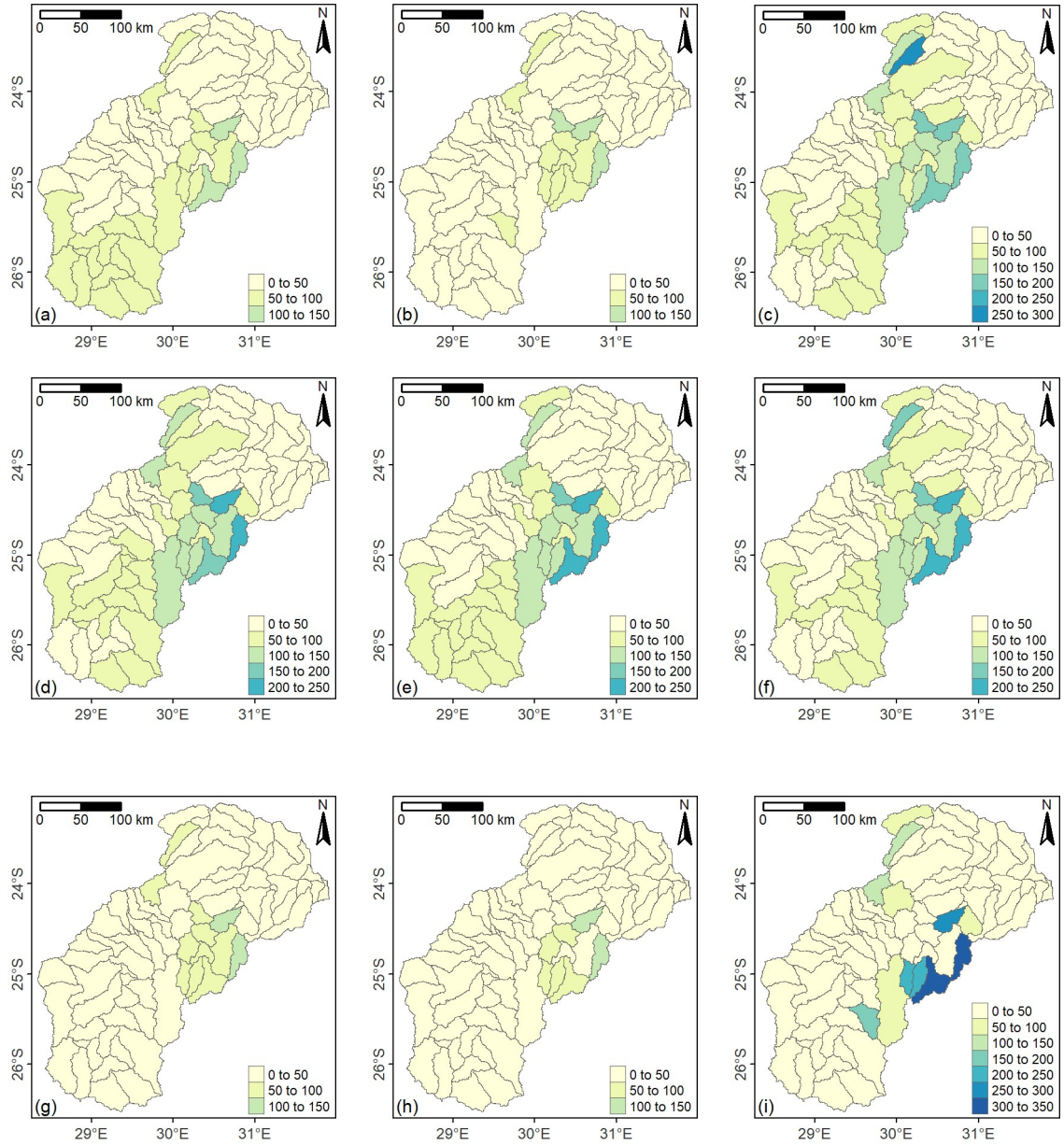


Figure A6-4: Projected annual water yield in the Olifants River basin for end-century under rcp 8.5 climate projections (The units are in mm).

Annexure 7: Projected Flow Duration Curves at Mamba for future periods

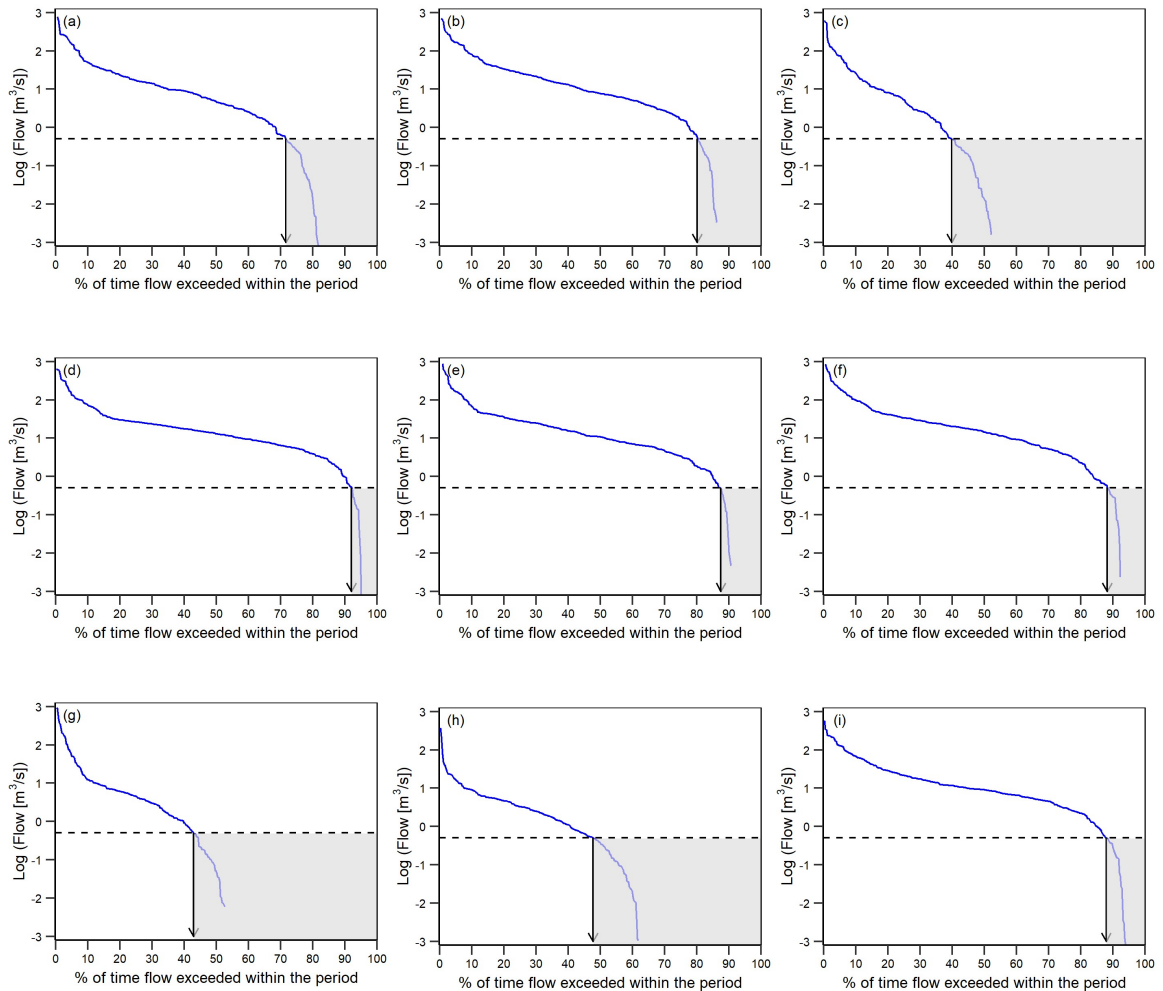


Figure A7-1: Flow duration curve at B7H015 for mid-century under rcp 4.5 climate projections (The dotted line is representing the minimum flow required at this station to maintain environmental flow for KNP and the shaded area is showing minimum flow unavailability period).

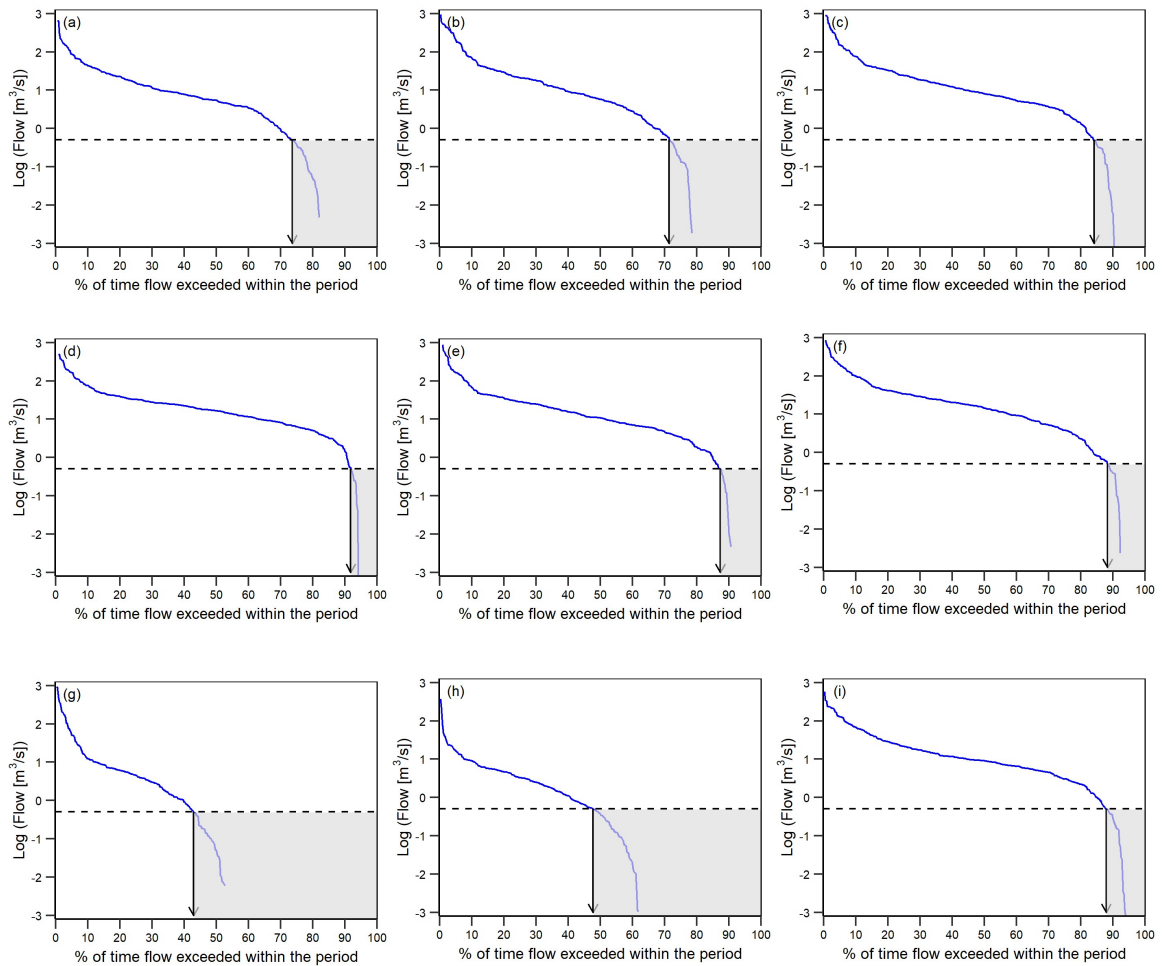


Figure A7-2: Flow duration curve at B7H015 for mid-century under rcp 8.5 climate projections (The dotted line is representing the minimum flow required at this station to maintain environmental flow for KNP and the shaded area is showing minimum flow unavailability period).

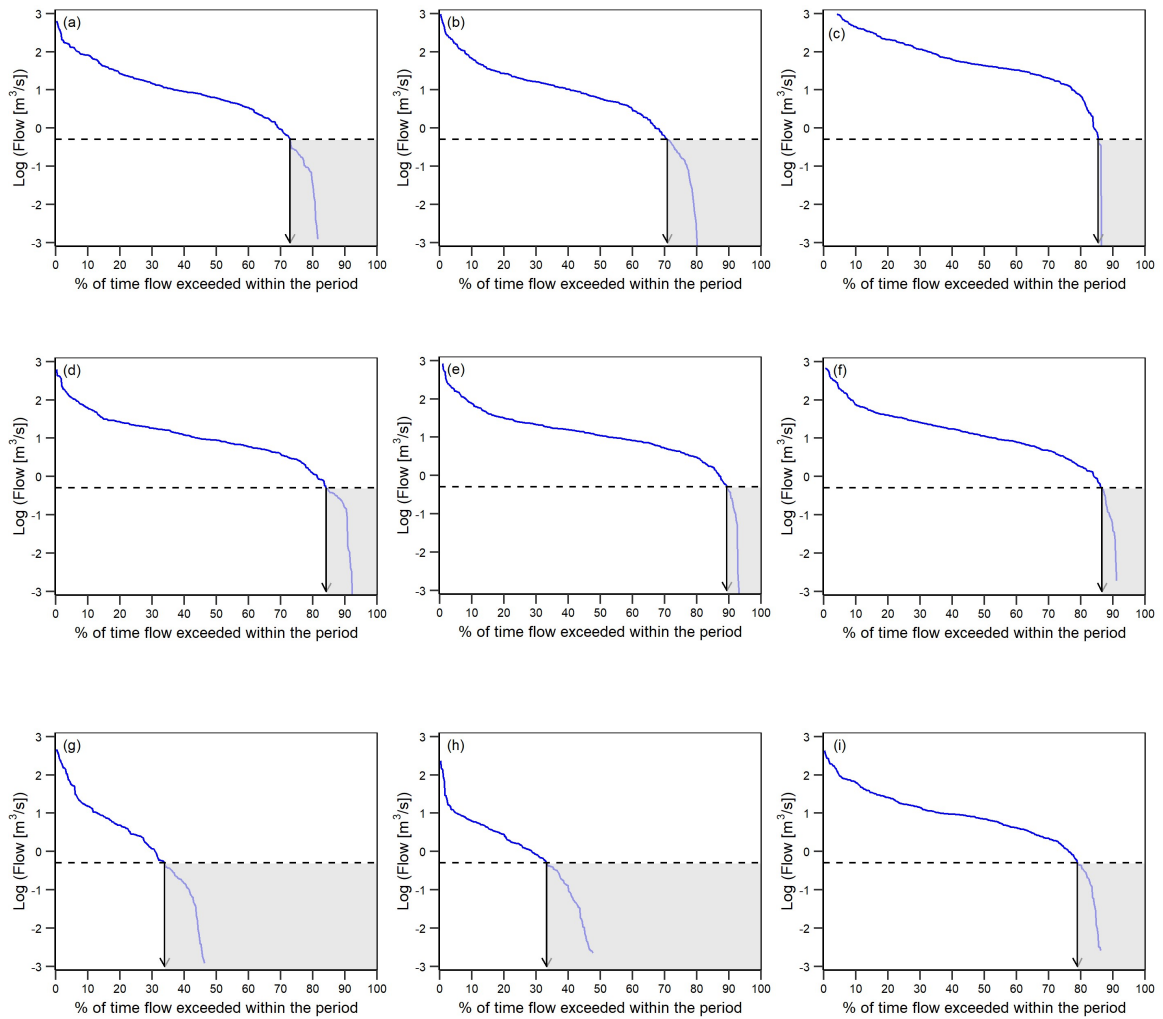


Figure A7-3: Flow duration curve at B7H015 for end-century under rcp 4.5 climate projections (The dotted line is representing the minimum flow required at this station to maintain environmental flow for KNP and the shaded area is showing minimum flow unavailability period).

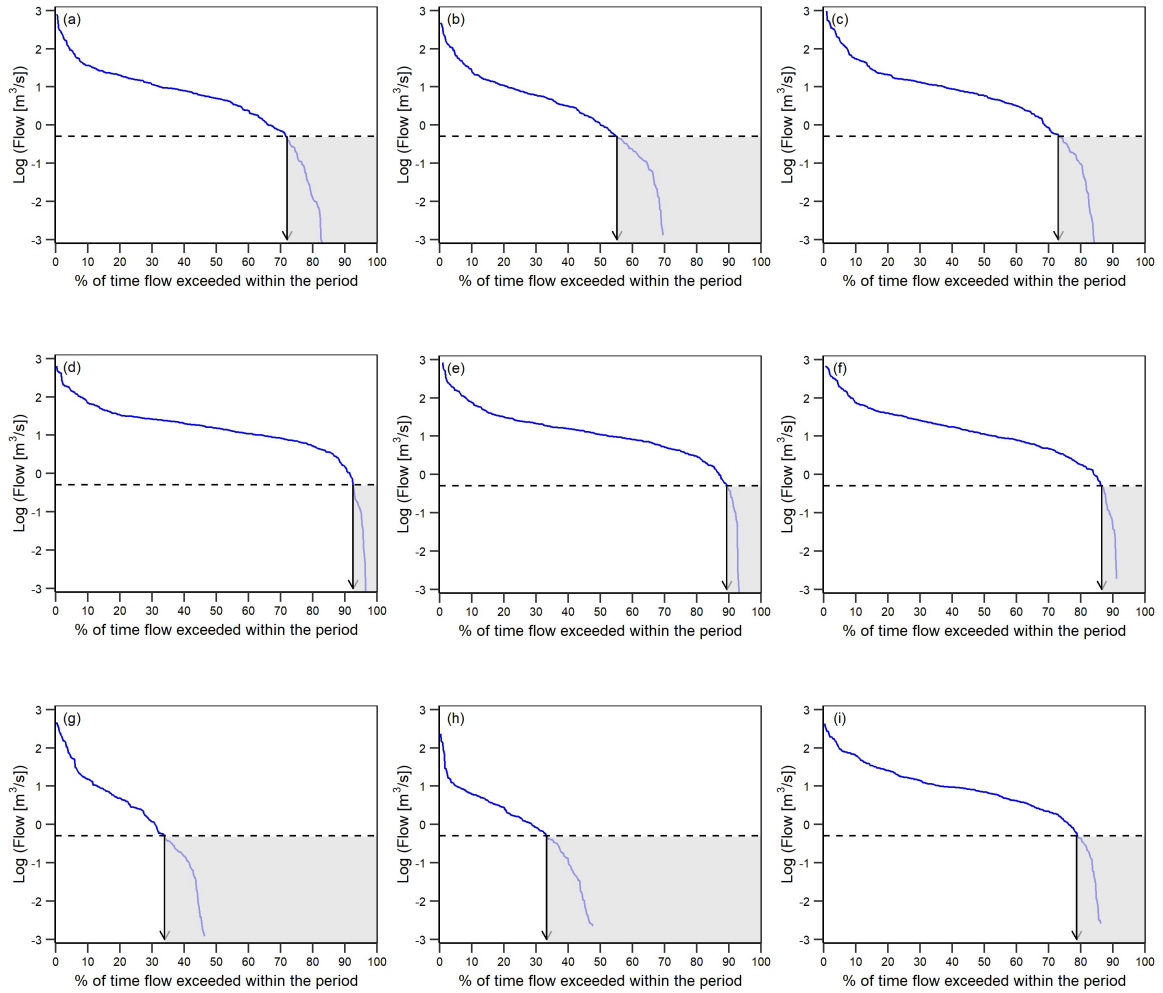


Figure A7-4: Flow duration curve at B7H015 for end-century under rcp 8.5 climate projections (The dotted line is representing the minimum flow required at this station to maintain environmental flow for KNP and the shaded area is showing minimum flow unavailability period).

Annexure 8: Trend analysis plots for projected temperatures

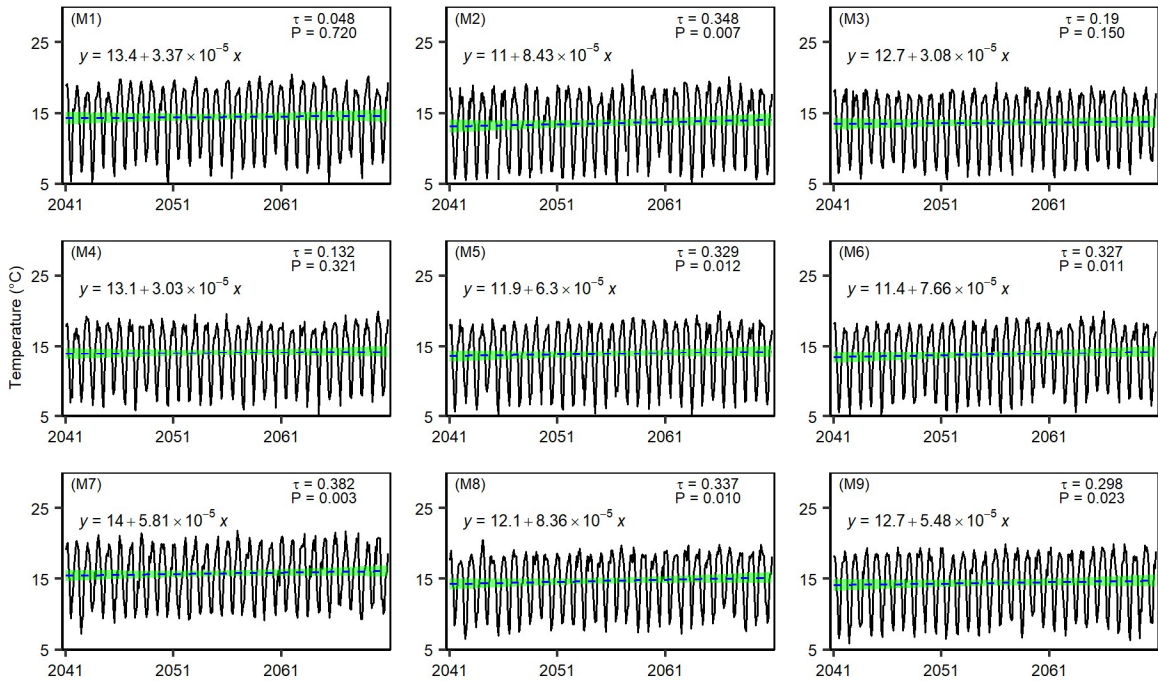


Figure A8-1: Monthly timeseries, linear regression analysis and annual Mann-Kendall statistics of daily minimum temperature for rcp 4.5 mid-century for the study area.

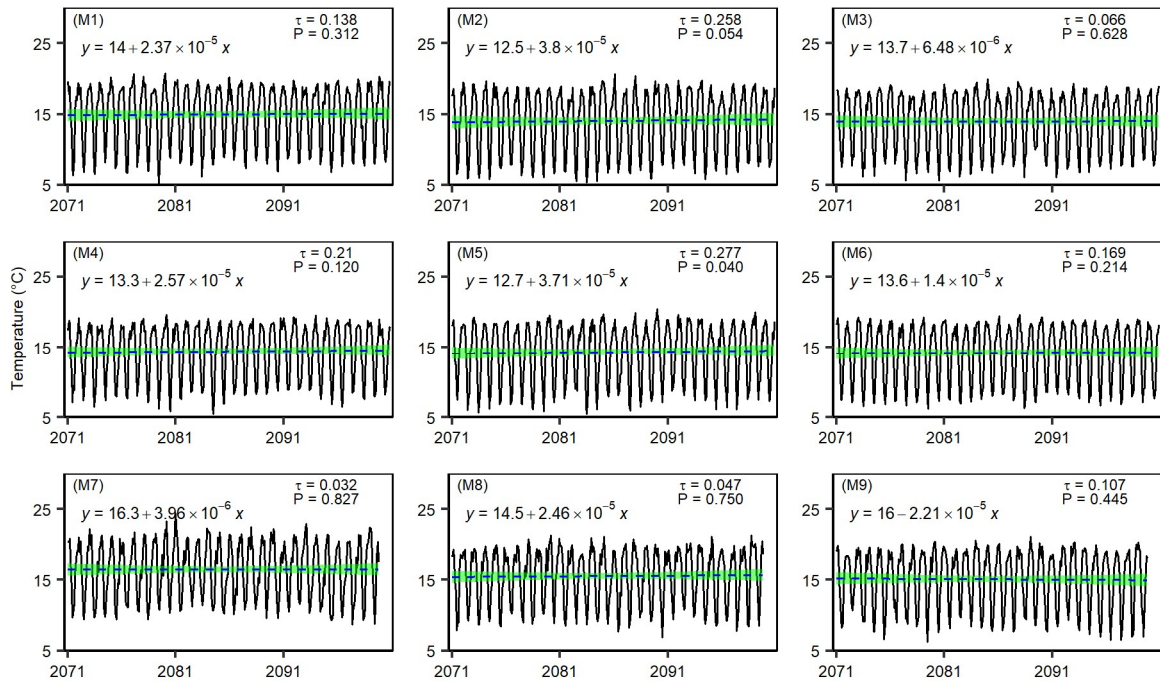


Figure A8-2: Monthly timeseries, linear regression analysis and annual Mann-Kendall statistics of daily minimum temperature for rcp 4.5 end-century for the study area.

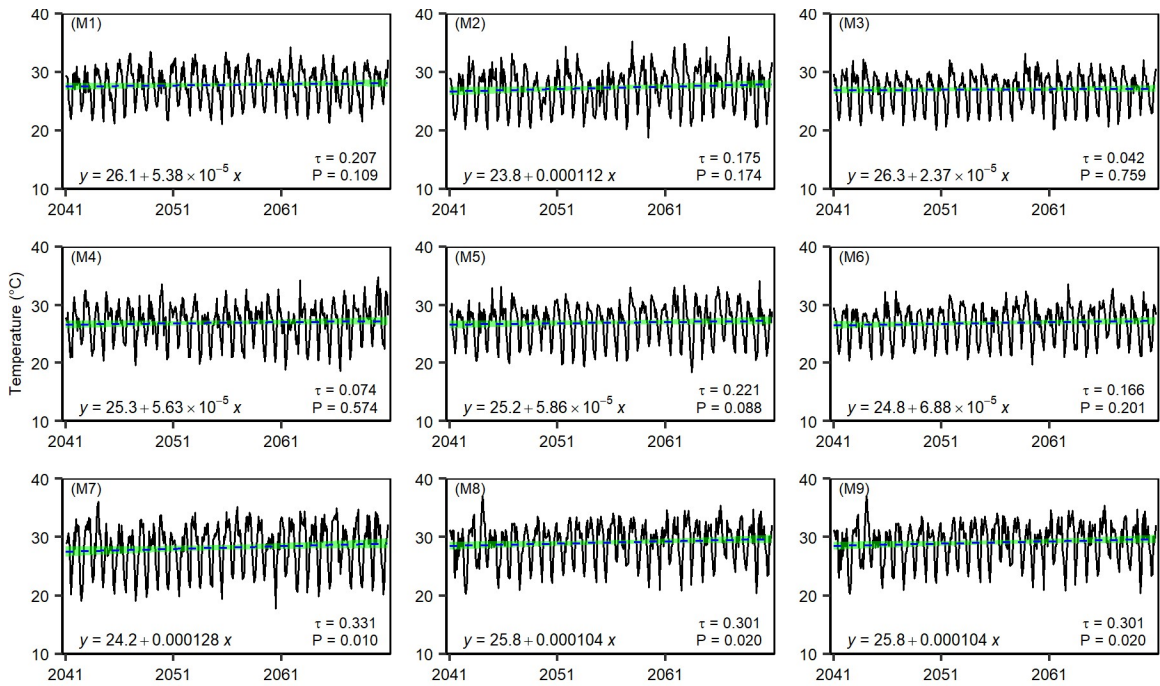


Figure A8-3: Monthly timeseries, linear regression analysis and annual Mann-Kendall statistics of daily maximum temperature for rcp 4.5 mid-century for the study area.

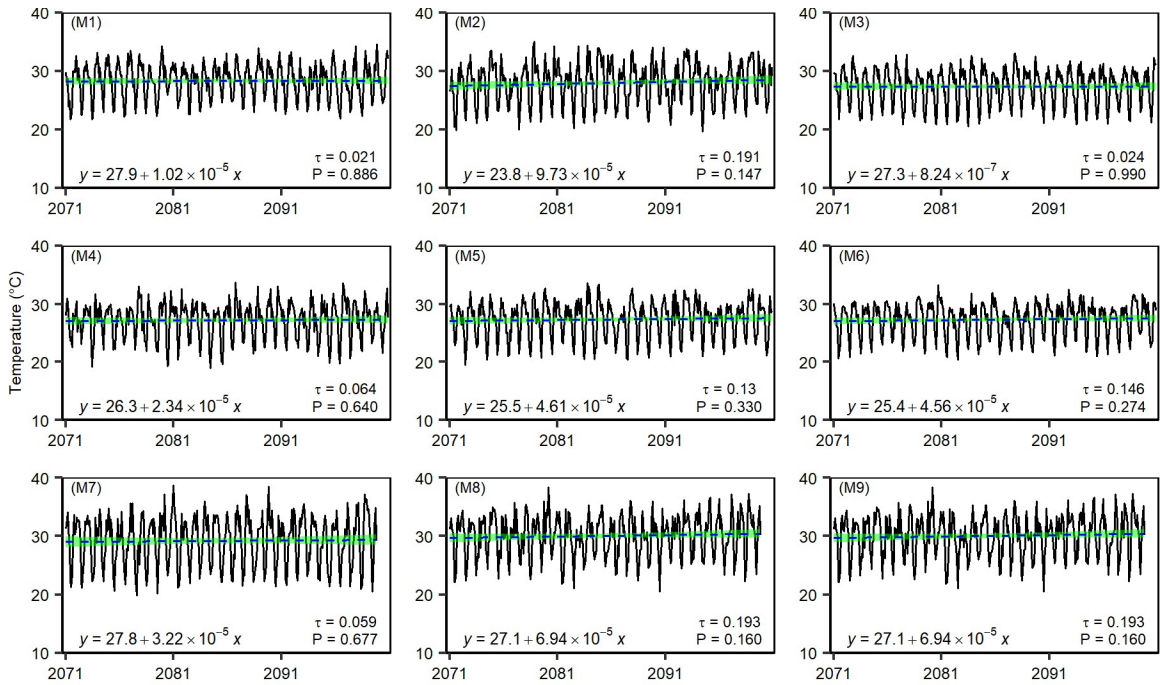


Figure A8-4: Monthly timeseries, linear regression analysis and annual Mann-Kendall statistics of daily maximum temperature for rcp 4.5 end-century for the study area.

Annexure 9: Change in annual hydrological components from base period

Table A9-1: Change in mean annual precipitation in future from base period (in mm)

Sub	Base	rcp4.5 MC		rcp4.5 EC		rcp8.5 MC		rcp8.5 EC	
		Model	(%)	Model	(%)	Model	(%)	Model	(%)
1	690	502	-27	482	-30	561	-19	505	-27
2	629	373	-41	376	-40	400	-37	333	-47
3	626	454	-27	458	-27	488	-22	405	-35
4	835	627	-25	599	-28	705	-16	600	-28
5	538	304	-43	310	-42	339	-37	282	-48
6	538	304	-43	310	-42	339	-37	282	-48
7	417	290	-30	296	-29	322	-23	270	-35
8	546	338	-38	343	-37	360	-34	301	-45
9	480	327	-32	327	-32	339	-29	294	-39
10	480	327	-32	327	-32	339	-29	294	-39
11	472	336	-29	319	-32	361	-23	326	-31
12	444	367	-17	358	-19	394	-11	350	-21
13	953	486	-49	488	-49	530	-44	430	-55
14	502	359	-28	340	-32	399	-20	343	-32
15	580	395	-32	395	-32	411	-29	341	-41
16	476	387	-19	362	-24	421	-12	379	-20
17	476	387	-19	362	-24	421	-12	379	-20
18	615	416	-32	422	-31	455	-26	361	-41
19	496	374	-25	374	-25	386	-22	321	-35
20	551	347	-37	324	-41	379	-31	344	-38
21	497	405	-19	405	-19	409	-18	353	-29
22	497	405	-19	405	-19	409	-18	353	-29
23	476	387	-19	362	-24	421	-12	379	-20
24	497	405	-19	405	-19	409	-18	353	-29
25	564	502	-11	503	-11	539	-4	445	-21
26	426	394	-8	394	-8	407	-4	346	-19
27	525	613	17	574	9	639	22	574	9
28	512	435	-15	435	-15	447	-13	386	-25
29	535	436	-19	436	-19	455	-15	387	-28
30	476	452	-5	413	-13	460	-3	419	-12
31	519	407	-21	375	-28	418	-19	382	-26
32	590	308	-48	302	-49	310	-48	289	-51
33	426	394	-8	394	-8	407	-4	346	-19
34	592	481	-19	487	-18	513	-13	447	-24
35	371	338	-9	344	-7	364	-2	315	-15
36	743	590	-21	595	-20	630	-15	528	-29
37	356	318	-11	317	-11	314	-12	285	-20
38	796	783	-2	762	-4	807	1	767	-4
39	762	345	-55	323	-58	343	-55	333	-56
40	439	331	-24	320	-27	332	-24	326	-26

Sub	Base	rcp4.5 MC		rcp4.5 EC		rcp8.5 MC		rcp8.5 EC	
		Model	(%)	Model	(%)	Model	(%)	Model	(%)
41	356	318	-11	317	-11	314	-12	285	-20
42	356	318	-11	317	-11	314	-12	285	-20
43	563	405	-28	381	-32	441	-22	395	-30
44	491	514	5	523	7	546	11	476	-3
45	713	543	-24	531	-26	564	-21	538	-25
46	517	427	-17	438	-15	459	-11	396	-23
47	484	392	-19	397	-18	397	-18	364	-25
48	829	561	-32	575	-31	621	-25	487	-41
49	499	411	-18	393	-21	413	-17	403	-19
50	523	400	-24	378	-28	403	-23	393	-25
51	962	822	-15	794	-17	848	-12	801	-17
52	523	400	-24	378	-28	403	-23	393	-25
53	639	543	-15	549	-14	597	-7	472	-26
54	639	543	-15	549	-14	597	-7	472	-26
55	722	556	-23	564	-22	606	-16	477	-34
56	585	503	-14	495	-15	505	-14	466	-20
57	850	646	-24	587	-31	655	-23	600	-29
58	850	646	-24	587	-31	655	-23	600	-29
59	585	503	-14	495	-15	505	-14	466	-20
60	473	445	-6	419	-11	443	-6	430	-9
61	496	437	-12	405	-18	439	-11	436	-12
62	585	503	-14	495	-15	505	-14	466	-20
63	685	855	25	779	14	865	26	786	15
64	787	558	-29	558	-29	569	-28	549	-30
65	613	513	-16	479	-22	518	-16	511	-17
66	671	564	-16	561	-16	570	-15	525	-22
67	664	560	-16	521	-21	561	-15	569	-14
68	746	598	-20	576	-23	621	-17	600	-20
69	735	559	-24	528	-28	588	-20	589	-20
70	809	684	-16	682	-16	692	-15	667	-18
71	706	554	-22	521	-26	560	-21	594	-16
72	688	566	-18	539	-22	596	-13	601	-13
73	711	577	-19	544	-23	582	-18	618	-13
74	684	544	-20	509	-26	549	-20	583	-15
75	706	554	-22	521	-26	560	-21	594	-16
76	751	644	-14	597	-21	669	-11	649	-14
77	710	569	-20	547	-23	607	-14	600	-15
78	711	577	-19	544	-23	582	-18	618	-13
79	658	589	-10	555	-16	593	-10	633	-4
80	768	618	-20	601	-22	648	-16	671	-13
81	787	613	-22	593	-25	647	-18	662	-16

Sub-Subbasin number, Base-Base period, Model-Mean of the climate models, (%) – Precipitation change percentage, MC- Mid Century and EC- End Century

Table A9-2: Change in mean annual PET in future relative to base period (in mm)

Sub	Base	rcp4.5 MC		rcp4.5 EC		rcp8.5 MC		rcp8.5 EC	
		Model	(%)	Model	(%)	Model	(%)	Model	(%)
1	1723	1836	7	1903	10	1836	7	1911	11
2	1786	2018	13	2018	13	1974	11	2117	19
3	1791	1986	11	1987	11	1939	8	2074	16
4	1686	1791	6	1870	11	1799	7	1879	11
5	1945	2122	9	2122	9	2101	8	2237	15
6	1887	2122	12	2122	12	2101	11	2238	19
7	1954	2126	9	2126	9	2107	8	2244	15
8	1912	2014	5	2014	5	1969	3	2110	10
9	1971	2095	6	2095	6	2083	6	2228	13
10	1988	2096	5	2096	5	2084	5	2228	12
11	1996	2167	9	2167	9	2129	7	2278	14
12	2008	2199	10	2237	11	2163	8	2269	13
13	1753	1965	12	1965	12	1915	9	2083	19
14	2005	2184	9	2212	10	2165	8	2265	13
15	1880	1999	6	1999	6	1968	5	2133	13
16	2011	2149	7	2149	7	2111	5	2233	11
17	2014	2148	7	2148	7	2110	5	2231	11
18	1859	1900	2	1900	2	1841	-1	1982	7
19	1947	2012	3	2012	3	1979	2	2144	10
20	1992	2156	8	2156	8	2119	6	2238	12
21	1983	2096	6	2096	6	2073	5	2206	11
22	1956	2098	7	2098	7	2075	6	2208	13
23	1997	2151	8	2151	8	2112	6	2234	12
24	1954	2095	7	2095	7	2072	6	2205	13
25	1813	1889	4	1889	4	1825	1	1969	9
26	1901	2007	6	2007	6	1964	3	2134	12
27	1699	1799	6	1805	6	1744	3	1863	10
28	1941	2086	7	2086	7	2060	6	2194	13
29	1881	1997	6	1997	6	1954	4	2125	13
30	1708	1822	7	1822	7	1764	3	1888	11
31	1693	1830	8	1830	8	1781	5	1903	12
32	1687	1815	8	1815	8	1787	6	1895	12
33	1892	2004	6	2004	6	1961	4	2131	13
34	1728	1778	3	1781	3	1738	1	1898	10
35	1736	1787	3	1804	4	1755	1	1915	10
36	1732	1881	9	1881	9	1816	5	1957	13
37	1781	1860	4	1870	5	1840	3	2000	12
38	1686	1712	2	1774	5	1715	2	1787	6
39	1676	1803	8	1820	9	1782	6	1867	11
40	1758	1874	7	1901	8	1869	6	2031	16
41	1799	1860	3	1870	4	1840	2	2001	11

Sub	Base	rcp4.5 MC		rcp4.5 EC		rcp8.5 MC		rcp8.5 EC	
		Model	(%)	Model	(%)	Model	(%)	Model	(%)
42	1800	1861	3	1872	4	1841	2	2002	11
43	1947	2141	10	2141	10	2101	8	2222	14
44	1715	1768	3	1768	3	1723	0	1883	10
45	1762	1736	-1	1801	2	1743	-1	1828	4
46	1725	1772	3	1780	3	1730	0	1889	9
47	1790	1845	3	1845	3	1795	0	1933	8
48	1667	1747	5	1759	6	1718	3	1816	9
49	1787	1867	4	1881	5	1853	4	2019	13
50	1731	1867	8	1867	8	1809	4	1949	13
51	1654	1686	2	1751	6	1686	2	1763	7
52	1732	1868	8	1868	8	1809	4	1950	13
53	1584	1746	10	1759	11	1710	8	1815	15
54	1585	1748	10	1761	11	1712	8	1817	15
55	1576	1722	9	1742	11	1689	7	1787	13
56	1778	1752	-1	1752	-1	1704	-4	1832	3
57	1503	1543	3	1580	5	1521	1	1631	9
58	1470	1541	5	1578	7	1518	3	1628	11
59	1680	1755	4	1755	4	1708	2	1836	9
60	1714	1808	5	1860	8	1764	3	1897	11
61	1720	1826	6	1863	8	1785	4	1915	11
62	1680	1755	4	1755	4	1707	2	1836	9
63	1472	1515	3	1551	5	1493	1	1584	8
64	1570	1662	6	1662	6	1609	3	1744	11
65	1630	1815	11	1849	13	1767	8	1898	16
66	1577	1746	11	1746	11	1693	7	1826	16
67	1633	1730	6	1783	9	1646	1	1769	8
68	1492	1508	1	1548	4	1471	-1	1575	6
69	1572	1695	8	1748	11	1618	3	1731	10
70	1447	1656	14	1656	14	1600	11	1729	19
71	1544	1593	3	1639	6	1593	3	1663	8
72	1556	1698	9	1752	13	1624	4	1737	12
73	1535	1586	3	1632	6	1586	3	1654	8
74	1555	1600	3	1647	6	1600	3	1671	7
75	1522	1592	5	1638	8	1592	5	1661	9
76	1473	1513	3	1549	5	1494	1	1566	6
77	1506	1583	5	1635	9	1554	3	1639	9
78	1500	1585	6	1631	9	1585	6	1654	10
79	1511	1584	5	1631	8	1584	5	1653	9
80	1501	1517	1	1575	5	1560	4	1622	8
81	1481	1547	5	1586	7	1560	5	1627	10

Sub-Subbasin number, Base-Base period, Model-Mean of the climate models, (%) – PET change percentage, MC- Mid Century and EC- End Century

Table A9-3: Change in mean annual water yield in future relative to base period (in mm)

Sub	Base	rcp4.5 MC		rcp4.5 EC		rcp8.5 MC		rcp8.5 EC	
		Model	(%)	Model	(%)	Model	Sub	Base	Model
1	86	47	-45	44	-49	54	-37	56	-35
2	65	17	-73	19	-70	21	-68	14	-78
3	65	31	-52	35	-46	38	-42	23	-65
4	129	76	-41	74	-42	94	-27	82	-36
5	42	12	-72	12	-70	14	-67	12	-72
6	40	11	-73	12	-71	13	-68	11	-72
7	15	7	-53	7	-53	8	-48	7	-52
8	41	12	-72	13	-69	14	-65	10	-75
9	18	7	-62	5	-72	7	-63	5	-71
10	18	7	-62	5	-72	6	-64	5	-72
11	26	9	-64	8	-68	11	-58	11	-59
12	28	24	-14	21	-25	24	-14	22	-21
13	182	39	-79	36	-80	43	-77	25	-86
14	35	21	-39	19	-46	21	-39	20	-41
15	30	10	-68	6	-79	11	-64	7	-78
16	34	23	-30	23	-30	28	-18	23	-33
17	33	23	-30	23	-30	27	-18	22	-33
18	32	15	-53	13	-60	20	-39	10	-70
19	27	15	-47	12	-57	15	-43	11	-61
20	42	13	-69	13	-69	16	-61	15	-65
21	25	15	-39	13	-49	17	-32	14	-43
22	26	15	-40	13	-49	17	-33	14	-44
23	33	23	-31	23	-31	27	-19	22	-33
24	25	15	-40	13	-50	17	-33	14	-45
25	31	29	-6.4	25	-18	40	29	19	-38
26	15	16	2.8	12	-24	17	9	11	-30
27	52	86	65	82	58	99	90	84	61
28	27	20	-26	16	-39	22	-17	17	-36
29	31	22	-30	17	-45	23	-26	13	-58
30	60	62	3.2	54	-11	64	6	56	-7
31	43	31	-27	26	-38	31	-27	28	-35
32	50	10	-81	8	-84	10	-80	8	-84
33	17	17	-0.2	13	-22	18	5	12	-31
34	55	52	-6.3	46	-16	45	-19	31	-43
35	12	16	34	12	4	13	13	10	-17
36	151	99	-34	100	-34	124	-18	81	-47
37	4	4	6.2	3	-16	4	-4	3	-16
38	143	142	-0.1	147	3	153	7	153	7
39	102	7	-93	7	-93	7	-93	7	-93
40	8	2	-78	2	-77	2	-79	2	-77
41	4	4	5.8	3	-16	3	-3	3	-16

Sub	Base	rcp4.5 MC		rcp4.5 EC		rcp8.5 MC		rcp8.5 EC	
		Model	(%)	Model	(%)	Model	Sub	Base	Model
42	2	2	19	2	-18	2	12	2	-18
43	39	16	-60	16	-60	21	-46	16	-59
44	21	39	82	37	72	36	69	22	6
45	74	36	-51	36	-51	41	-45	41	-45
46	25	24	-4.4	20	-21	20	-18	13	-48
47	14	7	-48	7	-52	7	-48	5	-61
48	155	75	-52	79	-49	97	-38	63	-59
49	19	7	-64	7	-62	7	-64	7	-64
50	27	7	-73	7	-74	7	-73	7	-76
51	195	150	-23	151	-23	165	-15	158	-19
52	27	7	-73	7	-74	7	-73	7	-75
53	66	48	-28	48	-27	64	-3	41	-38
54	80	60	-25	61	-24	78	-3	52	-35
55	104	62	-41	65	-38	80	-23	50	-52
56	30	25	-18	25	-17	21	-33	15	-51
57	136	81	-40	71	-48	92	-33	79	-42
58	152	88	-42	76	-50	99	-35	84	-45
59	33	25	-23	26	-22	21	-37	15	-53
60	13	11	-13	12	-9.1	12	-7	13	-4
61	26	17	-34	17	-35	15	-42	14	-45
62	33	26	-22	26	-21	22	-35	16	-53
63	74	139	86	118	58	149	101	123	66
64	75	43	-43	37	-51	38	-50	37	-51
65	50	28	-44	28	-43	27	-45	26	-48
66	49	39	-21	40	-20	34	-31	26	-47
67	61	41	-33	43	-29	44	-28	50	-18
68	81	58	-28	58	-29	63	-23	60	-27
69	85	39	-54	41	-51	50	-41	48	-43
70	88	77	-13	68	-23	72	-18	69	-21
71	62	34	-45	32	-48	38	-39	40	-35
72	74	42	-44	45	-39	55	-27	54	-28
73	42	26	-39	26	-39	31	-25	31	-26
74	63	39	-38	36	-43	43	-31	44	-30
75	56	29	-48	28	-50	33	-42	36	-37
76	53	44	-17	37	-31	45	-15	46	-13
77	47	39	-17	25	-47	39	-17	35	-25
78	44	27	-38	27	-38	33	-25	33	-24
79	28	27	-1.8	27	-2.9	34	20	33	20
80	56	32	-43	36	-35	48	-15	51	-9
81	62	35	-43	38	-39	49	-21	50	-19

Sub-Subbasin number, Base-Base period, Model-Mean of the climate models, (%) – Water yield change percentage, MC- Mid Century and EC- End Century

Annexure 10: Extracting climatic data from CHIRPS or CORDEX in R

```
# Extracting data from CHIRPS or CORDEX stored in netcdf format
# Load Required packages -----
library(ncdf4)
library(raster)
# Loading CHIRPS or CORDEX netcdf File-----
file01<-'chirps-v2.0.1990.days_p25.nc'
file02<-'chirps-v2.0.1991.days_p25.nc'
# Reading netcdf files -----
ncin01<-nc_open(file01)
ncin02<-nc_open(file02)
# parameter names of the netcdf files -----
names(ncin01$var)
# Build gridded dataset from netcdf -----
pre01 <-brick(file01,varname="precip")
pre02 <-brick(file02,varname="precip")
# Load required station data with Name, Longitude and Latitude -----
pcp_stations <- read.csv("req station.csv", header = T, row.names = "NAME", sep = ",")
# Overlay stations on netcdf grid to check location accuracy -----
points(pcp_stations,pch=16)
# Extract data for the given stations -----
pre.sites01 <- data.frame(extract(pre01, pcp_stations, ncol=2))
pre.sites02 <- data.frame(extract(pre02, pcp_stations, ncol=2))
# Match the column name of extracted data with given stations -----
row.names(pre.sites01)<- row.names(pcp_stations)
row.names(pre.sites02)<- row.names(pcp_stations)
# Order the chronologically -----
pre.sites1990<-t(pre.sites01)
pre.sites1991<-t(pre.sites02)
# Compile the dataset -----
pre.sites <- rbind(pre.sites1990,pre.sites1991)
# Save the file in csv format -----
write.csv(pre.sites, file="Extracted_Precipitation_CHIRPS_1990_1991.csv")
# End -----
```

Annexure 11: Publisher's permission



PARTIES:

1. **Cambridge University Press** [CompanyNumber] (Licensor); and
2. **Afanur Rahman Talukder** (Licensee).

Thank you for your recent permission request. Some permission requests for use of material published by the Licensor, such as this one, are now being facilitated by PLSclear.

Set out in this licence cover sheet (the **Licence Cover Sheet**) are the principal terms under which Licensor has agreed to license certain Licensed Material (as defined below) to Licensee. The terms in this Licence Cover Sheet are subject to the attached General Terms and Conditions, which together with this Licence Cover Sheet constitute the licence agreement (the **Licence**) between Licensor and Licensee as regards the Licensed Material. The terms set out in this Licence Cover Sheet take precedence over any conflicting provision in the General Terms and Conditions.

Free Of Charge Licence Terms

Licence Date: 19/10/2019
PLSclear Ref No: 19673

The Licensor

Company name: Cambridge University Press
Address: University Printing House
Shaftesbury Road
Cambridge
CB2 8BS
GB

The Licensee

Licensee Contact Name: Afanur Rahman Talukder
Licensee Address: 401 Sunset Avenue Windsor
University of Windsor
Center for Engineering Innovation
Center for Engineering Innovation
Windsor
N9B 3P4

Licensed Material

title: Hydrology An Introduction
ISBN: 9780521824798

publisher:	Cambridge University Press
figure number & title / caption	1.1 Sketch of some of the main processes in the land phase of water cycle
Are you requesting permission to reuse your own work?	No. I am NOT the author
page number	3
position on page	Top
reproduction colour	Black and White
reproduction size	Half page
positioning	inside or later pages

For Use In Licensee's Publication(s)

usage type	Book, Journal, Magazine or Academic Paper...-Thesis
language	English
number of pages	120
other relevant information	I need the permission to use the figure in my MASc thesis at University of Windsor, Canada.
publication title	Impacts of climate change on the hydrological regime in the Olifants River, South Africa.
type of document	Thesis

Rights Granted

Exclusivity:	Non-Exclusive
Format:	Thesis
Language:	English
Territory:	
Duration:	Lifetime of Licensee's Edition
Maximum Circulation:	0

GENERAL TERMS AND CONDITIONS

1. Definitions and Interpretation

1.1 Capitalised words and expressions in these General Terms and Conditions have the meanings given to them in the Licence Cover Sheet.

1.2 In this Licence any references (express or implied) to statutes or provisions are references to those statutes or provisions as amended or re-enacted from time to time. The term including will be construed as illustrative, without limiting the sense or scope of the words preceding it. A reference to in writing or written includes faxes and email. The singular includes the plural and vice versa.

2. Grant of Rights

2.1 The Licensor grants to Licensee the non-exclusive right to use the Licensed Material as specified in the Licence Cover Sheet.

2.2 The rights licensed to Licensee under this Licence do not include the right to use any third party copyright material incorporated in the Licensed Material. Licensee should check the Licensed Material carefully and seek permission for the use of any such third party copyright material from the relevant copyright owner(s).

2.3 Unless otherwise stated in the Licence Cover Sheet, the Licensed Material may be:

2.3.1 subjected to minor editing, including for the purposes of creating alternative formats to provide access for a beneficiary person (provided that any such editing does not amount to derogatory treatment); and/or

2.3.2 used for incidental promotional use (such as online retail providers' search facilities).

2.4 Save as expressly permitted in this Licence or as otherwise permitted by law, no use or modification of the Licensed Material may be made by Licensee without Licensor's prior written permission.

3. Copyright Notice and Acknowledgement

3.1 Licensee must ensure that the following notices and acknowledgements are reproduced prominently alongside each reproduction by Licensee of the Licensed Material:

3.1.1 the title and author of the Licensed Material;

3.1.2 the copyright notice included in the Licensed Material; and

3.1.3 the statement "Reproduced with permission of The Licensor through PLSclear."

4. Reversion of Rights

4.1 The rights licensed to Licensee under this Licence will terminate immediately and automatically upon the earliest of the following events to occur:

4.1.1 the Licensed Material not being used by Licensee within 18 months of the Licence Date;

4.1.2 expiry of the Licence Duration; or

4.1.3 the Maximum Circulation being reached.

5. Miscellaneous

5.1 By using the Licensed Material, Licensee will be deemed to have accepted all the terms and conditions contained in this Licence.

5.2 This Licence contains the entire understanding and agreement of the parties relating to its subject matter and supersedes in all respects any previous or other existing arrangements, agreements or understandings between the parties whether oral or written in relation to its subject matter.

5.3 Licensee may not assign this Licence or any of its rights or obligations hereunder to any third party without Licensor's prior written consent.

5.4 This Licence is governed by and shall be construed in accordance with the laws of England and Wales and the parties hereby irrevocably submit to the non-exclusive jurisdiction of the Courts of England and Wales as regards any claim, dispute or matter arising under or in relation to this Licence.

VITA AUCTORIS

NAME	Afanur Rahman Talukder
PLACE OF BIRTH	Jamalpur, Dhaka, Bangladesh
YEAR OF BIRTH	1985
EDUCATION	<ul style="list-style-type: none">• Bachelor of Science (Civil Engineering), Bangladesh University of Engineering and Technology (BUET), 2008.
EXPERIENCE	<ul style="list-style-type: none">• Research Assistant, Department of Civil and Environmental Engineering, University of Windsor, Sep 2017 to Dec 2019.• Executive Engineer, Dhaka Water Supply and Sewerage Authority, Dhaka, Bangladesh, Sep 2014 to Jun 2017• Sub Divisional Engineer, Dhaka Water Supply and Sewerage Authority, Dhaka, Bangladesh, Jan 2011 to Aug 2014• Assistant Engineer, Dhaka Water Supply and Sewerage Authority, Dhaka, Bangladesh, Jul 2009 to Dec 2010• Junior Engineer, Institute of Water Modelling, Dhaka, Bangladesh, Aug 2008 to Jun 2009